RADIATION EFFECTS ON YTTERBIUM-DOPED OPTICAL FIBERS

DISSERTATION

Briana J. Singleton, Major, USAF

AFIT-ENP-DS-14-J-15

DEPARTMENT OF THE AIR FORCE

AIR UNIVERSITY

AIR FORCE INSTITUTE OF TECHNOLOGY

Wright-Patterson Air Force Base, Ohio

DISTRIBUTION STATEMENT A.

APPROVED FOR PUBLIC RELEASE; DISTRIBUTION UNLIMITED

The views expressed in this thesis are those of the author and do not reflect the official policy or position of the United States Air Force, Department of Defense, or the United States Government. This material is declared a work of the U.S. Government and is not subject to copyright protection in the United States.

AFIT-ENP-DS-14-J-15

RADIATION EFFECTS ON YTTERBIUM-DOPED OPTICAL FIBERS

DISSERTATION

Presented to the Faculty

Department of Engineering Physics

Graduate School of Engineering and Management

Air Force Institute of Technology

Air University

Air Education and Training Command

In Partial Fulfillment of the Requirements for the

Degree of Doctor of Philosophy

Briana J. Singleton, MS
Major, USAF

June 2014

DISTRIBUTION STATEMENT A.
APPROVED FOR PUBLIC RELEASE; DISTRIBUTION UNLIMITED

AFIT-ENP-DS-14-J-15

RADIATION EFFECTS ON YTTERBIUM-DOPED OPTICAL FIBERS

Briana J. Singleton, MS
Major, USAF

Approved:

//signed//	28 May 2014
James C. Petrosky, PhD (Chairman)	Date
//signed//	28 May 2014
John W. McClory, PhD (Member)	Date
//signed//	28 May 2014
Robert L. Hengehold, PhD (Member)	Date
//signed//	28 May 2014
Michael C. Pochet, Major, USAF, PhD (Member)	Date

Accepted:

Adedeji B. Badiru, PhD Dean, Graduate School of Engineering and Management	Date

AFIT-ENP-DS-14-J-15

Abstract

Assuming on-board satellite high-bandwidth communications will utilize passive optical fibers as a communication channel, this work focused on the impact of gamma and mixed gamma/neutron radiation on transmission through single-mode and multi-mode ytterbium-doped single-mode fibers operated as amplifiers for a 1060-nm light source. Standard optical patch cables were evaluated along with active ytterbium -doped double-clad fibers in the same radiation environment. Exposure times and signal transmission wavelength variations were used to investigate the degradation of the fibers exposed to total doses above 100 krad(Si). Further, the effect on the amplified signal gain was studied for the ytterbium -doped fibers. The increased attenuation in the fibers across a broad wavelength range in response to multiple levels of gamma radiation exposure, along with the effect that increased attenuation has on the actively pumped ytterbium -doped fiber amplifier performance was evaluated.

Ytterbium-doped optical fibers demonstrate sensitivity to gamma and mixed neutron/gamma radiation exposures that is independent of the operational configuration of the fiber during irradiation. No identifiable dose rate damage production mechanism was encountered. However, fiber damage recovery following irradiation was found to be dependent on the radiation dose rate.

Dedicated to my grandmother.

Acknowledgements

I would like to thank my project sponsors at the Air Force Nuclear Weapon Center for supporting my work. None of this would have been possible without them. I would like to thank the members of my committee for their extreme patience and confidence in me to complete this project. I would like to thank the exemplary researchers at Sandia CA and to the personnel at the Annular Core Research Reactor and those of the Qualification Alternatives to the Sandia Pulsed Reactor project for all of their assistance and accommodation. Thanks to the personnel at The Ohio State University Nuclear Reactor Lab and their flexibility and assistance with my experiments that were conducted over 9 months. Thank you to Dr. Nick G. Usechak at the Air Force Research Laboratory's Sensors Directorate. He made his lab, resources and expertise available whenever I needed them. Thanks are owed to the chairman of my committee, Dr. James Petrosky for his enthusiasm and resourcefulness. He made every mountain into a molehill. He kept me focused by consistently reminding me of the joy of teaching and advising that is my reward for completing this dissertation. I would like to thank my fellow graduate students—those who have moved on, those in the thick of it, and those just beginning—for their support, feedback, and friendship.

To my husband, thank you for your unwavering support and love. You knew I would succeed way before I did. Last, but not least, I thank my son. We began this journey together and you are an ever-present reminder of the joy of exploration that initially attracted me to science.

Briana J. Singleton

Table of Contents

List of Figures

List of Tables

List of Abbreviations

ABBREVIATION	MEANING
ASE	Amplified spontaneous emission
dB	Decibel
DCF	Double-clad fiber
LMA	Large mode area
MM	Multi-mode fiber
NBOHC	Non-bridging oxygen hole center
ODC	Oxygen deficient center
OHC	Oxygen hole center
RE	Rare-earth
RIA	Radiation-induced attenuation
SiE’	Silicon E-prime center
SMF	Single-mode fiber
YDF	Ytterbium-doped fiber

RADIATION EFFECTS ON YTTERBIUM-DOPED OPTICAL FIBERS

1 Introduction

1.1 Overview

Ytterbium (Yb) doped optical fibers (YDFs) are susceptible to gamma and mixed gamma/neutron radiation to a degree greater than standard optical fibers. The damage results in degraded power transmission in broad spectral bands within the fibers, due to the production of color centers related to Al atomic defects, and to a lesser degree O,Yb, Si, and impurities within the fiber. The production is dependent on radiation total dose, and has no measureable dose rate, operational employment, or specific radiation type dependence. However, the recovery rate of the fibers following irradiation is highly sensitive to the dose rate.

A set of single-mode (SM) and multi-mode (MM) fibers were separately exposed to radiation from a Co-60 gamma source and from two reactor sources. The reactor sources were a university research reactor operated in a steady state mode and a national laboratory thermal pulsed reactor operated in the pulse mode. The SM fibers were tested both as Yb-doped fiber amplifiers (YDFAs) and in passive configurations. The MM fibers were evaluated with a white light source during the experiment.

The lack of sensitivity to dose rate for fiber transmission degradation over several magnitudes is a welcome result. It precludes the requirement to expose YDFs to multiple radiation environments to determine radiation sensitivity in a mixed dose rate environment, such as space. The YDFs can be tested at available radiation facilities and the damage to the fibers in other environments can be extracted as a function of total dose. The dependence of the recovery on the dose rate however changes this view if the radiation dose is time dependent, or operations

do not include “operate through” standards. Since the recovery was found to have an inverse relationship with dose rate (i.e., the higher the dose rate, the faster the recovery rate), this may change the time in which a system is held off-line following a radiation burst. Understanding the recovery rate is essential so that the recovery time for different environments can be established and mitigation methods can be most efficiently employed.

1.2 Motivation

Optical fiber-based components have characteristics that are ideal for applications in complex environments. They are small, lightweight, robust, impervious to electromagnetic field interference, and can handle multiple signal types. When doped with rare-earth (RE) elements, optical fibers can be designed to both amplify and transmit signals. The RE element typically doped in a low concentration within the core is an element that can be stimulated to emit light (Hecht, 2006). RE-doped optical fibers are primarily used as signal amplifiers in complex optical systems such as fiber gyroscopes and laser devices (Girard, et al., 2009).

Erbium (Er^{3+}) has long been the most prevalent RE dopant because of erbium’s ability to amplify signals at common communications wavelengths (1330 and 1550 nm). Ytterbium (Yb^{3+})-doped fiber, however, exhibits high output power coupled with excellent power conversion efficiency while avoiding some of the complications that are experienced with Er-doped fibers (Paschotta, Nilsson, Tropper, & Hanna, 1997). YDFs have also found increasing use in fiber-based laser systems. Their ability to amplify light over a broad range of wavelengths (975 to 1200 nm) has made them even more attractive for applications in other fields such as communications. Another advantage of Yb-doping is the ability to dope concentrations greater than what is achievable with Er-doping. This increased doping enables higher gain to be achieved with shorter lengths of fiber. For laser operation, the wide range of possible pump

wavelengths allows for greater flexibility of pumping schemes, including pumping by diode lasers (Paschotta, Nilsson, Tropper, & Hanna, 1997).

One undesirable effect of the use of any optical fiber in a radiation environment is the atomic scale production of point defects (aka color centers), which may absorb light, resulting in a reduction of signal power and data loss. In RE-doped glass fibers, energy transfer from excited RE ions to color centers can also degrade the amplification capacity of the fiber (Dragic, Carlson, & Croteau, 2008). Radiation interactions have been shown to change the fiber refractive index and pull strength. The primary means to characterize the radiation-induced degradation to the fiber transmission mechanism is through the measurement of the increase of the linear absorption in the fiber, also known as the radiation-induced attenuation (RIA). RIA is typically characterized at the wavelengths of interest and is measured in decibel (dB) per unit length (Berghmans, et al., 2008). This light absorption can be detrimental to the fiber's performance if the color centers absorb light that is near the operating wavelengths of the fiber.

Previous studies have shown that RE-doped fibers are more sensitive to radiation and experience RIA of the optical signal at typically an order of magnitude or more above that of the standard telecommunications optical fiber, the SMF28 (Girard, et al., 2012). However, studies have shown that optical fibers doped or co-doped with Yb demonstrate a higher radiation tolerance than Er-doped fiber amplifiers (Henschel, Köhn, Schmidt, Kirchhof, & Unger, 1998). Although the lengths of RE-doped fibers used for amplification and high-power laser applications are relatively short (0.5 to 10 m), there is nonetheless a need to investigate the fiber sensitivity in order to improve the understanding of radiation effects on these materials.

The broad variety of fiber types and environments in which optical fibers are used present additional challenges in the study of radiation effects. The response of optical fibers can change

drastically depending on a wide variety of intrinsic and extrinsic factors such as the type of optical fiber and the radiation environment considered. The amplitude and kinetics of the RIA greatly differ from one fiber type to another, depending on the composition of the core and cladding along with dopants (intentional or inadvertent) (Friebele, 1992), preform production and fiber drawing process parameters (Girard, Ouerdane, Boukenter, & Meunier, 2006). The manner in which fibers are employed with regards to temperature, signal wavelength and signal strength add another layer of research complexity (Brichard & Fernandez, 2005). In addition, the complexity of the damage mechanisms requires the use of complementary investigation methods to identify the color centers created.

There has been extensive research regarding the radiation effects on various types of RE-doped optical fibers in environments representative of civilian nuclear and space operations (Ott, 2004; Lezius, et al., 2012). However, the literature is sparse for research on RE-doped optical fibers in a radiation environment characteristic of military nuclear operations. In particular, a review of recent research dating back to the 1980s, concludes that the properties and response of RE-doped optical fibers to high dose rate radiation remain poorly documented.

In the past year, a group at Sandia National Laboratory (SNL) has designed and developed the first power-scalable all-fiber passively Q-switched laser using a large mode area (LMA) Yb-doped fiber as a gain medium, which is adiabatically tapered to an unpumped single-mode Yb-doped fiber that serves as a saturable absorber (Soh 2011). Their design enables the production of nanosecond optical pulses using approximately a meter length of fiber that can be compactly packaged and ruggedized. The system developed by SNL is one of several optical RE-doped fiber based systems being considered for implementation in future defense platforms.

The present research is oriented upon an effort to evaluate emerging technologies that are envisioned for use in future nuclear weapon system upgrades. This work is supported by the Air Force Nuclear Weapons Center (AFNWC) and applies to an effort to determine the feasibility of employing various materials prior to the more advanced stages of design and procurement.

There already exist several experimental results published on Yb-doped optical fiber designs irradiated while in the passive mode (Fox B. P., et al., 2007; Dicks, Heine, Petermann, & Huber, 2001; Girard, et al., 2009). However, to date, there are scant published results on the radiation effect to Yb-doped fibers while in the active mode (Girard, et al., 2012; Fox B. P., Simmons-Potter, Moore, Fisher, & Meister, 2009). The overall reliability of the Yb-doped fiber laser system is the sum of many variables, and this dissertation will focus on the RIA of the optical signal in the fiber and how it affects the signal amplification performance. In particular, this work will focus on the RIA caused by high dose rate radiation ($>10^5$ rad(Si)/sec) in continuous and pulsed operations. Figure 1 details the radiation dose rates and total doses that are typical of certain radiation environments. The scope of published work to date has been focused on the space environment and conducted at dose rates of 10^2 rad(Si)/sec and lower.

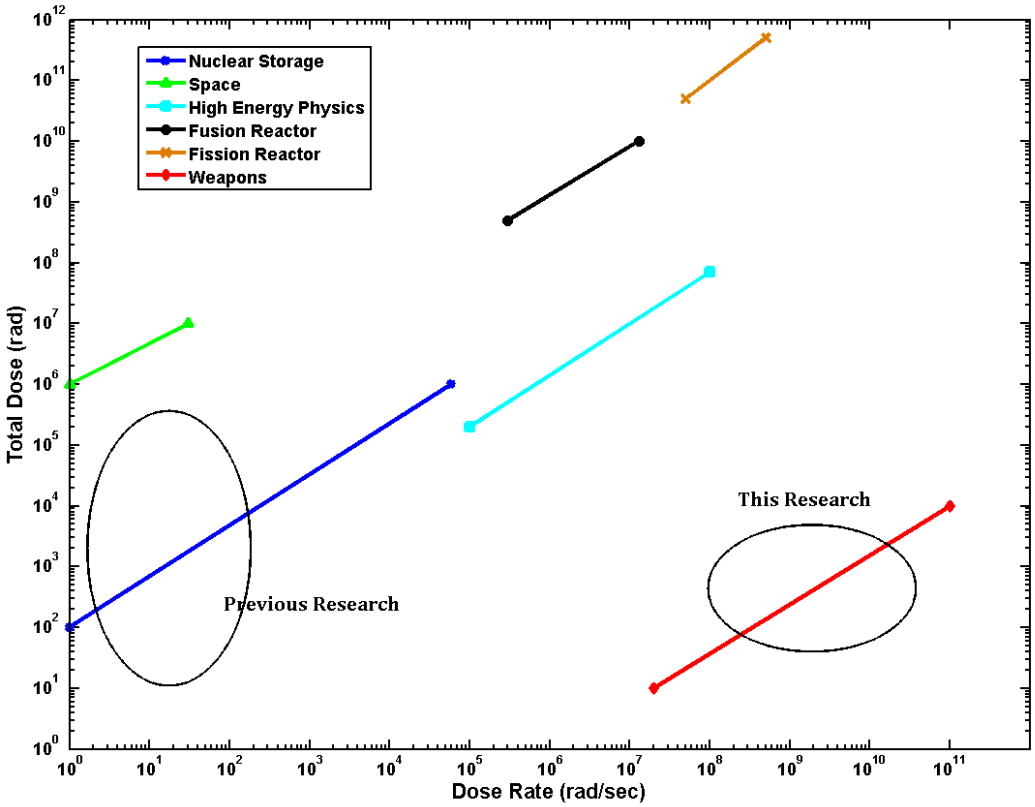

Figure 1. Dose rate and total dose values typical of specific radiation environments. Reproduced from data in (Girard S., 2003) .

1.3 Problem Statement

The goal of this dissertation is to determine the fundamental causation of effects to Yb-doped fibers from high dose rate radiation during and in the short times following exposure. The data from experiments conducted across several magnitudes of dose-rates will be used to model and then verify the degradation that would be experienced by a fiber laser system that is in close proximity to a nuclear detonation. This work is the only documented, to date, examination of actively pumped Yb-doped fibers in a high-dose rate, short-pulse, mixed neutron/gamma radiation environment. The focus of the experiments and analysis will be to:

1. Determine how radiation dose rate affects the performance of the Yb-doped fibers using a continuous radiation source and a short-pulse source.

2. Determine whether the results from the continuous dose rate experiments can be used to extrapolate the damage from high dose-rate, short-pulse radiation exposures.
3. And to determine whether actively pumping the Yb-doped fibers during exposure affects the radiation sensitivity.

The information will be used to determine the degree of damage to the fiber laser operation and whether or not experiments utilizing continuous exposure at lower dose rates can be used to estimate damage to systems exposed to extremely high dose-rate pulsed radiation.

This dissertation briefly discusses the theory of optical fibers and the operation of RE-doped fibers as amplifiers and fiber lasers along with a review of their sensitivity to radiation in Chapter 2. Chapter 3 will discuss the experimental techniques that are employed to evaluate RE-doped fibers, before, during, and following irradiation to study the RIA and its effects. Chapters 4-5 summarize the results of gamma irradiation on single-mode (SM) Yb-doped fibers, very rapid reactor pulse rate exposure, and steady state research reactor exposure, respectively. Synthesis of these results is presented in Chapter 6.

2 General Theory

2.1 Chapter Overview

This chapter provides a general overview of the theory behind optical fiber operation and damage from radiation exposure. An in-depth summary of the most current research into the radiation response of RE-doped fibers, focusing on YDFs is also provided.

2.2 Rare-earth doped optical fibers

The concept of total internal reflection of light has been well known and demonstrated since 1840. Using glass fibers to transmit optical signals began in the 1920s. Nonetheless, there were few real-world applications until the development of the laser to provide the equivalent of a pure carrier frequency in 1960. Following this, the use of optical fibers made from silica glass for telecommunication signal transmission became rapidly popular (Hecht, 2006). In the same decade, rare-earth doping of silica fiber was first conducted, along with the first demonstration of an Nd^{3+}-doped silica fiber amplifier (Koester & Snitzer, 1964). This was quickly followed by the first silica fiber laser doped with Er^{3+} and Yb^{3+} in 1965 (Snitzer & Woodcock, 1965). The first widespread use of RE doped optical fibers was the Er-doped fiber amplifier (EDFA), which emerged to increase the transmission distance of optical telecommunications fiber (Hecht, 2006). The use of RE-doped optical fibers as amplifying media has since branched out into various industries including defense, medical, and manufacturing, with optical output powers extending from the mW in the telecommunications range to the multiple tens of kW range for materials processing (Sumimura, Yoshida, Hisanori, & Nakatsuka, 2006).

2.3 Overview of silica-based optical fibers

Silica glass (SiO_2) is the most common optical fiber material. Subsequently, the majority of Yb-doped fibers are based on a silica matrix. Amorphous silica consists of a random network of Si atoms each bonded to four O atoms. The structure lacks periodicity, extended symmetry and long-range order. The ideal silica network, depicted in Figure 2, consists of corner-sharing SiO_4 tetrahedra without broken or homopolar bonds (Wright, 2000). In most cases, the SiO_4 tetrahedra can be treated as rigid units, linked together to form silica. For amorphous silica, the bond angle between the tetrahedra, α, varies from 120° to 180°, resulting in a lack of long-range order. In addition to its amorphous nature, natural silica contains an assortment of structural defects and impurities. The most prevalent defects arise from oxygen deficiencies or oxygen excesses (Skuja, Optical Properties of Defects in Silica, 2000). The chemical properties of these defects, the electron transitions of the bonding oxygen atoms, and the resonance vibrations of the Si-O bonds, define the optical absorption spectra of amorphous silica (Brückner, 1970). Therefore, it is essential to begin fiber production with ultrapure glass in order to optimize the transmission.

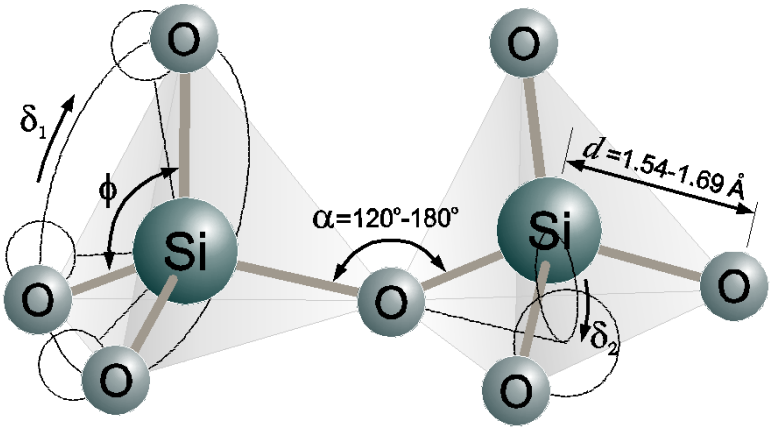

Figure 2. Three-dimensional schematic of a pure fragment of the ideal silica structure. The Si-O bond length is defined as d and typical lengths are shown. The tetrahedral angle is φ, the inter-tetrahedral bond angle is α, and the bond torsion angles are defined as δ_1 and δ_2 (Salh, 2011). Used with permission granted by Creative Common License 3.0.

The impurity concentration in glass used to make quality optical fibers is required to be on the order of one part per billion. In order to achieve this level of purity, synthetically produced fused silica is used as the starting material for optical fiber production. Fused silica glass cylinders are the standard preform shape in fiber production. There are several techniques that enable the doping of different element concentrations on the cylindrical preform's inner and/or outer surfaces. They all include tightly controlled methods to deposit a vaporized material onto the surfaces which is then melted (sintered) into place. Optical fiber production begins by heating one end of the glass preform until it softens. The fiber is then created by a controlled pulling of the heated glass out into very thin strands (Hecht, 2006).

Although silica is the most widely used material for RE-doped optical fibers, it requires the inclusion of other elemental dopants along with the RE-ions in order to stabilize the RE-ions and prevent them from clustering, which can degrade amplifying performance (DiGiovanni, Shubochkin, Morse, & Lenardic, 2007). The Yb-doped fibers used in this research are manufactured by nLight Corporation and are doped using the Direct Nanoparticle Deposition (DND) process. This process enables fabrication of fibers with extremely high rare-earth concentrations, which minimizes the required fiber length for amplification and laser systems, and raises the threshold power for nonlinear processes. In this process, the rare earth dopants are mixed with the refractive index changing materials (Al, Ge, P, for example) prior to deposition. The DND process improves the homogeneity of the glass composition before the sintering phase and can increase the radiation resistance for Er-doped fiber amplifiers exposed to gamma radiation (Kokki, Koponen, Laurila, & Ye, 2010; Gusarov, Van Uffelen, Hotoleanu, Thienpont, & Berghmans, 2009)

Yb, and Er ions are incorporated into glasses in the trivalent state. The resulting electron structure is similar to Xe with only the partially filled electron f^{N-1} orbital which is effectively shielded by the outer 5s and 5p shells. The partially filled orbital results in relatively well-defined energy levels that lead to narrow absorption and emission bands. The levels are broadened by interactions with the silica matrix and the degeneracy of the levels can be relaxed somewhat allowing f-f transitions to occur (DiGiovanni, Shubochkin, Morse, & Lenardic, 2007). For Yb^{3+} ions in silica, the lower level, $^2F_{7/2}$ is split into four Stark levels and the upper level, $^2F_{5/2}$, is split into three, as shown in Figure 3. Homogenous and inhomogeneous broadening enables transitions between sublevels to occur at a wide range of wavelengths. The large energy gap between the $^2F_{5/2}$ and $^2F_{7/2}$ levels inhibits concentration quenching and nonradiative decay via multiphonon emission from the $^2F_{5/2}$ level. These features, along with the closeness of the pump and amplification wavelengths, enable high efficiency operation (Pask, et al., 1995).

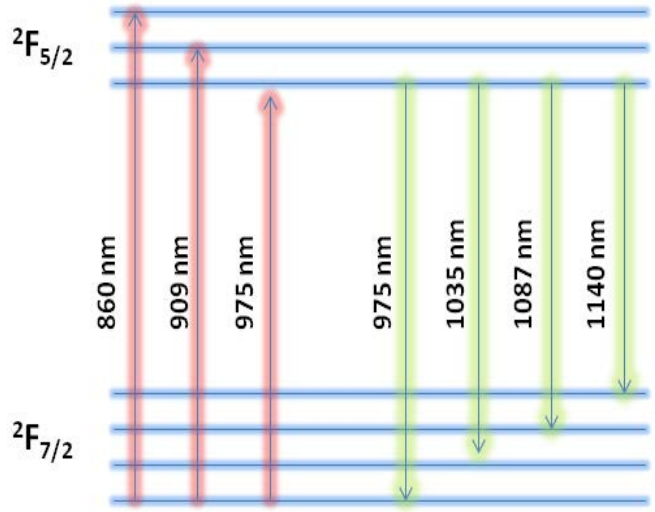

Figure 3. Energy level structure of Yb^{3+} in silica glass (Pask, et al., 1995).

2.4 Characteristics of RE-doped optical fibers

The rare earth ions incorporated into silica glass are optically active as a result of the splitting of their energy levels by the silica matrix. They absorb light at specific wavelengths and

can then emit light at longer wavelengths. For a doped fiber amplifier, pump light coupled into the fiber elevates the RE ion into an excited state. The signal light that is propagated in the fiber interacts with these excited ions and, through stimulated emission, can cause the release of a coherent photon traveling in the same direction as the signal photon, thus amplifying the signal. For Yb^{3+} ions in silica, both the absorption and emission are peaked at a wavelength of approximately 975 nm. However, the broad range of the absorption and emission cross-sections as shown in Figure 4 allows for a flexibility in both pumping and amplification wavelengths. In most applications, Yb-doped fibers are pumped by light in the region from 950-980 nm and emission is at higher wavelengths, e.g. 1047 or 1064 nm (Paschotta, Nilsson, Tropper, & Hanna, 1997).

In addition to stimulated emission, the excited ions can also decay spontaneously (spontaneous emission). When population inversion occurs, some of the excited ions will spontaneously relax to the ground state before interacting with a signal photon. This relaxation is completed by emitting a photon which is not coherent with the signal light or other spontaneous emissions. Light that is emitted at a wavelength and in a mode that can be guided by the fiber can be subsequently amplified as it propagates forward or backward through the fiber. This amplified spontaneous emission (ASE) can contribute significantly to signal distortion. ASE is the main source of background noise for Yb-doped fiber amplifiers. This optical noise is produced along the length of the fiber as long as population inversion is occurring, whether the signal light is present or not.

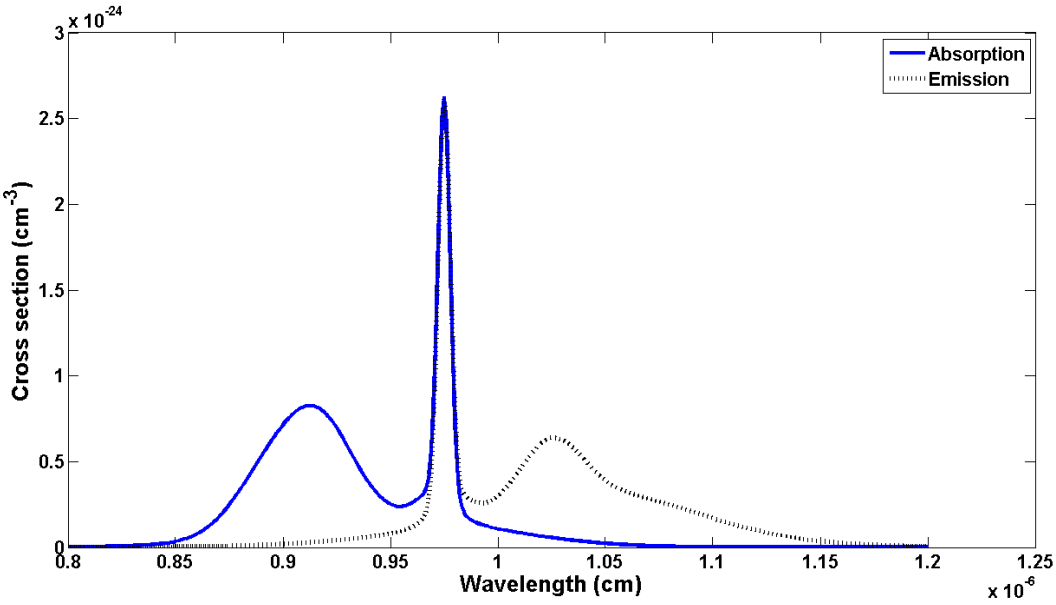

Figure 4. Calculated absorption (solid) and emission (dotted) cross sections of Yb in silica glass (Rumbaugh, 2013).

In order to enable light propagation, optical fibers typically consist of a core, a cladding, and in certain instances, a second (outer) cladding surrounding the silica cladding. Fibers are typically protected by a polymer sheath that does not propagate light. The glass core has the highest refractive index while the refractive index of the cladding is lower in order to allow for total internal reflection. For RE-doped fibers, a double cladding scheme is often used. In double clad fibers the outer cladding has the lowest refractive index. This format increases the acceptance angle of pump light in the cladding, which is then absorbed into the core doped with the active rare earth ion (Hecht, 2006). The difference in the refractive index from the core to the cladding can be very small (from 0.001 to 0.2). In addition, the cladding cross section of a doped fiber is typically not circular, as shown in Figure 5. This is done to enhance the propagation of pump light from the cladding to the core and reduce the buildup of nonlinear effects (Koponen, 2008). Pump light is directed into the doped core where amplification takes place.

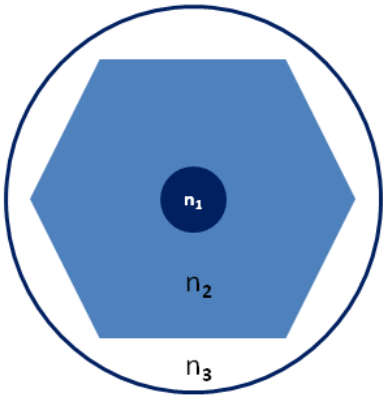

Figure 5. Representative double-clad fiber cross section ($n_1>n_2>n_3$).

Rare earth-doped fiber amplifiers and lasers function on the principles of excited state population inversion and stimulation emission. The energy levels of rare earth ions incorporated into a glass structure are split due to the electrostatic interactions between the ion and the host material. Pump light is injected into the cladding and propagated to the core where it excites the optically active elements, say Yb^{3+} ions. With a strong enough pump light, a significant portion of the Yb^{3+} ions will remain in an excited state. A signal beam with wavelength close to the emission of the Yb^{3+} ions is then propagated through the fiber. When this signal light interacts with the excited Yb^{3+} ions, the ions release a photon of the same wavelength through the process of stimulated emission. The signal is thereby amplified when passing through the doped fiber (Hecht, 2006).

For laser operations, the principles of amplifier function apply, but there is no external signal light. The system is pumped strongly enough so that the population of Yb^{3+} ions that are in an excited state exceeds those in the ground state (population inversion). The signal light is initially generated by spontaneous emission and then reflected back into the doped fiber core in order to produce a larger quantity of signal photons. The length of the cavity is such that a

resonance occurs and the light moving back and forth through the core becomes coherent. One end of the fiber is coated to reflect the majority of the signal light until the power reaches an upper threshold. At that point, the coherent light will pass through that end and the fiber will 'lase' (Hecht, 2006).

For optically active materials, the small-signal gain is a factor measured and used to characterize the gain of the medium per unit length at a signal level well below gain saturation. If a beam of power P_0 enters the medium and is amplified in a length L to a power, P, the small signal gain, g_0 is given by (1)**.**

$$g_0 = \left[\frac{1}{L}\right] \times \log\frac{P}{P_0} \tag{1}$$

The concentration of optically active ions in a medium is limited; the gain coefficient at higher signal powers will decrease. This phenomenon is called gain saturation and is a result of the depopulation of the excited state that occurs with an increasing number of signal photons. The gain coefficient, g, can be written as follows in (2).

$$g = \frac{g_0}{1 + P/P_s} \tag{2}$$

In (2), P is the incident signal power and Ps is the saturated signal power, defined as the power required for the gain to drop by half of its small-signal value. The saturation power is an important characteristic of an optical amplifier because it defines the input power for which the most possible output power can be achieved (Bjarklev, 1993).

Rate equations to model the propagation of light through a fiber amplifier can be written assuming that the power of a beam is P [W] in a doped fiber amplifier core with emission and absorption cross-sections of σ_e and σ_a [m^2] respectively. The total concentration of dopants is N_T with the concentrations of dopants in the ground and excited states denoted as N_1 and N_2 [per m^3]

and $N_T = N_1 + N_2$. When a beam with power P travels through the active medium, the amount of power absorbed by the ground state atoms (pumping them to excited states) per unit length is given by:

$$P_{abs} = \sigma_a \times P \times N_1, \tag{3}$$

and the gain of the signal power, P per unit length is given by:

$$Gain = \sigma_e \times P \times N_2. \tag{4}$$

In an infinitesimal distance, *dz*, if the stimulated emission and absorption contribution is considered the expected change of the power should be:

$$dP = (\sigma_e N_2 - \sigma_a N_1) \times P \times dz. \tag{5}$$

In a scenario in which ASE does not extract significant power, rate equations for the spatially-dependent population and power-propagation are given by (6) through (8).

$$\begin{aligned} \frac{dN_2}{dt} = \frac{D}{hcA}\sum_{j=1}^{J} \lambda_j^p \left[\sigma_a(\lambda_j^p)N_1 - \sigma_e(\lambda_j^p)N_2\right] \times P_p(\lambda_j^p) \\ + \frac{\Gamma}{hcA}\sum_{k=1}^{K} \lambda_k^s [\sigma_a(\lambda_k^s)N_1 - \sigma_e(\lambda_k^s)N_2] \times P_s^{\pm}(\lambda_k^s) \\ - \frac{N_2}{\tau} \end{aligned} \tag{6}$$

$$\frac{dP_p(\lambda_j^p)}{dz} = D \times \left[\sigma_e(\lambda_j^p)N_2 - \sigma_a(\lambda_j^p)N_1\right] \times P_p(\lambda_j^p) - \alpha P_p(\lambda_j^p) \tag{7}$$

$$\frac{dP_s^{\pm}(\lambda_k^s)}{dz} = \Gamma \times [\sigma_e(\lambda_k^s)N_2 - \sigma_a(\lambda_k^s)N_1] \times P_s^{\pm}(\lambda_s^k) - \alpha P_s^{\pm}(\lambda_k^s) \tag{8}$$

In (6) through (8), the pump and signal powers are divided into separate spectral channels, $P_p(\lambda_j^p)$, which denotes the pump power of the jth channel. $P_s^{\pm}(\lambda_k^s)$ represents the signal power of the kth signal channel propagating forward or backward with respect to the pump beam, c is the speed of light in vacuum, α is the background attenuation coefficient of the fiber, A is the doped effective area of the fiber, τ represents the fluorescence lifetime of the upper level, confinement factors of the pump and signal beams in the doped area are represented by D and Γ (Liu, 2011).

Equation (6) provides the change to the upper population density due to stimulated absorption and emission of both the pump and signal beams. The subsequent equations provide the evolution of the pump and signal power along the fiber. Assumptions used to simplify these rate equations are that the gain medium is assumed to be homogenous (the Yb concentration is assumed to be uniformly distributed in the core), and that the pump and signal intensity profile over the area of the inner cladding and core area are assumed to be uniform.

2.5 All fiber laser

The potential uses for an all-fiber laser are numerous. The system as designed by Sandia/CA can be easily packaged and transported and utilized in multiple fields, including weapons, manufacturing, telecommunications, remote sensing, and medicine. The all fiber laser power node consists of a large mode area (LMA) fiber adiabatically tapered and spliced to a single mode fiber that is then spliced to a fiber Bragg grating (FBG). The laser cavity is formed by the reflection from the flat-cleaved LMA fiber and the FBG. The LMA fiber acts as the gain medium and is cladding pumped and the smaller single mode fiber acts as the saturable absorber. The saturable absorber has a high absorbance (loss) of the light generated in the gain medium at low light intensities. This allows the gain in the LMA fiber to increase without saturating. Once the

intensity of the light reaches a certain upper threshold, the saturable absorber becomes 'transparent' and allows for the generation of a high energy pulse from the gain medium. The taper between the two fibers provides a mode filtering effect and allows single mode operation of the laser when using the LMA fiber (Soh, Bisson, Patterson, & Moore, 2011).

2.6 Radiation damage mechanisms in silica optical fibers

For purposes of clarity, the various forms of radiation can be divided into two main categories; purely ionizing and particle radiation. Purely ionizing radiation, such as x-rays and γ-rays interact with atoms within a material and deposit energy through the creation of secondary electrons and positrons, depending upon the amount of energy transferred. These secondary particles can further ionize atoms, but typically through small energy scattering, as they travel. Particle radiation, consisting of neutrons, protons, and heavy ions, can cause both ionization in a material and non-ionizing energy loss through displacement or vibration of targeted atoms (Brichard & Fernandez, 2005). Energetic radiation of both types can create a cascade effect where primary ionizations and/or displacements lead to a series of subsequent damage affecting the electronic and atomic structure, as depicted in Figure 6. In addition, incident radiation can interact with existing defects (precursors) in the material to cause additional defects and changes to the material properties (Berghmans, et al., 2008).

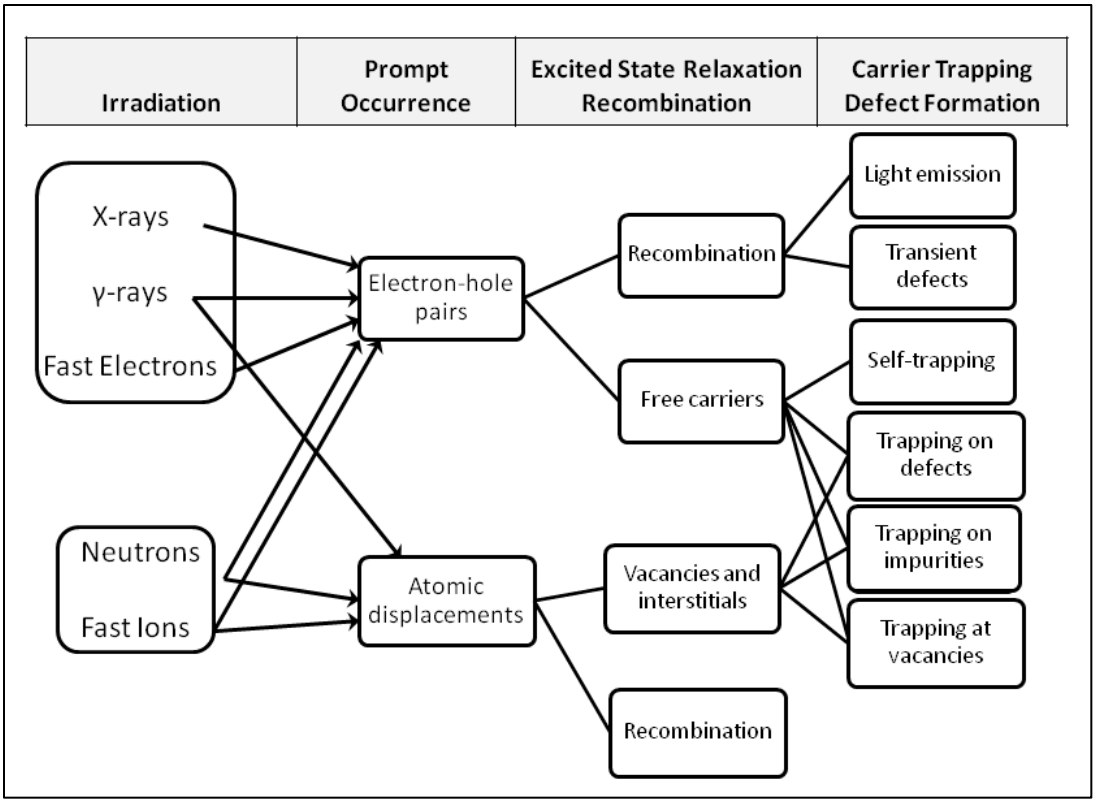

Figure 6. Creation and evolution of radiation-induced defects in silica glass. Figure derived from (Girard S. , 2003).

The main concern for transparent materials are defects caused by irradiation that become absorption (or color) centers. Color centers, depending on their electronic structure and behavior, absorb light at specific wavelengths. The concentration of defects created along with the wavelength of light that is absorbed is dependent upon the intrinsic and extrinsic characteristics of the fiber along with the radiation environment. The measurement of the wavelength-dependent increased absorption as a result of irradiation is called the radiation-induced attenuation (RIA). RIA is measured by comparing the absorption at a wavelength following irradiation to the absorption before irradiation. RIA, as a function of wavelength, time and dose is calculated with (9).

$$RIA(\lambda, t, D) = -\frac{10}{L} \times \log_{10} \frac{P(\lambda, t)}{P(\lambda, t_0)} \ (dB/m) \tag{9}$$

In (9), L is the length of the fiber in meters, $P(\lambda,t)$ is the power output of the test sample at a time t, and $P(\lambda, t_0)$ is the power output of the test sample before irradiation (Girard S. , 2003). For several types of optical fibers across several magnitudes of doses, RIA growth follows a power law with respect to radiation dose as demonstrated in (10).

$$RIA(D) = \alpha D^{\beta} \tag{10}$$

In (10) α and β are fiber dependent parameters. The parameter β is typically 0.7 to 1.0 and the parameter α can vary widely and dominate the RIA growth. At low dose rates of <1 rad/sec, RIA growth in Er-doped fiber has been demonstrated to follow the Power Law behavior from total doses of 10^3 to 10^6 rads (Lezius, et al., 2012). At low dose rates, the growth of the RIA tends to saturate at an upper dose level particular to the fiber, above which, the increase in RIA is sublinear or static.

The power loss due to the creation of color centers can be both permanent and temporary with mechanisms such as optical bleaching potentially affecting the rate of recovery during and after irradiation. Optical bleaching, also called photobleaching occurs when incident photons cause color centers to anneal (Johnston, 2004). The RIA is determined by the competing processes of creation and annealing (plus activation and de-activation) of color centers. Annealing is dependent on the operating temperature of the fibers along with the optical power being transmitted. Higher temperatures and higher optical powers are more conducive to annealing. Optical power losses due to radiation damage is therefore sensitive to both total dose and dose-rate, in addition to factors such as transmission wavelength, injected light power and temperature (Gill, Grabit, Persello, Stefanini, & Vasey, 1997).

In addition to characterizing the degradation to the performance of the fiber via RIA, decades of research through various means has identified and characterized the defects responsible. To

date, there are approximately a dozen identified intrinsic defect types (those constructed of silicon and/or oxygen atoms or ions) and around ten times as many defect varieties involving the presence of intentional and/or unintentional dopants. Many such defects in amorphous SiO_2 have been associated with specific optical absorption and emission bands. Absorption spectrometry can provide direct linkages to the presence and quantity of absorbing species in the silica (Skuja, 2000).

Intrinsic defects can be loosely divided into two categories consisting of those that are associated with oxygen deficiencies and those that are associated with oxygen excesses. Among the former group are a family of SiE' centers – defects based on a hole trapped at an oxygen vacancy and neutral oxygen vacancies known as oxygen-deficiency centers (ODCs). The group of defects resulting from oxygen excess consists of the non-bridging oxygen hole center (NBOHC), peroxyl radical, peroxy bridge and interstitial oxygen molecules (O_2 and O_3) (Griscom D. L., 1985).

The SiE' center is the most studied color center in amorphous silica. It consists of a hole trapped at an oxygen vacancy that is being orbited by an electron. During formation of this defect, the silicon atom may move from the tetrahedral configuration to a planar one. Several studies have attributed an absorption band around 215 nm (5.8 eV) to SiE' defects in irradiated amorphous silica. Figure 7 is a diagram of a generic SiE' center and Table 1 lists several potential methods for SiE' center formation in irradiated silica.

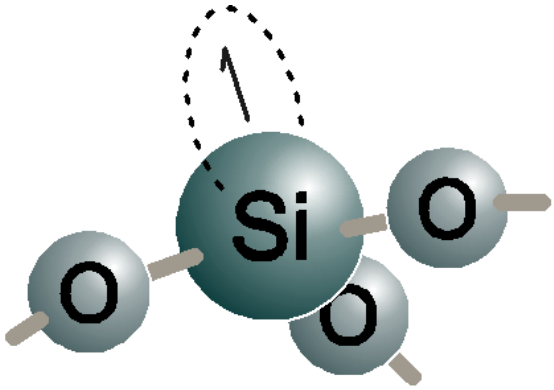

Figure 7. Generic E' center comprised of an unpaired electron of a silicon atom bonded to three oxygen atoms (Salh, 2011). Used under permission granted by Creative Common License 3.0.

The NBOHC consists of an O atom that forms a single bond with a silicon atom and has a hole trapped on a sp^2-type orbital. It is the best-characterized intrinsic defect in silica in regards to optical characteristics (Skuja, 2000). Two absorption bands at 275 nm (4.5 eV) and 620 nm (2.0 eV) have been attributed to this defect. In addition, the NBOHC can be excited to produce a luminescence band at 650 nm (1.9 eV).

A defect of particular interest that has received no attention at all in the study of radiation-induced damage to Yb-doped fibers is related to the formation of oxygen molecules in the fiber. Interstitial oxygen molecules, O_2, can be formed in silica fibers during the manufacturing process or afterwards due to the transformation of incomplete Si-O bonds. First principles research shows that the lowest energy equilibrium position for the O_2 molecules is at the center of the void rings created by the SiO_2 network (Bakos, 2003). The absorption edge for the O_2 molecules begins at 7 eV and the molecule has been identified through characteristic luminescence at 1270 nm that can be preferentially excited by 765 nm (second excited state) and 1064 nm light. The energy of the transition of the molecule to the first excited vibronic state is around 1.2 eV (~1066 nm) which gives rise to the luminescence produced at 1270 nm from 1064

nm light excitation (Skuja, Güttler, Schiel, & Silin, 1998). By measuring the concentration of O_2 molecules in both 'wet' (high OH^- content) and 'dry' (low OH^- content) silica, it was proposed that the formation of O_2 under irradiation is not a result of the destruction of O-H groups. The increase in concentration in both types of fibers was of the same magnitude under the same irradiation conditions, so therefore, the interaction of bridging oxygen atoms was identified as a precursor for O_2 formation. The Smakula relation has been used to calculate the density of O_2 molecules in pristine and irradiated wet and dry silicas. The concentration of O_2 in pristine unirradiated fibers was calculated to be on the order of $10^{18}cm^{-3}$ for 'wet' silicas and undetectable levels (below 10^{14} cm^{-3}) for 'dry' silicas. In most cases, the concentration increased following irradiation. The magnitude of increase was similar for both wet and dry silicas as well as for gamma and neutron dose.

Measuring the absorption and emission of the fibers before and after irradiation provides insight into the concentration of light absorbing and emitting species in the material. During irradiation it is anticipated that the Yb^{3+} atoms may be converted through reduction or ionization to non-active species. Radiation defects may also be induced through the interaction of the other dopants that are used to stabilize the Yb^{3+} ions in the silica matrix. Energy transfer from the silica matrix or from excited Yb^{3+} ions to these defects may significantly decrease the amplification performance of the fiber.

Table 2 details a number of known defects that can evolve in silica and absorb light at energies from 1.17 to 8 eV. Analyzing the wavelength-dependent absorption of the fibers can help to identify defect species that are created by irradiation and contribute to changes in the fiber performance.

Table 1. Conditions and reactions leading to the formation of SiE' centers (S. Girard, 2003)

Formation conditions	**Reactions leading to the formation of SiE' centers**
Formation by evaporation of O_2 upon stretching silica into a fiber.	$Si\text{-}O\text{-}Si \rightarrow Si\cdot Si^{+} + e^{-} + \frac{1}{2}O_2$
Formation from Si-Si precursors in oxygen deficient silica	$h\nu + Si\text{-}Si \rightarrow Si\cdot Si^{+} + e^{-}$
Formation under irradiation as a result of oxygen displacement	$h\nu + Si\text{-}O\text{-}Si \rightarrow Si\cdot Si^{+} + O^{-}$
Impurities present in silica can lead to E' center formation (i.e., chlorine)	$h\nu + Si\text{-}Cl \rightarrow Si\cdot + \cdot Cl^{0}$
The diffusion of radiolytic hydrogen can lead to formation of E' centers	$Si\text{-}Si + H0 \rightarrow Si\cdot + Si\text{-}H$
Under irradiation, a highly stressed normal link can lead to the formation of an E' center and a NBOHC	$h\nu + Si\text{-}O\text{-}Si \rightarrow Si\cdot + \cdot O\text{-}Si$

Table 2. Characteristics of certain radiation-induced defects in silica (Girard & Marcandella, 2010)

Defect	**Optical Absorption Energy (eV)**	**Optical Absorption Wavelength (nm)**
SiE'	5.8	214
Si-NBOHC	4.8	258
	6.8	182
SiODC(I)	7.6	163
SiODC(II)	3.15	394
	5.0	248
	7.0	177
Per-oxyl radical (POR)	5.4	230
	7.7	161
STH	2.61	475
Ozone (O_3)	4.9	253
Interstitial O_2	1.17	1067
	1.62	765

2.7 Radiation effects on RE-doped optical fibers

For a several decades, studies have been conducted on rare earth doped optical fiber amplifiers operating in a radiation environment, with the bulk of the research conducted on Er-doped fiber amplifiers (Lezius, et al., 2012; Ahrens, et al., 1999; Ahrens, Jaques, LuValle, DiGiovanni, & Windeler, 2001; Ott, 2004; Henschel, Köhn, Schmidt, Kirchhof, & Unger, 1998; Mattern, Watkins, Skoog, & Barsis, 1975). These studies have used the RIA of the RE-doped fibers, particularly at the pump and emission wavelengths, as the primary means of characterizing the effect of irradiation on their performance. It has been shown that the RIA for rare earth doped fibers can be an order of magnitude or higher than that of standard optical telecommunication fibers (i.e. SMF-28) (Fox B. P., et al., 2008; Girard, et al., 2009). Understanding the RIA is essential to the developing and fielding of practical fiber lasers and amplifiers in applications requiring predictable performance in long-term operational settings (Girard, et al., 2012).

Deschamps et al. from 2013, unambiguously concluded that in Yb-doped fibers, the primary cause of radiation induced darkening is the aluminum oxygen hole center (Al-OHC) point defect. However, their work was done on gamma irradiated fiber preforms and not pulled fibers. They used a combination of annealing temperature studies and EPR temperature measurements to correlate the decrease in absorption to the concentration of the Al-OHC.

Deschamps et al. also studied the structure of the pristine glass samples using Raman scattering and pulsed-EPR spectroscopy. Raman spectroscopy provided them information on the arrangement of Al and P in the silica network, while the pulsed-EPR provided insight into the local environment of the Yb^{3+} ions. They deduced that when the concentration of Al is less than that of P, Al-P coupling exists. This in turn, demonstrates the proximity of Al and P nuclei in the

vicinity of Yb^{3+}. No Al-P correlation is observed when Al>P. No POHC centers encountered post-irradiation even for samples with very high P concentrations relative to Al. The concentration of induced Al-OHC defects was shown to be linearly dependent on the Al/P ratio and not just the Al concentration. The Al-OHC are created only when P is not introduced in excess to Al. When there is an excess of P, the P not used to bond Yb^{3+} form P-O-P and P=O bonds. In this scenario, the absence of Al-OHC shows that $AlPO_4$ structures inhibit their creation. On the other hand, when Al is in excess, the overage, which is not located in $AlPO_4$ linkages, is ionized by gamma rays creating absorption centers.

There are a host of different trapped-electron centers which could be created along with the Al-OHC during the pair generation process, such as Si-E', Ge-E', Al-E' or P-related electron-trapped paramagnetic defects. In the work of Deschamps et al, they were not able to identify these due to the high magnitude of Ge-related defects in the post-irradiated EPR spectra. Another potential candidate they identified is the Yb^{2+} specie, which can be formed by Yb^{3+} reduction mechanism. This possibility was rated as highly probable considering the proximity between Al and Yb^{3+} revealed in previous works and confirmed in this one.

Several factors have been determined to affect the sensitivity of the rare earth (RE) doped optical fibers. They include the manufacturing process, the rare-earth dopant, and the type of co-doping, operating temperature, operating conditions, type of radiation, dose and dose rate. In regards to manufacturing, fibers in which the rare earth ion is uniformly incorporated into the core exhibit a higher radiation tolerance than those fibers in which the rare earth ions may be clustered together (Lezius, et al., 2012; Gusarov, Van Uffelen, Hotoleanu, Thienpont, & Berghmans, 2009). Although, Er^{3+} has long been the most prevalent rare earth dopant, studies have shown that optical fibers doped or co-doped with Yb^{3+} demonstrate a higher radiation

tolerance than Er-doped fiber amplifiers (Girard, et al., 2009). Even more important than the RE dopant, the presence of other elemental dopants in the fiber core, such as Al, Ge, and P that are used to stabilize the RE ions and adjust the glass refractive index have been shown increase the radiation sensitivity of RDFs (Lezius, et al., 2012).

The majority of these radiation tests have been conducted in the passive mode (sending light through the fiber without creating inversion or amplification) during irradiation. Fox et al. conducted a series of experiments on Yb-doped optical fibers in the Gamma Irradiation Facility (GIF) at Sandia National Laboratory in New Mexico (Fox B. P., Simmons-Potter, Moore, Fisher, & Meister, 2009). The experiments were focused on simulating radiation that the fibers may encounter in space as part of an orbiting satellite and included doses up to 160 krad(Si) at dose rates ranging from 14 to 120 rad(Si)/sec. At the total dose levels indicative of an earth orbit for a few years, 2 to 5 krad(Si), the fibers exhibited very little attenuation of light following irradiation. However, at higher total dose levels, they documented significantly reduced transmission of optical light in the fibers following irradiation with little to no recovery following irradiation, even with subsequent heating to 120° C for 30 minutes.

Lezius et al. performed proton, neutron and gamma irradiation of rare earth doped fibers and compiled results from nine separate studies published on the radiation response of rare earth doped fibers. The results of their study, published in early 2012, suggest that the concentration of the RE dopant does not significantly impact the radiation sensitivity of the fibers. However, the concentration of co-dopants, such as Al, P, and Ge play a major role in radiation sensitivity. These co-dopants are often included to increase the energy transfer to the RE dopants, to stabilize the silica structure and to adjust the refractive index of the fiber core. Their study found that there are some general trends apparent in the response of RE-doped fibers to radiation, such

as an increase in RIA with dose and minimal dose rate effects at lower dose rate levels. However they concluded that predicting the radiation response for a particular fiber is extremely difficult and that the RIA needs to be 'directly derived from irradiation experiments'. In addition, their work cites the need for studies on fibers that are irradiated while being actively pumped as this may drastically alter the radiation sensitivity (Lezius, et al., 2012).

A few recent studies have tested RE doped fibers under active pumping conditions (Rose, Gunn, & Valley, 2001; Bussjager, Hayduk, Johns, & Taylor, 2002; Fox B. P., Simmons-Potter, Moore, Fisher, & Meister, 2009). Rose et al. reported on experiments conducted on Er-doped amplifiers in both active and passive configurations. They used their results to develop a computer code to simulate the effects of long term, low dose rate exposure to the fiber amplifiers. From a comparison between the experiments and the simulations, they concluded that the effects from passive measurements may overestimate the damage to an actively pumped fiber amplifier under certain conditions and speculated that the active pumping may assist in annealing (Rose, Gunn, & Valley, 2001). In a 2002 study, two Er-doped fiber lasers were irradiated above 1 Mrad(Si) with a Co-60 source, with one system actively pumped and the other operated in a passive mode. The laser system that was actively pumped during irradiation experienced decreased laser pulse width and output power for increasing dose. Before the end of irradiation, the system suffered catastrophic failure and did not recover post-irradiation. The passively operated fiber laser failed to perform immediately following irradiation, but experienced recovery to a degraded level a few days following irradiation (Bussjager, Hayduk, Johns, & Taylor, 2002). An experiment reported in 2009 by Fox et al. using actively pumped Yb-doped fiber amplifiers irradiated at the Gamma Irradiation Facility (GIF) at Sandia National Labs in New Mexico measured a significant decrease in amplifier output versus diode pump current

during and following irradiation. However the magnitude of the decrease of transmittance at the signal wavelength was similar to that observed during passive operation. They concluded that the degradation at the signal wavelength is not significantly affected by the fiber amplifier being operated in active mode, but is mainly affected by color centers created at the pump wavelength (Fox B. P., Simmons-Potter, Moore, Fisher, & Meister, 2009).

Girard et al. tested Er, Yb and Er/Yb-doped fibers in several published works that demonstrated that Yb and Er/Yb-codoped fibers have a higher resistance to radiation induced attenuation than Er-doped fibers (Girard, et al., 2009; Girard, et al., 2007). They also studied the effects of co-doping with cerium (Ce) and hydrogen preloading of the fibers before exposure to radiation. The result for both techniques was an increase in radiation tolerance. They also tested the fibers in a passive mode and in an actively pumped mode using a laser diode. Their evaluation of the effect of pump power on the radiation induced attenuation demonstrated that the induced losses at the signal wavelength remained constant for different pump powers at a particular total radiation dose (Girard, et al., 2012).

Dose rate effects were studied by Ahrens et al. in Yb- and Er-doped fiber amplifiers. The tests were conducted using a Co-60 source with several dose rates from 5.5×10^{-3} to 4 rad(Si)/sec. They found that higher dose rates of gamma radiation lead to higher RIA at the same total dose levels. They speculated that the increase in RIA at higher dose rates is due to the differences in the rate of defect production coupled with simultaneous thermal annealing. By measuring the recovery in transmission as a function of temperature at both 110° C and 160° C, they concluded that lower activation energy defects are annealed during the lower dose irradiations, thus providing a lower overall RIA (Ahrens, et al., 1999). Lezius et al. found that at ‘high’ gamma dose rates of approximately 21 rad(Si)/sec and above, the RIA increased with a relationship to

the fourth power of the total dose during the first 10 minutes as opposed to the exponential growth that is widely experienced at lower dose rates (Lezius, et al., 2012). Alam et al. irradiated pumped Yb/Er co-doped amplifiers at two dose rates (10 and 20 rad(Si)/sec). Their results demonstrated an increase in the degradation of the system at the higher dose rate.

When the type of radiation is considered, the consensus is that at low dose rates, the RIA at an equivalent radiation dose is comparable from irradiation by gammas, x-rays, and protons. Rose et al. evaluated the effect of gammas and protons up to total doses of 50 krad(Si) on RE doped fibers (Rose, Gunn, & Valley, 2001). Girard et al. compared the effect from gamma, proton, and X-ray irradiation up to total doses of 50 krad(Si) (Girard, et al., 2009). Lezius et al. irradiated Er- and Yb-doped fibers with 20 MeV and 180 MeV neutrons, yet observed only minor RIA after exposure to fluxes of approximately 3×10^4 neutrons/cm^{2}sec for several hours (Lezius, et al., 2012). No studies encountered thus far have looked at the performance of YDFAs in a mixed neutron/gamma environment. This may be due to the expectation in the silica fiber research community that, in un-doped silica fibers, the total ionizing dose from the most common types of irradiation provides equivalent levels of damage. The foremost reference on this behavior is from Mattern et al, in which it is demonstrated that at low dose rates, the effects from gamma, beta, and 14 MeV neutron irradiation on un-doped silica fibers are the same for equivalent total ionizing dose levels up to 60 krad(Si) (Mattern, Watkins, Skoog, & Barsis, 1975).

Table 3 summarizes the published radiation experiments conducted on Yb- and Yb/Er-doped fibers. Only three of the published experiments (highlighted in yellow) involve actively pumping the fiber during irradiation. The dose rates used in these experiments range from mrads(Si)/sec to tens of krad(Si)/sec, with irradiations being carried out over several minutes to hours. From this

series of tests, there is evidence that the damage to the fibers may not be linear with radiation dose rate. The effect of actively pumping the fiber amplifiers during irradiation has not been conclusively demonstrated. Another important area of research that has yet to be covered is the effect of high dose rate continuous and pulsed radiation that is indicative of nuclear weapon environments on rare earth doped fiber amplifiers. Because of the extreme variability of the response of fibers to radiation, there is a need to evaluate fiber and fiber-based systems that are proposed for use in military nuclear systems in anticipated threat environments.

Table 3. Summary of radiation tests published on Yb- and/or Yb/Er-doped fibers. The highlighted experiments involved actively pumping the fiber during irradiation.

Reference	RE Dopants	Radiation Type	Dose Rate rad(Si)/sec	Total Dose krad(Si)
(Henschel, Köhn, Schmidt, Kirchhof, & Unger, 1998)	Yb	Gamma	3	15
(Ahrens, et al., 1999)	Yb/Er	Gamma	$5.6\text{-}4\times10^{-3}$	100
(Taylor & Liu, 2005)	Yb	Gamma	2.1	97.1
			3	14
(Alam, Abramczyk, Madasamy, Torruellas, & Sanchez, 2007)	Yb/Er	Gamma	10 & 20	41
(Fox B. P., et al., 2007)	Yb	Gamma	14.31 to 120	2 - 160
(Girard, et al., 2009)	Yb Yb/Er	X-rays (10 keV)	10^2 to 10^4	0.1 - 10^5
		Gamma	0.3	20
		Protons (105 MeV)	10	50
(Fox B. P., Simmons-Potter, Moore, Fisher, & Meister, 2009)	Yb	Gamma	7	7.6
(Fox B. P., Simmons-Potter, Thomes Jr., & Kliner, 2010)	Yb	Gamma	14.31 to 120	200
(Mady, Benabdesselam, Mebrouk, & Dussardier, 2010)	Yb	X-rays (45 keV)	4.2	50
		UV (deuterium lamp)		
(Girard, et al., 2012)	Yb/Er	Gamma	0.3	50
(Lezius, et al., 2012)	Yb	Gamma	1 to 48	~106
		Protons (20 & 180 MeV)	1.2×10^4 & 710	~10^4
		Neutron	5×10^5 n/cm^2 sec	~10^9 n/cm^2
(Deschamps, Vezin, Gonnet, & Ollier, 2013)	Yb	Gamma		
(Fox B. P., Simmons-Potter, Kliner, & Moore, 2013)	Yb	Cosmic	Flew on space station for 18 months	~2.4 to 12.6

2.8 Damage Recovery

In regards to RE-doped fibers, generally the recovery is wavelength dependent and not linear with respect to time. This indicates that there are higher-order recovery kinetics going on within the fiber (Lezius, et al., 2012). Photodarkening studies use the measurement of light

transmission in the 550 to 633 nm range as an analog for the degradation and recovery of the signal transmission at the 1060 nm range (Koponen, 2008). Thermal studies have shown that recovery rates can be increased by annealing the fibers under temperatures above 350°C (Mady, Benabdesselam, Mebrouk, & Dussardier, 2010).

With respect to irradiation time, it is generally theorized that the recovery rate decreases with increasing irradiation time (Henschel & Köhn, 1993). The damage that occurs during shorter irradiation times is primarily due to population of the defect precursor sites, which are typically unstable at room temperature. Higher order, more stable defects do not have time to form in significant concentrations and therefore, following irradiation, damage from these shorter irradiations anneals more rapidly than that experienced at longer irradiation times. In regards to dose rate, the same mechanisms lead to a similar effect for fibers irradiated up to the same total dose. The higher the dose rate, the faster the recovery, because at the faster dose rate, the irradiation time to a set dose level occurs more over a shorter time period (Henschel, Köhn, Schmidt, Kirchhof, & Unger, 1998).

A recent test of undoped silica fibers designed to transmit signals to and from YDFAs or YDF based lasers was conducted at the ACRR. Following pulse irradiation, the recovery of the un-doped silica fibers occurred over a matter of seconds. There was no permanent damage detected to the transmission of 1064 nm laser light through the fibers following irradiation. Fibers that were irradiated with subsequent pulses experienced full recovery between irradiations. However, there was an increase in the transient transmission loss with subsequent radiation exposures. This was attributed to the neutrons inducing permanent damage of a type and concentration that did not affect the light transmission during normal operation. However,

these neutron-induced damage sites, during irradiation, served as formation sites for temporary defects (Cheeseman, Bowden, Akinci, Knowles, & Webb, 2012).

2.9 Summary

Although the amount of research conducted on Yb-doped fibers has increased in recent years, there is still a need for examining the sensitivity of RE doped fibers when exposed to mixed neutron/gamma environments along with the effect of operational configuration during radiation exposure. In addition, all works that have postulated the defects responsible for the RIA in Yb-doped fibers has focused on absorption centers that peak below 800 nm. It is assumed that these broad absorption centers have tails that reach into the IR region thus explaining the increased attenuation at the signal wavelengths (above 1000 nm). However, there is reason to believe that there could be defects more directly responsible for the increased attenuation at the signal wavelength.

3 Methodology

3.1 Chapter overview

Primarily, this work is the only documented, to date, examination of actively pumped Yb-doped fibers in a mixed neutron and gamma radiation environment. In addition, the results cover steady-state exposure and high-dose rate, short-pulse radiation. The experiments and analysis were designed to produce the following results:

1. Dose rate does not significantly affect the degradation to the Yb-doped fibers. However, the recovery rate is inversely dependent on dose rate.
2. Absorption from Al-based defects produced in the UV increases degradation of SM YDFA gain through Yb^{3+} de-activation.
3. The results from the continuous steady state experiments can be used to extrapolate the damage from high dose rate, short-pulse radiation exposures.
4. Actively pumping the Yb-doped fibers during exposure does not affect the radiation sensitivity. However, the results gathered from unpumped fiber tests may not be sufficient to predict the degradation of the amplifier performance if only the loss at the signal wavelength is considered.

Three different radiation sources were employed in this research. Gamma only irradiation was carried out at the Co-60 irradiator cell at The Ohio State University (OSU). YDFs were exposed to mixed gamma/neutron radiation environments at the OSU Nuclear Reactor Lab (OSU-NRL) and the Sandia National Laboratory Annular Core Research Reactor (ACRR). Continuous gamma/neutron experiments were accomplished at the OSU-NRL, and pulsed gamma/neutron exposure experiments were accomplished at the ACRR. The bulk of the experiments were conducted with SM YDFs. Multi-mode YDFs were used in the OSU Co-60

irradiation cell and research reactor. The MM YDFs were not actively operated as amplifiers during irradiation experiments. A white light source was used to measure transmission through the MM fibers during irradiation. The SM YDFs were operated in an amplifier configuration and also kept dark during some irradiations.

3.2 Characterization of experimental materials and equipment

Previous work has been conducted on rare-earth doped pulled crystal fibers, namely Ce- doped Y-Al-garnet (YAG:Ce). The pulled YAG:Ce crystal fibers were exposed to 1 MeV electron irradiation and changes in their absorption and emission characteristics measured. The results were presented at the 2011 IEEE Nuclear Science Symposium (Singleton, et al., 2011). The work provided a foundation for experimentation with optically active materials.

All equipment used throughout this research was commercially available standard optical components, see Table 4. All equipment was fully characterized before irradiation began and subsequently checked for performance prior to each use in an actual experiment.

Table 4. Equipment list for experiments conducted in this study

Item	**Specification**
Yb-doped fiber	YB1200 6/125DC manufactured by nLight
Passive double-clad (DC) fiber	6/125 DC manufactured by nLight
Passive single mode (SM) fiber	SM980-5.8-125 970-1650 nm 125 micron cladding
980/1060 nm WDM	WD202E - FC/APC connectors
980 nm pump lasers	PLD-33-A-974
Benchtop laser diode/TEC controller	ITC4020 - 20 A / 225 W
Fiber optic isolator (high power capability)	1064 nm isolator
Pump combiners	(6+1)×1 High Power
White light source (tungsten-halogen)	Fiber coupled
Splitters	95/5 ratio

The attenuation of the doped fiber before irradiation was evaluated by measuring the transmission of the light source through a fiber that has a known and very low attenuation at the wavelengths being considered. The output, P_A from this fiber is then coupled to the doped fiber and used as the input power for the doped fiber. The wavelength-dependent output power from the doped fiber is then measured, P_B. The attenuation (dB/m) can be calculated from the following (11) in which L_B is the length of the doped fiber.

$$A(\lambda) = \frac{10}{L_B} \times \log \frac{P_B(\lambda)}{P_A(\lambda)} \tag{11}$$

3.3 Fiber preparation

SM YDFs were fusion spliced to passive fiber patch cables with FC/APC ferrules on the ends to facilitate coupling the light into and out of the SM YDFs during irradiation. The transmission loses from the splicing was very low in all cases. The process of splicing did preclude the use of an exact length of doped fiber for all prepared SM YDF samples. The lengths of doped fiber used varied from 22 to 33 cm.

MM YDFs were stripped and cleaved at each end and universal temporary connectors were attached at each end. These universal connectors were configured with SMA ferrules for ease of connection to the white light source and the CCD spectrometer. Both devices were designed for SMA connection. The cleaving process again prevented the use of exact lengths of the MM YDF for each sample. However, there was less variability in the lengths used. The fiber lengths varied from 25.4 to 30.5 cm.

3.4 SM YDFA operation

Signal and laser light, at 1064 nm and 975 nm respectively, were coupled into the SM YDF using a wavelength division multiplexer (WDM) designed for these specific wavelengths. The pump laser used was a fiber-coupled diode laser with a maximum power output of 500 mW.

The signal laser was a fiber-coupled GaAs substrate based quantum well high power laser with a maximum output of 200 mW.

The loss through the WDM for both laser sources was measured at 2 dB for the pump laser light and 4 dB for the signal laser light. This loss has been incorporated into the analysis. The WDM output was transferred through a passive fiber to the YDF under test. The output from the YDF was fed through a 50/50 splitter (loss < 1 dB) to a power meter (PWM) and then an optical signal analyzer (OSA). The performance of the fibers as signal amplifiers was evaluated and characterized. The fiber amplifier set up is shown in Figure 8. The YDFAs were evaluated in the same configuration before, during and after irradiation.

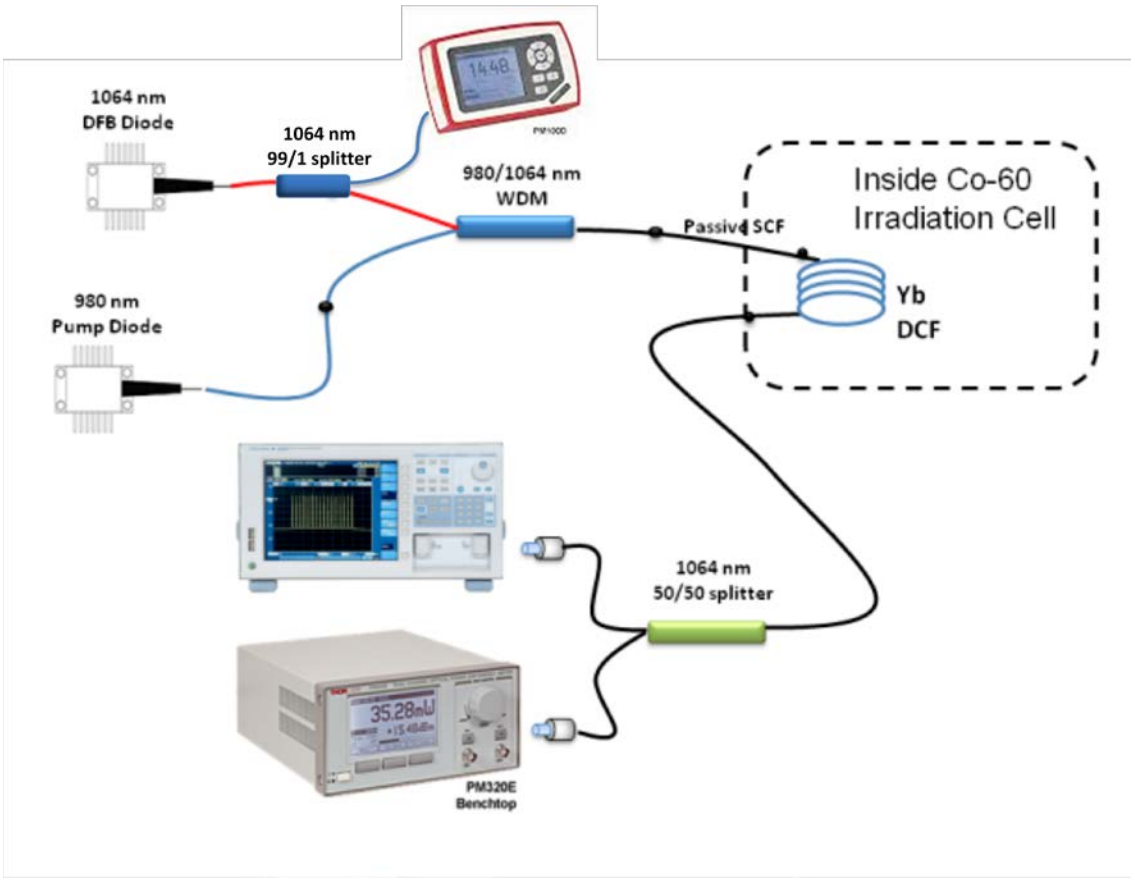

Figure 8. Nominal set up for YDFA operation experiments.

Amplified spontaneous emission (ASE) is generated in a fiber as long as population inversion exists, even without an input signal. Therefore, the ASE spectrum is easily measured by pumping the fiber without propagating a signal. The spectral output of the Yb-doped fiber consists of the transmitted (unabsorbed) pump light and the propagated ASE photons. A 1 m length of single-mode double-clad Yb-doped fiber was spliced to a length of standard optical cable (SMF-28) and pumped with a 980 nm diode laser. The output spectrum is plotted in Figure 9 and clearly shows the partial transmission of the 980 nm signal along with the ASE spectrum at higher wavelengths (peaking around 1080 nm in this case). The peak wavelength of the ASE spectrum shifts to lower wavelengths as the input power (and subsequently inversion) increases. This is due to the higher gain values of the fiber at the lower wavelengths (see Figure 4). The Yb^{3+} ions have a higher absorption coefficient for spontaneously emitted photons in the shorter wavelengths. Higher density of excited Yb^{3+} ions will lead to preferential amplification of the spontaneously created photons at lower wavelengths. The ASE is an important feature to understand because it puts an upper limit on the gain that is possible in a single pass through a fiber amplifier (Bjarklev, 1993).

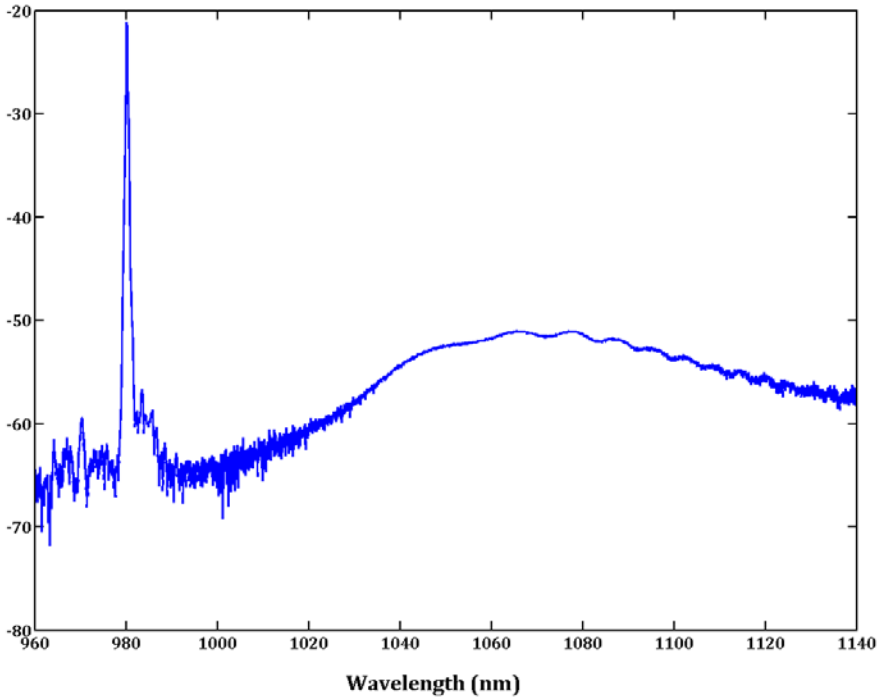

Figure 9. Spectral output of Yb-doped fiber pumped with fiber-coupled laser diode at 980 nm.

Gain, power input, and the amplifier output profile were characterized by setting the signal power at a low value and then the pump power was varied. The signal power was then increased and the pump power varied and the process repeated until the operating range of the amplifier is defined. The pump power for which the output signal power is equal to the input signal power denotes the threshold pump power. The region of pump and signal powers for which the gain of the fiber remains relatively constant, i.e. gain is saturated, is important to determine as well, because this is the region in which the system is operated during the irradiation tests.

3.5 Amplified output power

The amplified output power measured at the signal transmission wavelength, 1064 nm, was measured before, during and following irradiation. The performance of the YDFA can be measured by the overall gain in signal power with relation to the input signal power. This gain is

reported in dB/m for the purposes of this work and comparison to the work of others. Changes to amplified signal gain are used to define the degradation to the YDFA during and following the irradiation experiments. Amplifier performance can also be characterized by the change in the ASE intensity. The ASE intensity will become an important factor when considering YDFA performance in a radiation environment using data collected from passive YDF irradiation tests.

3.6 Multi-mode YDF operation

A broad band white light source was coupled to the MM YDFs before, during and following irradiation, as shown in Figure 10. The white light source was power and temperature stabilized with output spectrum from 300 to 2600 nm, peaked at 1000 nm. The transmission spectrum of the fiber was measured using a CCD spectrometer controlled by a laptop. The spectrometer recorded the light transmission from 500 to 1100 nm. Prior to radiation exposure experiments, the output of the light source was characterized over a 10 hour period and showed very little change in intensity.

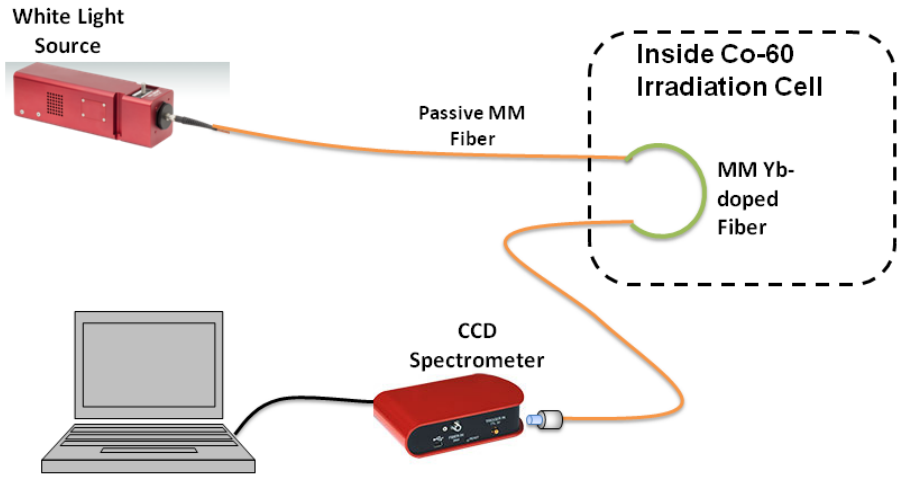

Figure 10. MM YDF set up including white light source and CCD spectrometer.

3.7 Absorption data presentation

The change in absorption of transmitted light in a fiber can be calculated from the change in the wavelength dependent intensity of transmission of a stable light source through the fiber. The data can be presented as either the decrease of light transmission or inversely as the increase in absorption. For purposes of this work, the change in the light absorption is reported as the radiation-induced absorption, RIA. The change is calculated relative to the absorption of the pristine fiber prior to radiation exposure.

3.8 Irradiation experiments

3.8.1 Gamma irradiation

The goal of the first set of experiments was to conduct a series of tests that could be used to analyze the response of the single-mode YDFs to gamma irradiation. These tests at relatively low dose rates provided confidence that exposing the fibers to high dose rate irradiation would not result in immediate darkening of the fibers; but that the fibers would degrade at a rate that will allow adequate measurements to be conducted. In addition, tests were configured to potentially provide additional information on whether or not the radiation induced loss is dependent on dose rate and whether or not pumped fibers have a different loss profile than fibers that are unpumped during irradiation. A total of twenty-two tests are included in the analysis that follows in Chapter 4.

The experiments included irradiation of a SM passive fiber in order to determine the extent of damage from the passive fiber that may have been influencing the results from the SM YDFA tests. Portions of the set of SM YDFAs were operated as an amplifier only during measurement periods taken at 10 minute intervals. The other SM YDFAs were continuously operated as an amplifier during irradiation. The passive fiber was kept dark during irradiation.

3.8.2 ACRR tests

The experiment set up for the ACRR tests of the SM YDFAs is detailed in Figure 8. The passive cables used for the ACRR experiments were both 20 meters in length. Short lengths of single mode passive fiber patch cables were spliced onto the ends of each single mode YDF sample. The samples were affixed to an experimental rig designed to fit in the center of the ACRR (Figure 11). Other devices under test and dosimeters were attached to the rig as well. The pump and signal laser were combined using a WDM and input into the fiber and the output was split between the power meter and the optical spectrum analyzer (OSA). Following the pulse, the amplifier was continuously operated for at least 24 minutes while it remained in the reactor core.

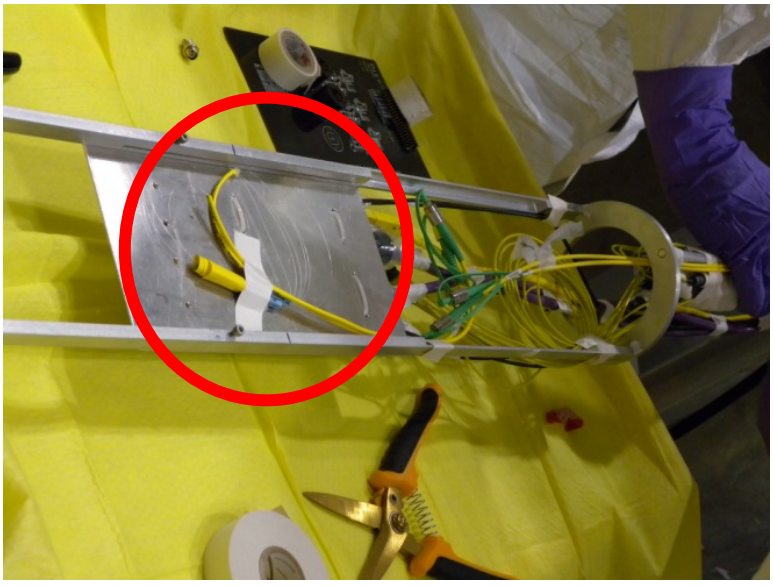

Figure 11. Fibers affixed to experiment rig at ACRR. The red circle highlights the location of the SM YDF fiber under test.

3.8.3 OSU-NRL experiments

The OSU-NRL tests were designed to expose the YDFs to a total neutron flux equivalent to the neutron flux that the single mode fibers were exposed to in the first series of ACRR tests. For these tests, MM and SM YDFs were fielded. The MM YDFs fibers were connected to a white light source during irradiation. The SM YDFs fibers were operated as signal amplifiers during irradiation. Recovery data of the fibers was recorded for approximately 40 minutes to several days following irradiation.

All of the fibers irradiated during the reactor tests were placed at the same location in a dry experiment tube that was situated adjacent to the reactor core. The reactor was operated at the same power level output for each irradiation (450 kW). The fibers were placed inside a cadmium box and lowered into position prior to the reactor start up. The Cd box selectively attenuates thermal neutrons below 0.5 MeV due to its high thermal neutron cross section, so that the spectrum is hardened, and radiation activation is reduced.

3.9 Recovery measurements

It has been shown that damage to the fibers may anneal, albeit quite slowly, at room temperature (Girard, et al., 2009). The recovery of the transmission of light through the fibers can be used to gauge the energy levels of the light absorbing color centers and therefore was closely monitored following irradiation. Due to the nature of the fiber samples, it was not feasible to measure and properly compare the fiber recovery in all cases. There were several instances in which the fiber was broken upon removal from the irradiation chamber. In addition, for the Co-60 tests, the only way to stop irradiating the fibers was to move them, via the hydraulic lift, from the irradiation cell. Once this was done and the fibers were shifted during their removal, the transmission values often changed due to the rearrangement of the fibers or adjustment of the fiber connectors. The best recovery data was collected from the ACRR and

OSU-NRL tests. In both scenarios, the fibers were able to remain in place for several minutes to several hours after the irradiation period. In the case of the OSU-NRL, the dry tube holding the fiber sample was moved several meters away from the reactor core immediately following irradiation.

3.10 System-level effects of radiation exposure on YDFA performance

Damage resulting in absorption of the pump light by radiation-induced defects in the fiber, the primary effect is the reduction of the excitation population of Yb^{3+} ions (see section 2.6). This will lead to a lower amplified signal output along with a lower ASE intensity (ASE will also shift to higher wavelengths), as illustrated in Figure 12.

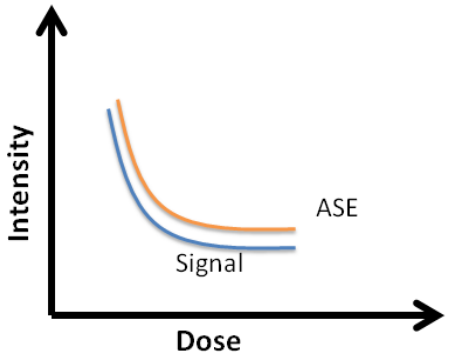

Figure 12. Anticipated changes in output power for signal and ASE wavelengths in an irradiated YDFA if pump absorption dominates.

A second mechanism due to deactivation of Yb^{3+} ions has the primary effect of reducing the number amplified signal photons. The color centers will compete with the signal photons as sources of Yb^{3+} relaxation from the excited state. The amplified signal will reduce significantly, however it logically follows that the ASE will not be affected as strongly. The increase of radiation-induced defects that can receive de-excitation energy from the Yb^{3+} ions will also lead to a decrease in the upper state lifetime.

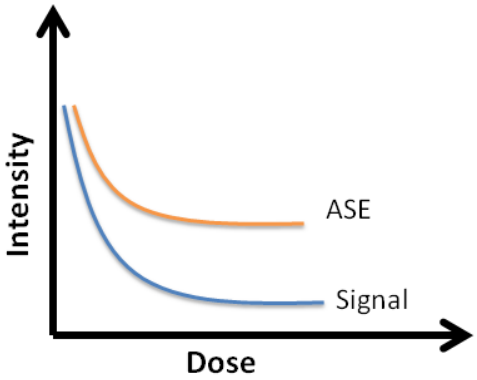

Figure 13. Anticipated changes in output power for signal and ASE wavelengths in an irradiated YDFA if deactivation of Yb^{3+} via non-radiative energy transfer dominates.

A third damage mechanism arises from the absorption of the signal light in the fiber. This causes the ASE to be reduced from absorption in the fiber as well. However, the reduction will be lessened and possibly overcome by the excited Yb^{3+} resulting in a lower intensity of signal photons. If the excited Yb^{3+} population is not strongly affected, this will enable more Yb^{3+} ions to relax via spontaneous emission and make more of the spontaneously emitted photons available for amplification.

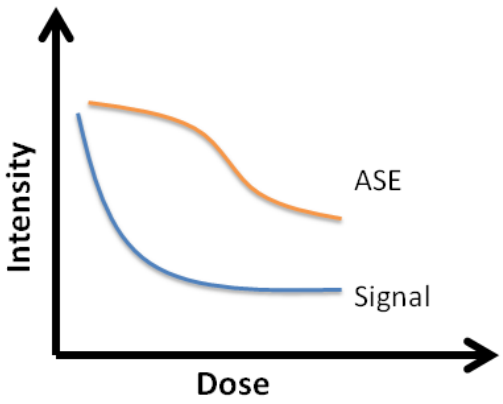

Figure 14. Expected change in output power for signal and ASE wavelengths in an irradiated YDFA if signal absorption dominates.

3.11 Numerical analysis

A model representing the performance of the SM YDFA was developed to analyze the measurements. The results of the model were used to provide bounds for the experiment parameters. Following irradiation, the change in the absorption spectrum was used to adjust the absorption coefficient calculations in the model. The model was also used to evaluate various parameters related to the absorption centers that contribute most to the additional absorption measured in the fibers during and after irradiation.

The previously defined equations (4) through (6) that model the rate of change in the excited state population, pump and signal powers can be modified to take into account the amplified spontaneous emission (ASE) as in equations (12 through (15) (Liu, 2011).

$$\begin{aligned}\frac{dN_2}{dt} = \frac{D}{hcA}\sum_{j=1}^{J}\lambda_j^p\left[\sigma_a(\lambda_j^p)N_1 - \sigma_e(\lambda_j^p)N_2\right]\times P_p(\lambda_j^p) \\ + \frac{\Gamma}{hcA}\sum_{k=1}^{K}\lambda_k^s[\sigma_a(\lambda_k^s)N_1 - \sigma_e(\lambda_k^s)N_2]\times P_s^{\pm}(\lambda_k^s) \\ + \frac{\Gamma}{hcA}\sum_{m=1}^{M}\lambda_m^{ASE}[\sigma_a(\lambda_m^{ASE})N_1 - \sigma_e(\lambda_m^{ASE})N_2] \\ \times [P_{ASE}^{+}(\lambda_m^{ASE}) + P_{ASE}^{-}(\lambda_m^{ASE})] - \frac{N_2}{\tau}\end{aligned} \tag{12}$$

$$\frac{dP_p(\lambda_j^p)}{dz} = D\times\left[\sigma_e(\lambda_j^p)N_2 - \sigma_a(\lambda_j^p)N_1\right]\times P_p(\lambda_j^p) - \alpha P_p(\lambda_j^p) \tag{13}$$

$$\frac{dP_s^{\pm}(\lambda_k^s)}{dz} = \Gamma\times[\sigma_e(\lambda_k^s)N_2 - \sigma_a(\lambda_k^s)N_1]\times P_s^{\pm}(\lambda_s^k) - \alpha P_s^{\pm}(\lambda_k^s) \tag{14}$$

$$\begin{aligned}\frac{dP_{ASE}^{\pm}(\lambda_m^{ASE})}{dz} = \Gamma\times[\sigma_e(\lambda_m^{ASE})N_2 - \sigma_a(\lambda_m^{ASE})N_1]\times P_{ASE}^{\pm}(\lambda_m^{ASE}) \\ - \alpha P_{ASE}^{\pm}(\lambda_m^{ASE}) + \Gamma\times\sigma_e(\lambda_m^{ASE})\times N_2\times\frac{2hc^2\Delta\lambda}{[\lambda_m^{ASE}]^3}\end{aligned} \tag{15}$$

In (12) through (15), $P_{ASE}^{\pm}(\lambda_m^{ASE})$ represents the forward and backward ASE power of the m^{th} ASE channel. The width between two channels is denoted by Δλ. Equation (12) modifies (4) by adding in the changes to the excited state population density due to the stimulation absorption and emission of ASE light. Equation (15) calculates the evolution of the ASE power along the fiber in both directions (Budz, Waisman, Tiedje, & Haugen, 2009).

The finite difference method can be used to solve these equations numerically under a steady state condition. To do so, a fiber of length, *L*, is divided into *n* segments along its length with the left end of the fiber defined as *z=0* and at the right end *z=L*. P[n] describes the power, including the pump, signal and ASE power in the n^{th} segment. $N_1[n]$ and $N_2[n]$ denote the population densities of the ground and excited states in the n^{th} segment, Figure 15.

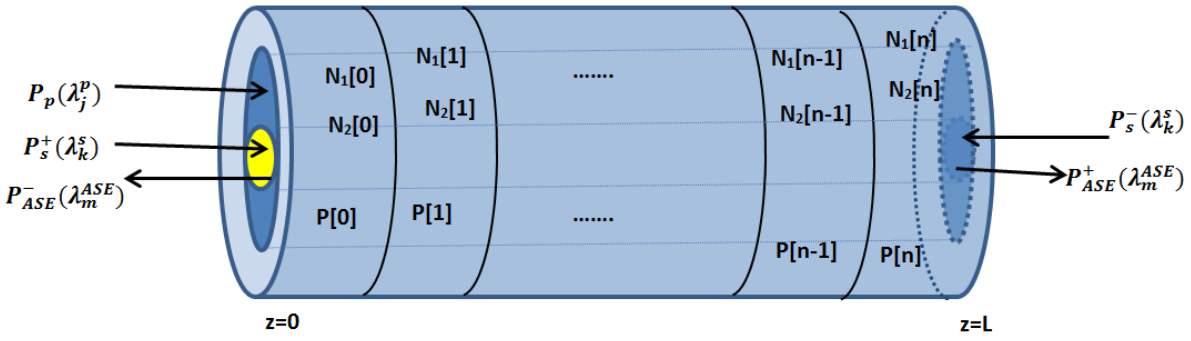

Figure 15. Schematic for the numerical simulation of the Yb-doped fiber amplifier (Liu, 2011). (See text for details.)

If the pump beam and signal beam are coupled into the fiber from the left end, the initial boundary conditions used to solve the equations are the powers of the incident pump and signal energies at *z=0*. Either the pump or the signal can be coupled into the fiber from the right end. The initial boundary conditions will then change to either the power of the injected pump or

signal energies at $z=L$. The forward and backward ASE powers start at zero and increase towards each end of the fiber.

A set of routines implementing this model were obtained from the open source MATLAB file exchange (Rumbaugh, 2013). The codes were validated using the gain characterization data from the SM YDFAs. Adjustments were made to the calculation of the absorption coefficients portion of the code in order to model the effects from the radiation induced absorption. The model was also used to evaluate the absorption centers that contribute most to the additional absorption measured in the fibers during and after irradiation.

The numerical analysis permits a large set of permutations to be tested that is not feasible to complete experimentally due to time and resource constraints. The absorption coefficients were adjusted to examine the effect of RIA at the signal wavelength (1064 nm) on the YDFA performance. The absorption coefficients were increased at 564 nm, 1064 nm, and a combination of both wavelengths.

The performance of the pristine YDFA was calculated and the results are depicted in Figure 16. As the pump power is absorbed within the YDF, the gain of the output signal increases steadily. Once the pump power absorption increases to nearly 100%, the gain of the signal power saturates. At this point, the excitation ratio of Yb^{3+} ions rapidly decreases due to the absence of any pump power and the transmitted signal encounters fewer excited ions to interact with and produce additional stimulated emission.

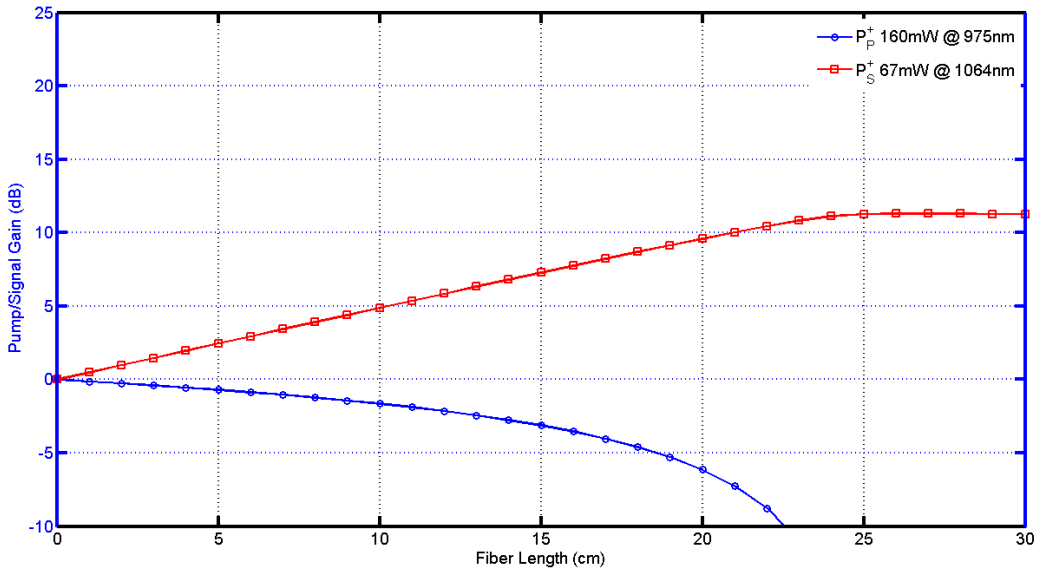

Figure 16. YDFA single pass gain calculated with 160 mW pump and 5 mW signal input. Gain for the signal is calculated to saturate at approximately 25 cm where the pump power is regulated by near complete absorption.

The presiding theory is that the gain degradation experienced at the signal wavelength of the YDFA following irradiation is a direct result of the increase in Al-based defects and their corresponding absorption features. In order to simulate this, the cross-section calculation of the code was updated with the absorption curve of the Al-OHC centered at 564 nm, as shown in Figure 17. The features of the curve were derived from results on Al-OHC absorption in YDF found in the work published by Deschamps et al. (Deschamps, Vezin, Gonnet, & Ollier, 2013).

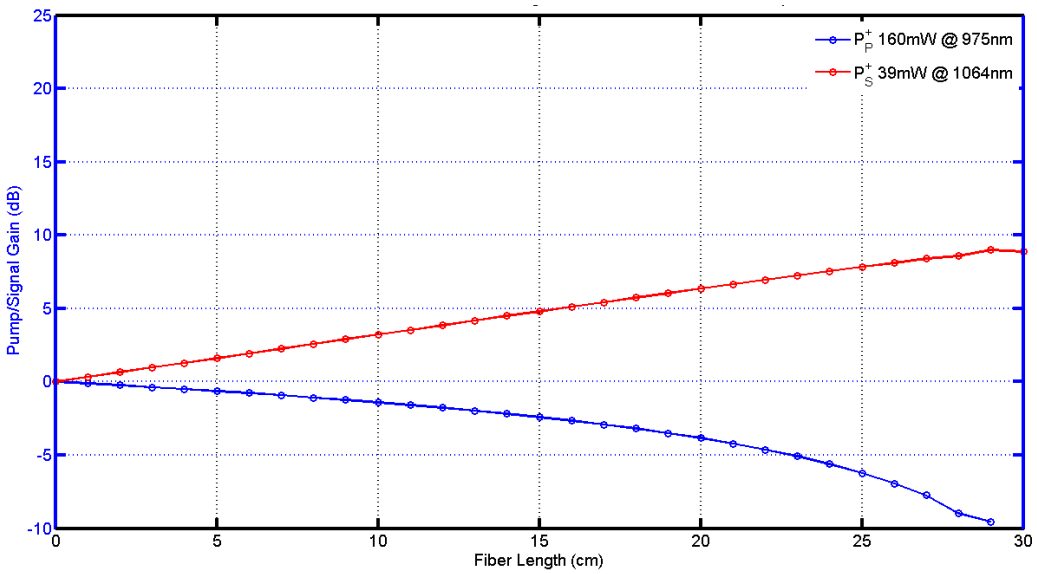

Figure 17. Calculated YDFA performance with absorption at 564 nm included in the cross section calculation.

The absorption of the pump light through the fiber actually decreases along the length of the fiber. The gain of the signal fiber is subsequently decreased significantly. The process is a reciprocal one in which the increased absorption of the signal photons leads to a higher number of excited Yb^{3+} ions having to de-excite through other mechanisms, which have lifetimes significantly longer than the stimulated emission process. This decreases the population of Yb^{3+} ions that are available to be excited as the pump light transmits through the fiber. The pump light photons encounter more Yb^{3+} ions that are already excited. YDFs are known for their lack of excited state excitation, therefore more of the pump light continues uninterrupted.

Examining the effect of an increase in the absorption at the 1064 nm wavelength only, shown in Figure 18, the signal gain profile is similar to that in Figure 17. The features of the Gaussian used to simulate the potential absorption at 1064 nm were formulated using details of the absorption of O_2 molecules published in a two papers (Jockusch, et al., 2007) (Skuja, Güttler, Schiel, & Silin, 1998). The increased absorption at the signal wavelength leads to a decrease in absorption of the pump light in the fiber with a subsequent decrease in the gain of the signal

power through the fiber. The difference in the performance of the YDFA between the two radiation-induced absorption scenarios shows up in the amount of ASE power transmitted.

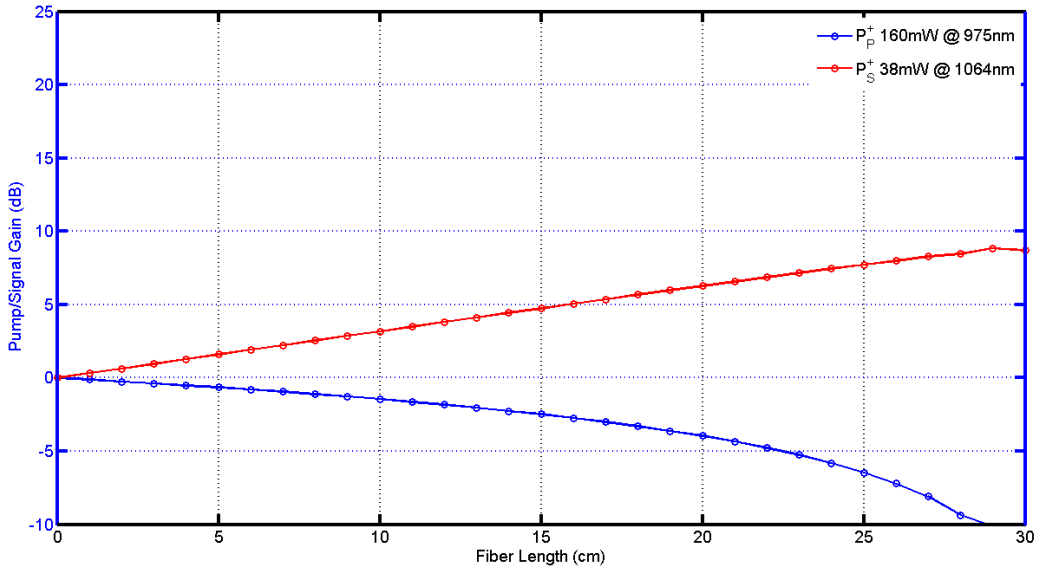

Figure 18. Calculated YDFA performance with absorption at 1064 nm added to the absorption coefficient calculation.

Figure 19 depicts the calculated forward ASE power through the YDFA for the pristine YDF, the YDF with added absorption at 564 nm and the YDF with added absorption at 1064 nm. For the absorption centered at 564 nm, the ASE goes through a slight decrease as it propagates through the fiber. For the scenario in which only 1064 nm absorption is considered, the ASE experiences an increase in output power.

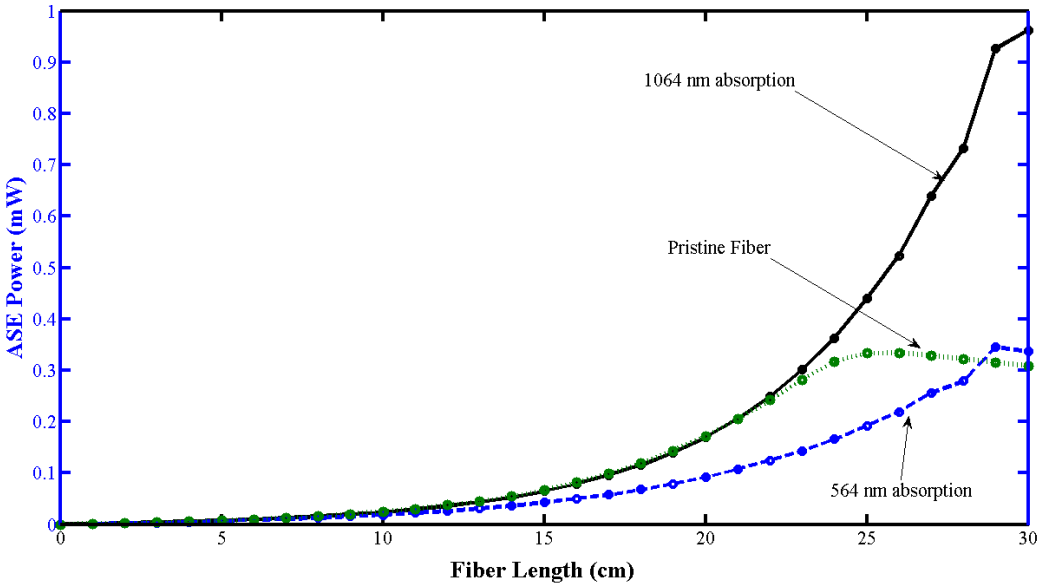

Figure 19. Forward ASE propagation power through YDFA. When 1064 nm absorption is considered, the ASE experiences an increase in power. When the 564 nm absorption is considered, the ASE power is slightly decreased through the fiber and remains relatively at the same level at the output.

Results from the gamma irradiations of the YDFAs presented in the following chapter indicate that both scenarios describe the ASE output power during irradiation. In the short time following the start of the radiation exposure, the ASE power initially increases while the signal power decreases. Later on, the ASE power slowly decreases at a rate much slower than the decrease of the output signal power. As mentioned earlier, this is a clear indication that deactivation of the Yb^{3+} emission and absorption of the signal light increase in the YDFA as a result of gamma irradiation.

4 Results of Gamma Irradiation on YDFs

4.1 Chapter overview

Passive optical fibers, Yb-doped MM and SM fibers were exposed to a Co-60 gamma source and the radiation-induced degradation was measured. The SM YDFs were operated *in-situ* as amplifiers for a 1064 nm laser light source. The MM YDFs transmitted light from a white light source during irradiation. The standard SM optical patch cables were evaluated with the pump and signal laser light sources used for the YDFA system. Varied exposure times and operational configurations were used to investigate the degradation of the fibers exposed to total doses above 100 krad(Si). The effect on the amplified signal gain was studied for the SM YDFAs and the change in transmission through the MM YDFs was measured from 500 to 1100 nm. This chapter provides the details related to the effects of radiation; an increased attenuation in the fibers across a broad spectrum with strong wavelength dependence, and the increase in attenuation when the Yb-doped fiber is pumped.

For optical fibers, the major mechanism of performance degradation is through the creation of absorbing species in the fiber, which in turn inhibit the transmission of light at certain wavelengths (Griscom, Gingerich, & Friebele, 1993) (Barnes & Wiczer, 1984) (Girard, et al., 2013). In recent years, the use of RE-doped optical fibers has expanded greatly. Nevertheless their ability to be used in harsh radiation environments has been the subject of only a limited number of studies. These fibers exhibit some of the same transmission decreases as with passive optical fibers, but the degree of degradation is significantly higher. The mechanisms responsible for the increase are still not fully identified (Lezius, et al., 2012). Previous studies have revealed that when operated in radiation environments, optical systems will be limited by the damage to

the YDFs because they are the most radiation sensitive component in such systems (Girard, et al., 2013).

In this study, SM YDFAs, MM YDFs, and the passive optical fibers of the type used with YDFs for transmitting amplified signals or laser light were evaluated during irradiation from the Co-60 gamma cell at The Ohio State University. Dose rates of 21.5 and 43 krad(Si)/hr (6 and 12 rad(Si)/sec) were used to expose the fibers to a maximum total dose that ranged from 90-250 krad(Si). The transmission of light through the fibers was measured *in-situ* which allowed the SM YDFs to be operated in two modes. Some fibers were actively operated as amplifiers while others were kept dark (no light) during irradiation, and only turned on as an YDFA for a short duration (15 sec) at approximately 5-10 minute intervals for the purpose of conducting a measurement. In order to gain further insight into the damage mechanisms, MM YDFs were irradiated in the same environment. The transmission of a white light source (from 500 to 1100 nm) through the MM YDFs was monitored.

4.2 Experiment

4.2.1 Description of tested fibers

Three different fiber sample sets were evaluated, as described in Table 5. The Yb-doped fibers consisted of two types of commercially available double clad fibers; a SM fiber with a core size of 6 µm and a cladding of 125 µm and a MM fiber with a core size of 40 µm. Passive single mode fibers of the standard SMF-28 jacketed variety were also evaluated. The Yb-doped fiber, manufactured by nLight, is a highly-doped fiber that enables signal gain using relatively short lengths (Tammela, Söderlund, Koponen, Philippov, & Stenius, 2006).

Table 5 Fibers used for *in-situ* analysis of the radiation damage

Optical fiber	*Core Dopant*	*Core/cladding diameters (μm)*
SM-YDF	Yb	6/125
SM-Passive	None	8/125
MM-YDF	Yb	20/400

The SM YDF fibers were operated as YDFAs using a pump laser at 975 nm and a signal laser at 1064 nm. The length of the fiber, pump and signal power, were selected to ensure that the YDFA was operated in the saturation region. This also guaranteed a uniform excitation ratio (50% for YDFs) across the length of the fiber.

4.2.2 Irradiation source description

The Co-60 gamma cell at The Ohio State University is a pool-type gamma irradiation facility using a common cobalt cylindrical rod irradiator submerged 20 feet into a water tank. A mechanical elevator in a 6 in dry tube lowers the sample to the irradiator for measurements, taking approximately 15 seconds to be fully situated. The sample location establishes the dose rate. The maximum available of 43 krad(Si)/hr was used in these experiments along with a half-maximum dose rate of 21.5 krad(Si)/hr.

4.2.3 Experimental setup

The experimental set up for the SM YDF irradiation is detailed in Figure 8. All experiments were conducted at room temperature. Five-meter long single mode fiber patch cables were connected to short lengths of passive fiber spliced onto the ends of each Yb-doped fiber sample. The YDF sample was lowered into the irradiation cell to the required location to obtain either the maximum or half-maximum dose rate exposure. The pump and signal laser were combined using a WDM and input into the fiber. The output was split using a 50/50 splitter between the power meter and the OSA. The OSA was used to measure the spectral

characteristics of the light transmission and amplification during irradiation. A 99/1 splitter was included on the output of the 1064 nm laser diode after the laser, but before the WDM splitter. The 1% output from the splitter was used to monitor signal power fluctuations during the irradiation. The pump laser had been previously characterized and fluctuations in its performance over a four hour period were insignificant.

Using this setup, the radiation-induced loss (RIA) of the amplified output signal was calculated using (16).

$$\mathrm{RIA}(\lambda,t) = \frac{-10}{l} \times \log\left(\frac{P_{out}(\lambda,t) * P_s(\lambda,t_0)}{P_{out}(\lambda,t_0) * P_s(\lambda,t)}\right) \tag{16}$$

RIA(λ,t) is the radiation induced attenuation at a specific time and wavelength measured in dB/m. $P_s(\lambda,t_0)$ is the initial measurement of the signal laser output through the splitter and $P_s(\lambda,t)$ is the measurement at time *t*. The power output from the SM YDF before and during irradiation are represented by $P_{out}(\lambda,t_0)$ and $P_{out}(\lambda,t)$, respectively.

The output from the YDF was sent through a 50/50 splitter. The power meter connected to the output of the YDF measured the light power at 1064 nm and the OSA provided spectral measurements from 970 to 1170 nm. All samples were characterized onsite using the exact set up used prior to lowering them into the irradiation cell.

The multi-mode YDFs were stripped and cleaved on both ends prior to irradiation. Bare fiber adapters with SMA connectors were attached to each cleaved end. The connectors were coupled to 5 m long 50 μm core passive fibers designed for transmission of 400 to 2400 nm light for the duration of the experiment. The MM YDFs were lowered and exposed while the transmission of a temperature stabilized white light source was measured through the fibers during and post irradiation. The transmission spectrum from 500 to 1100 nm was recorded using

a CCD spectrometer connected to a laptop. The power spectral density of this light source is not high enough to induce any appreciable amplification, fluorescence, or nonlinear effects in the MM YDFs (Figure 10).

4.3 Results and discussion

Degradation of the amplifier output gain was measured to estimate the system-level vulnerability of the Yb-doped fibers. Spectral RIA measurements were used to analyze the origin of the degradation. The degradation rates of the single mode and multi mode fibers were then correlated in order to determine the region of induced absorption that best explains the SM YDFA performance degradation.

4.3.1 Passive fiber degradation

The radiation-induced attenuation in the passive fiber was measured using the pump and signal lasers. A pristine 2 meter long passive patch cable with ceramic ferrules was characterized using a variety of pump and signal powers, and then placed in the Co-60 cell at a location for 21.5 krad(Si)/hr. The fiber remained in the chamber for approximately 26 hours resulting in a total dose of 560 krad(Si). At the pump wavelength, the attenuation measured is 0.25 dB/m or 4.4×10^{-4} dB/m*krad(Si). At the signal wavelength, the attenuation is 0.17 dB/m or 3.0×10^{-4} dB/m*krad(Si). This was only a fraction of the loss measured in signal and pump light output during irradiation of the YDF fibers and therefore contributes minimally to the error of the measuring the SM YDF amplifier output.

Henschel et al. studied the effects of Co-60 irradiation on ceramic single mode fiber connectors. They estimated that the upper limit of attenuation due to damage to the fiber optic connectors to be 0.15 dB following exposures to 1 Mrad(Si) at a dose rate 62.6 krad(Si)/hr (Henschel & Köhn, 1993). To examine this effect in the passive fiber of this research, a post-

irradiation measurement was conducted in which the fiber was cut in half and one end spliced to an unirradiated fiber. Taking fusion splicing losses into account, the degradation in the light transmission through the unirradiated fiber with the irradiated coupler was 0.07 dB and .04 dB for 1064 nm light and 975 nm light respectively. It was deduced that the majority of RIA attributable to the passive fiber was due to the darkening of the SM passive fiber rather than from the connectors.

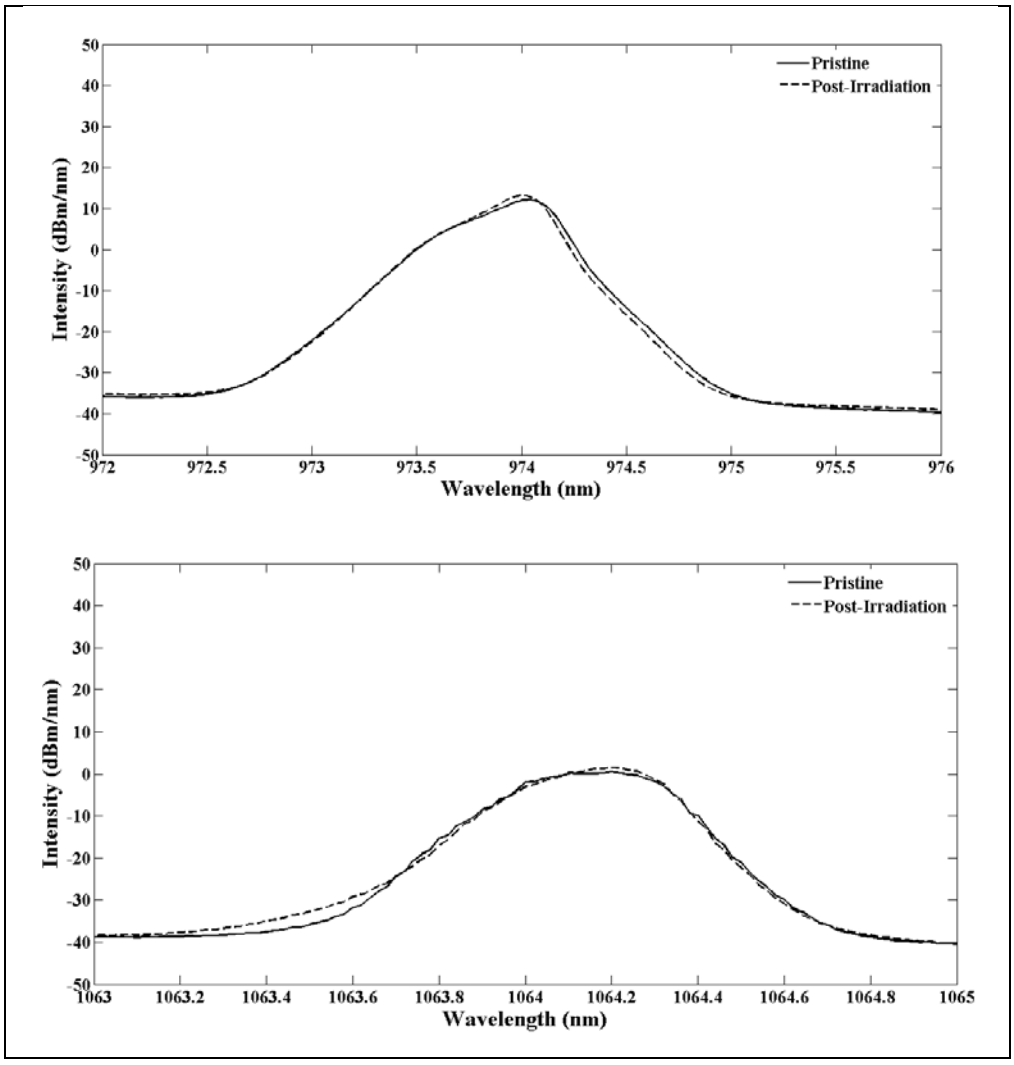

Figure 20. Transmission of 975 nm and 1064 nm light through passive fiber before and after 560 krad(Si).

4.3.2 SM YDF amplifier performance

During irradiation of the continuously pumped and intermittently pumped amplifiers, the output power decreased nearly monotonically with total dose. All RIA data for the amplifier performance is calculated with respect to the pre-irradiation output power for the YDF. The fibers were irradiated in the Co-60 cell at a dose rate of 21.5 and 43 krad(Si)/hr to a total dose of at least 90 krad(Si). One set of fibers was irradiated while actively operated as an YDFA during irradiation. The second set of fibers was unpumped (except during measurements) and the pump and signal lasers were turned on at regular intervals to measure their amplified signal output. The entire set of SM YDFs irradiated demonstrate a loss rate of 0.01 to 0.03 dB/m*krad(Si) following irradiation up to 100 krad. Using this rate to estimate damage at 150 krad(Si), the maximum loss experienced would be from 1.5 to 4.5 dB/m. For the set of fibers irradiated up to 150 krad(Si), the range of the RIA of amplified signal output is 1.42 to 3.94 dB/m. This set of experiments is sufficient to produce a range of potential damage to YDFA signal gain and lifetime estimates for systems before they are employed. For instance, the range of loss for a 3 m section of YDF, damage would be estimated from 0.03 to 0.09 dB/krad(Si) when operating in a radiation-harsh environment. If an acceptable total signal loss of 1.25 dB (reduction to 75% of initial power output), then the YDFA could be depended on to remain operational up to a minimum total dose of 14 krad(Si) and possibly to over 40 krad(Si).

At higher dose rates, YDFs from the same manufacturer of those used in this present research were shown to completely darken in the signal region (1 to 1.7 μm) (Fox B. P., et al., 2007). Fox et al. exposed a set of fibers to Co-60 irradiation at 14.3 and 40.1 rad(Si)/sec dose rates. At total doses over 200 krad(Si), complete loss of transmission in the signal region was experienced. The lowest dose rate used by Fox et al. is more than twice the highest dose rate used in this set of experiments. This indicated that there is a dose rate dependence on the rate of

RIA at the signal wavelength. Indeed the transmittance-rate decay, calculated by averaging the slopes for the set of YDFs tested by Fox et al. was 0.08 dB/(m*krad(Si)) at 1100 nm. Unfortunately both series of experiments only evaluated the fibers at two dose rates and for each individual experiment; there is no significant difference in the RIA with respect to dose rate when taken separately.

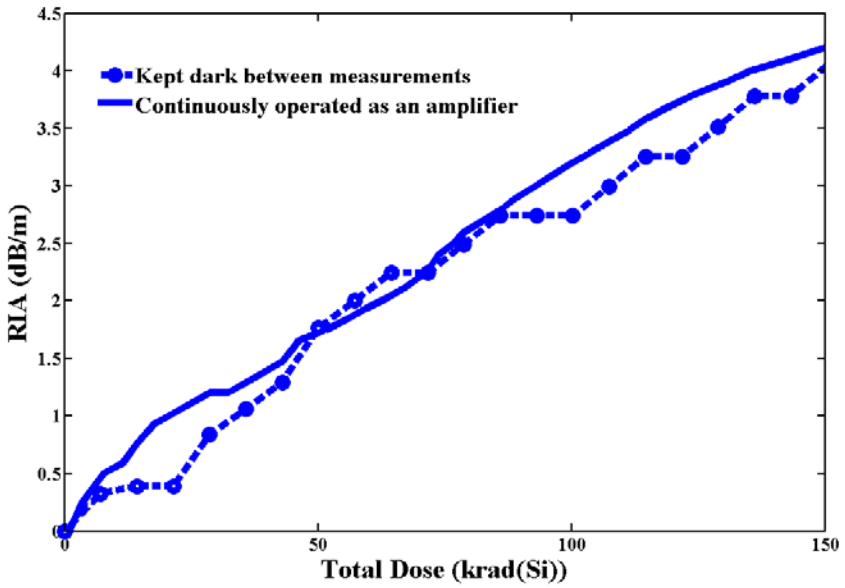

Figure 21. Data from two SM YDFAs irradiated at the same dose rate but with one continuously operated (solid line) and the other kept dark between measurements (dotted line).

As expected, the RIA for the SM YDFs follows a power law increase with increasing dose as defined in (17).

$$\mathrm{RIA}(D) = a \times D^{b} \tag{17}$$

In (17), D is the dose and a and b are fiber-specific parameters. The dose vs RIA curves for all of the SM YDFs were fit using the Power Law. The fit for both the fibers that were continuously pumped and those that were unpumped during irradiation returned the same average exponential value, b, of 0.83±0.05. In addition, there is no measurable indication that the

presence of the pump and signal laser has an effect on the degradation of the performance of the fiber amplifier system when exposed to gamma irradiation up to 150 krad(Si).

Therefore the RIA from a set of experiments on SM YDFAs with respect to the log-base-10 of the total dose is best fit with a linear relationship. The fits are averaged together and considered from the perspective of dose rates and operational condition. For both scenarios, there is not a statistically significant difference in the degradation experienced. For the scenario involving continuously pumped fibers, the fits predict a higher degradation, however, the error for both estimates overlaps, thus precluding any certainty of a real difference between the effects of the two operational configurations. The same is the case for the two different dose rates used.

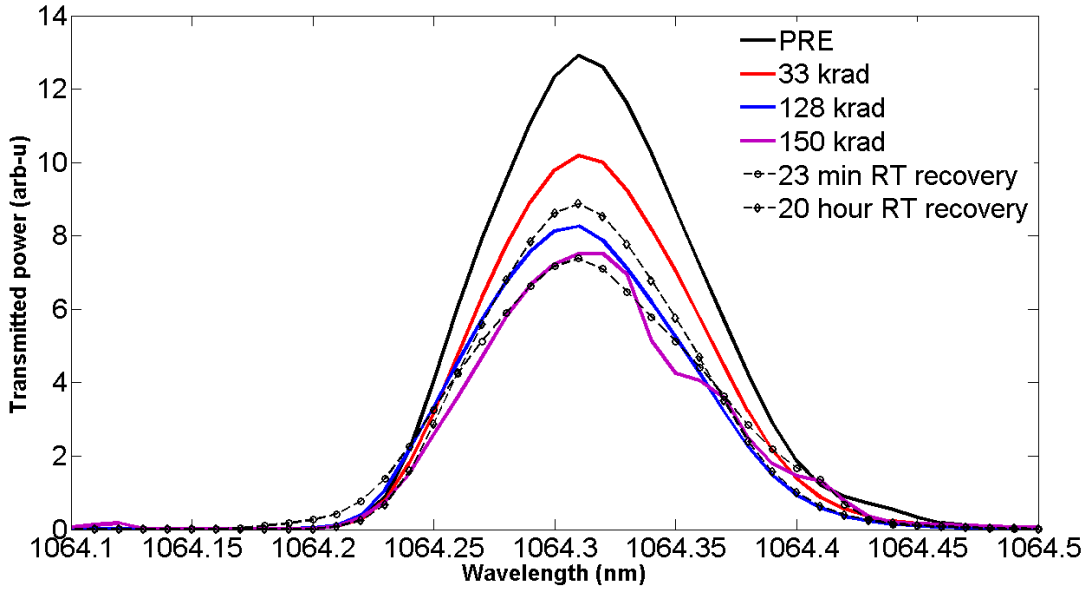

Figure 22. Transmitted power of the amplified signal before, during and after irradiation.

Figure 22 provides the spectral output at the amplified signal wavelength before, during, and after irradiation. Analysis of the signal indicates that the primary transmitted signal wavelength is invariant during and following irradiation (within the error due to variations induced by the 1064 nm laser source). The recovery time constant is long and following a

20 hour room temperature recovery, the output of the YDFA only recovered from a degradation of 70% to 78% of the total initial signal output power.

It is anticipated that heating of the fibers could increase the recovery rate. Fox et al. found that heating of the fibers to 170°C did not produce any annealing in completely darkened YDFs (Fox B. P., Simmons-Potter, Moore, Fisher, & Meister, 2009). However, Mady et al. conducted experiments of Yb-doped optical fiber performs and reported that thermal detrapping with temperatures up to 500°C corresponded to a recovery of light transmission (Mady, Benabdesselam, Mebrouk, & Dussardier, 2010). In their work, it is noted that recovery above 50% transmission did not occur until the temperature was raised to 350°C. Therefore it is speculated that in order to have a significant effect on recovery, the fibers would have to be heated above 350°C.

The derivative of the RIA with respect to dose, here referred to as the power loss rate, is plotted as a function of the total dose for the continuously pumped fiber irradiated up to 150 krad(Si) in Figure 23. The power loss rate decreases nearly monotonically with increasing dose. Although no saturation (power loss rate ≈ 0) was observed during the irradiation experiment, the rate declines at the higher total dose, suggesting a trend towards saturation. Saturation of the RIA occurs when either the potential defect sites become completely populated and/or when the rate of defect creation matches that of defect annealing.

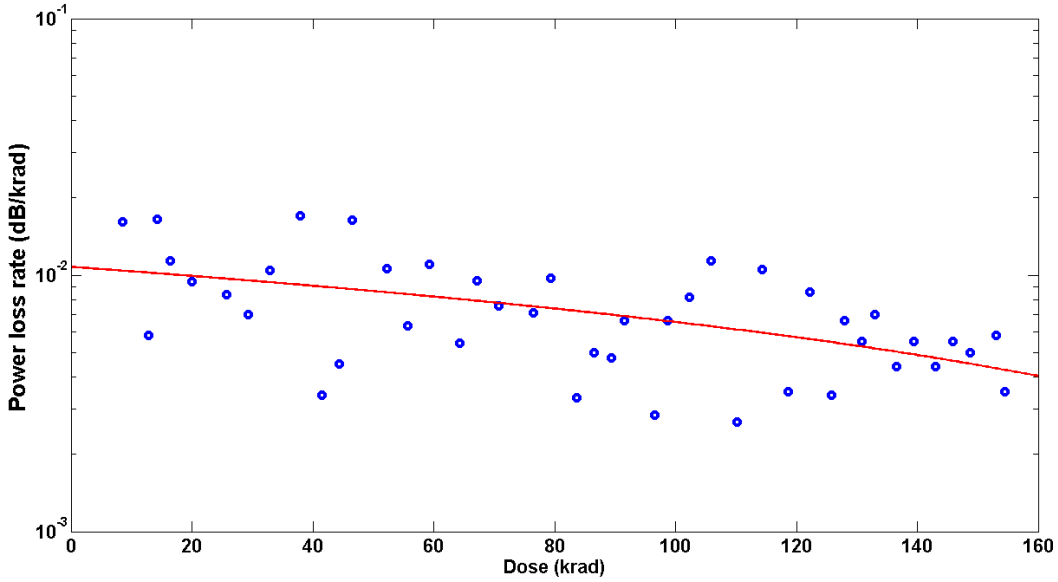

Figure 23. Power loss rate (dB/krad(Si)) as a function of total dose for a fiber irradiated up to 150 krad. The downward trending rate with dose is an indication of RIA saturation.

Following a 24 hour room temperature recovery during which no light source was transmitted through the fiber, the fiber was irradiated for an additional 150 krad under the same conditions (Figure 24). Fitting the curves in Figure 24 to a line results in a slope of 0.052 dB/m*krad(Si) for the first irradiation and 0.041 dB/m*krad(Si) for the second irradiation. These slopes represent the fiber radiation sensitivity. This lower sensitivity measured during the second irradiation is likely a continuation towards saturation that was observed in the previous irradiation.

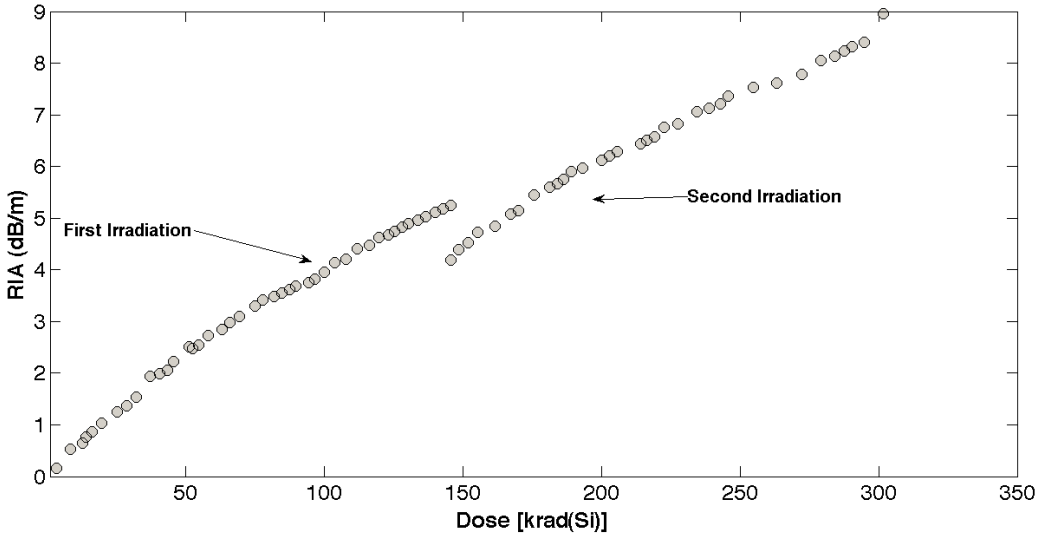

Figure 24. Radiation induced attenuation of the amplified signal output for a fiber that was irradiated twice. Fitting the curves shows that the RIA does not increase as rapidly during the second irradiation, suggesting a saturation of damage.

The amplified spontaneous emission (ASE) spectrum of the SM YDFs was measured by transmitting only 975 nm pump light through the fiber without the 1064 nm signal present. The ASE is the limiting factor for an unsaturated amplifier or laser system's maximum achievable gain. In addition, it is the dominant source of noise. As dose increases, the ASE power decreases and the peak of the curve shifts to longer wavelengths. Comparing the RIA for the peak as a function of dose for the ASE, and that of the amplified signal shows that the ASE intensity decreases more slowly with respect to dose than that of the amplified signal, as shown in Figure 25. This lack of correspondence between two RIA values indicates that the signal-to-noise ratio may not correlate well to the reduction in amplified signal output. Therefore increasing the degradation of an YDFA system performance beyond what may be expected by only considering the loss measured in a passive configuration at the signal wavelength.

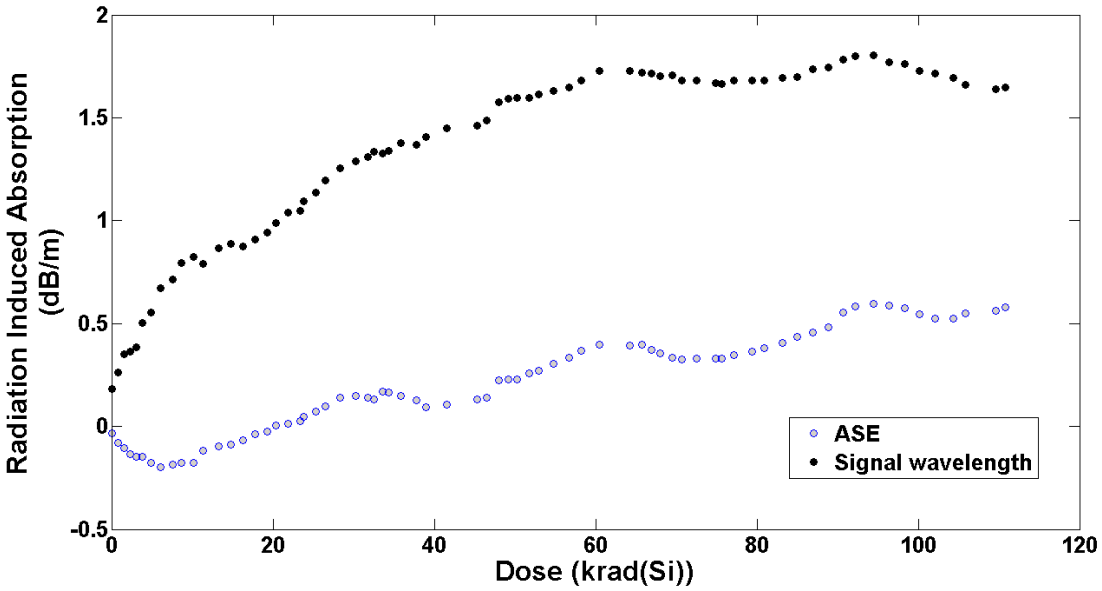

Figure 25. RIA at signal and ASE wavelengths in an irradiated SM YDFA

RIA data for fibers irradiated with three different total doses are normalized with respect to the total ionizing dose in krad(Si). The time axis is normalized with respect to the total irradiation time, with x=1 representing the end of irradiation. Figure 26 includes the data for SM YDFAs irradiated from 94 to 225 krad(Si). The magnitude of the RIA with respect to total dose decreases with increasing dose, indicating a saturation of the RIA at higher total doses.

The SM YDFAs demonstrate no difference in degradation when irradiated at two dose rate levels by gamma irradiation from a Co-60 source. There is a difference between the RIA of the amplified signal and that of the ASE. The RIA of the amplified signal increases faster with increasing dose than the RIA of the ASE wavelengths. This is a clear indication that the absorption of the pump light by defects is not the primary damage mechanism. The slow and saturating RIA of the ASE indicates that the concentration of excited Yb^{3+} ions is not decreasing at a rate commensurate with the decrease in the amplified signal output. In the chapter 5, the effect of de-activation of the excited Yb^{3+} ions and the absorption of the light at the signal wavelength will be examined in further detail.

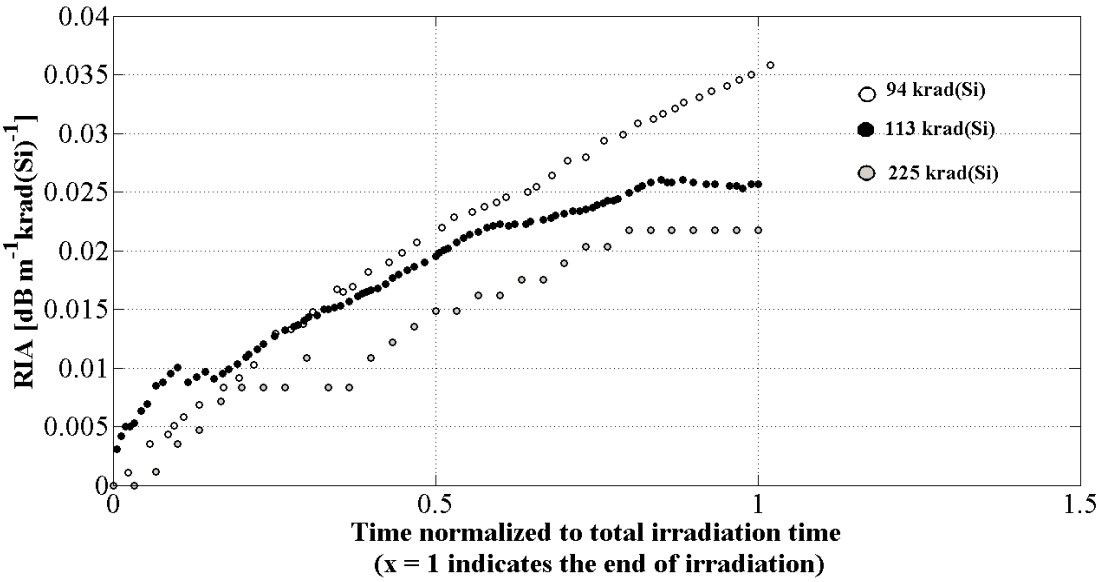

Figure 26. RIA of SM YDFA normalized to the total ionizing dose. The time scale is normalized to the total irradiation time.

4.3.3 Multi-mode fiber transmission

Attenuation of the transmission of light at 1064 nm through the MM YDFs follows a trend that matches that of the SM YDFAs (red curves in Figure 27). This further supports the result that the main source of YDFA degradation during irradiation arises from absorption of the signal light. Figure 28 represents a typical wavelength-dependent RIA spectrum from MM YDFs exposed to Co-60. Close examination of the difference between the curves plotted at 90 seconds, 12 minutes and 23 minutes, with increasing gamma exposure, provides evidence that the rate of RIA increase to dose is reduced. There is an increased RIA magnitude in the UV region and at the IR region above 1000 nm wavelength.

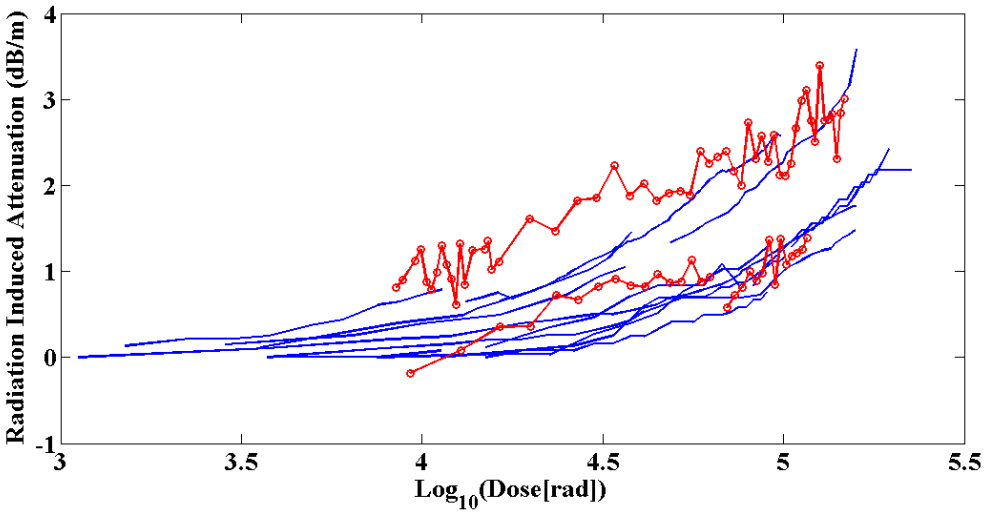

Figure 27. RIA as a function of the log of the dose in rads from Co-60 irradiations. Red lines represent data from MM YDFs measured at 1064 nm. Blue lines are from SM YDFAs.

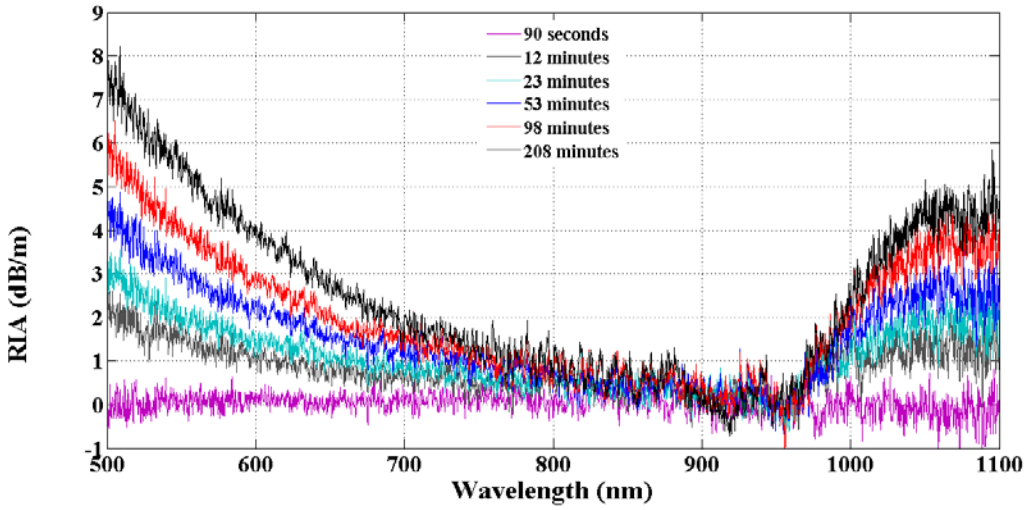

Figure 28. Radiation induced absorption in MM YDF as a function of wavelength presented at different irradiation times (total dose).

Examining the radiation induced absorption of the white light measured through the multi-mode fiber provides evidence that the greatest radiation-induced absorption occurs at the wavelength region below 900 nm. This gamma radiation induced absorption behavior is comparable to the result obtained by Deschamps et al. on Yb-doped fiber, performed with Co-60 up to 180 krad(Si) total dose (Deschamps, Vezin, Gonnet, & Ollier, 2013). In their work, along

with that of Arai et al., the primary source of increased absorption is attributed to defects arising from the Al doping of the fibers. The additional absorption spectra can be decomposed into a set of Gaussians by using known absorption curves of Al-based defects in amorphous silica detailed in (Hosono & Kawazoe, 1994) (Arai, Ichii, Tanigawa, & Fujimaki, 2009). The result of this technique is shown in Figure 29.

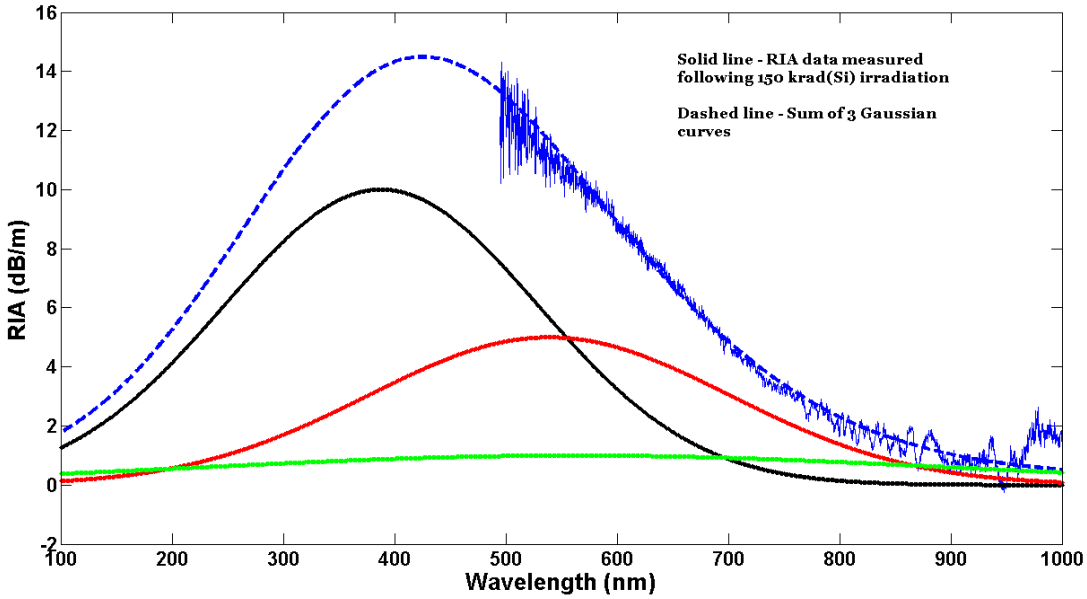

Figure 29. Fit of the RIA of light through the MM fiber following 150 krad(Si) irradiation. The heights of the three well-defined Al-based defect centers' Gaussians were adjusted to provide a good fit (dashed line) at wavelengths below 1000 nm.

It is notable that the absorption curves due to the Al-based defects in Figure 29, do not fit the RIA above 980 nm. In the MM YDFs operated in a passive configuration, with no excited Yb^{3+} population, the loss of light at 1064 nm is attributed to defect species that can directly absorb light at that wavelength. The increase in the absorption at the 1064 nm wavelength may be attributable to the radiation-induced creation of interstitial O_2 molecules in the silica. The first excited vibronic state of O_2 molecules in silica has been shown to be excited by 1064 nm light (Skuja, Güttler, Schiel, & Silin, 1998). Relaxation of the excited molecule is characterized by

luminescence around 1272 nm (Skuja, 2000). The measurements taken during this experiment did not cover light transmission up to 1272 nm, so there is no correlating emission to match with the increased absorption. An additional absorption curve was added to the result of Figure 29 centered at 1070 nm and the 539 nm and 564 nm curves were combined into a single Gaussian curve at 550 nm to model a more accurate decomposition.

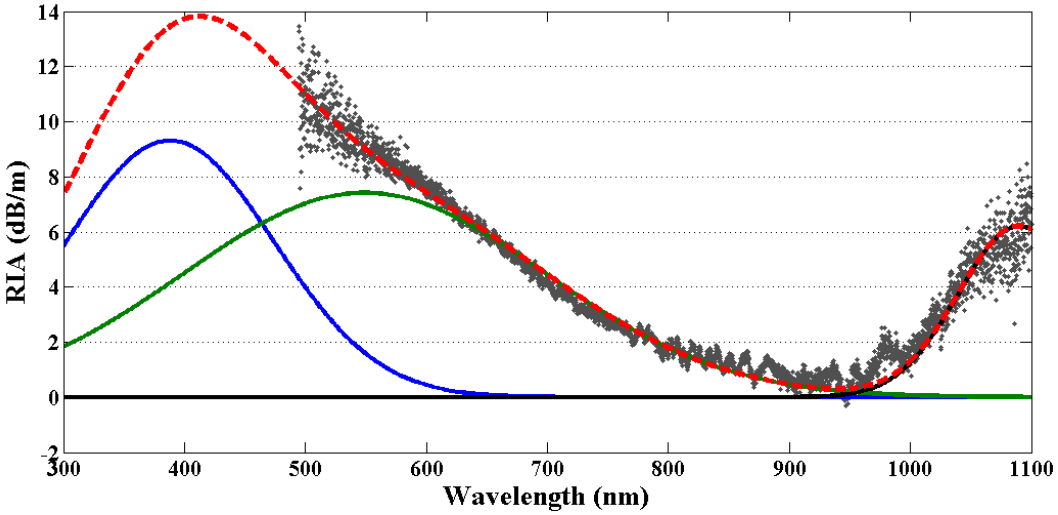

Figure 30. Fit of the RIA of light through the MM fiber following 150 krad(Si) irradiation. The heights of the three well-defined Al-based defect centers' Gaussians along with an absorption center at 1070 nm were adjusted to provide a good fit (dashed line).

In his PhD dissertation, Fox presents transmission loss measurements through similar YDFs under gamma irradiation from 1000 to 1700 nm. The results from both SM and MM YDFs irradiated in a passive configuration demonstrate that the highest magnitude of transmission loss is experienced at the 1000 to 1100 nm range in the fibers (Fox B. P., 2013). When taken with the results from the MM YDFs here, this leads to the conclusion that there is indeed a peak in the absorption in the fibers near 1060 nm.

Using a white light source of spectral intensity of less than 100 μW, Girard et al. measured increased RIA (~ 4 dB/m) in the region between 1 and 1.1 μm (Girard, et al., 2009) following proton exposure. They conducted the same experiment, but employed a supercontinuum source

that directly coupled light into the fiber core at powers > 10 mW. These measurements indicated minimal increased absorption (~ 1 dB/m) in the 1 to 1.1 μm region. The white light source transmitted light from 850 to 1700 nm, but the expected increase of absorption due to the interstitial O_2 absorption was not observed, even thought this is a known effect. One possible explanation is that the light from the supercontinuum light source may be bleaching out this defect in the post irradiation measurements. Skuja et al. demonstrated that bleaching of the O_2 content (via decrease of the O_2 absorption) takes place in the presence of UV light (4.4 eV) (Skuja, 2000). The light used for Girard's experiment had energy peaking at 550 nm (2.5 eV).

RIA at various wavelengths in this work through the MM YDF is plotted in Figure 31 as a function of the log-base-ten of the dose. The RIA at 1064 nm correlates well to the RIA at 550 nm as a function of dose. The RIA experienced at other wavelengths up to a dose >150 krad(Si) increases at lower rates. In studies of photodarkened fibers, the 1064 nm RIA has been correlated with the RIA at wavelengths between 550 and 633 nm (Koponen, 2008). In the work published by Koponen, the increased loss at 633 nm for YDFs demonstrated a 71:1 relationship to the increased loss at 1064 nm. It is evident that they follow a similar rate of increase. However, relating these two regions of absorption to the same defect is only partially justified based on known defects that absorb at the 500 to 633 nm range.

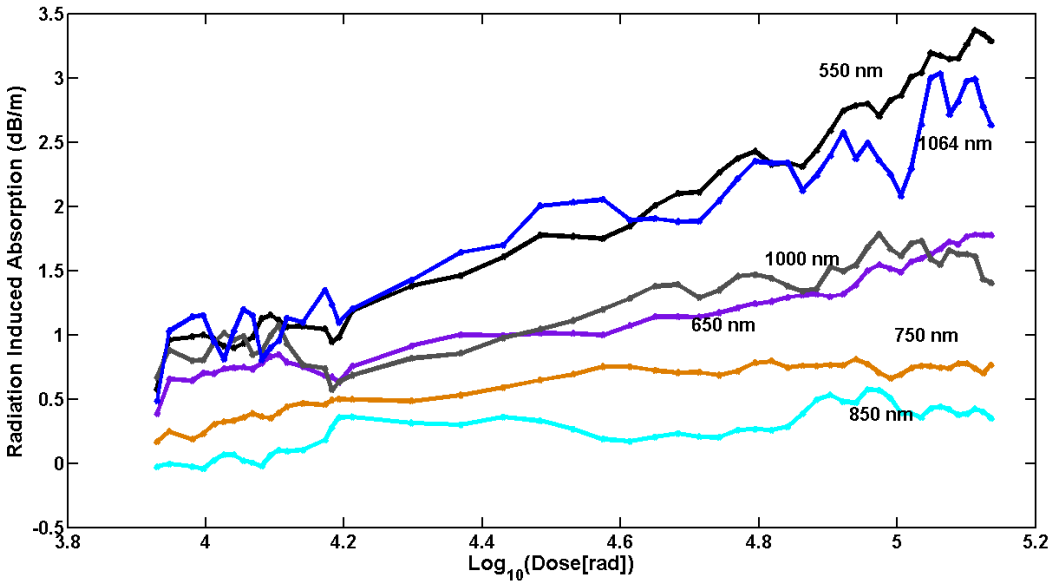

Figure 31. Wavelength dependent RIA for a MM YDF exposed to Co-60 irradiation

Although the RIA for the 550 nm and 1064 nm wavelengths increase at a similar rate with respect to dose, the rate of recovery following the end of irradiation at 550 nm, shown in Figure 32, is faster than the rate of recovery at 1064 nm (5 dB/m*hr compared to 3.4 dB/m*hr). Recovery of the Al-OHC absorption region of the spectrum initially proceeds at a higher rate than the 1064 nm absorption.

The RIA normalized to total dose from a SM YDFA irradiation is shown along with that for two sets of transmission data at 1064 nm for MM YDFs in Figure 33. The normalized RIA of the SM YDFA is higher than that of the transmission through the MM YDFs. The degradation to the output of the SM YDFA cannot be explained completely by the loss of transmission at the 1064 nm wavelength.

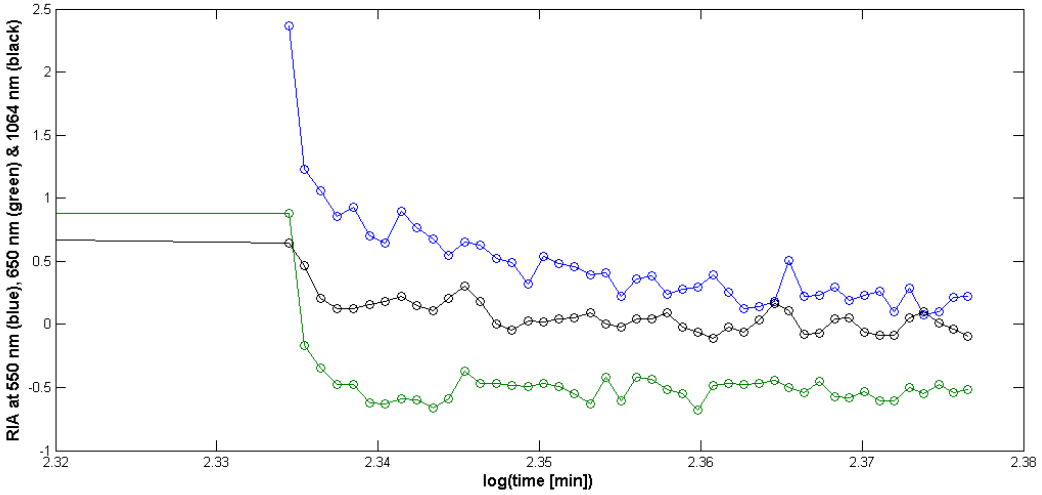

Figure 32. Recovery of light transmission through a MM YDF at three different wavelengths. The 1064 nm transmission recovery is slower than the recovery at the visible wavelengths.

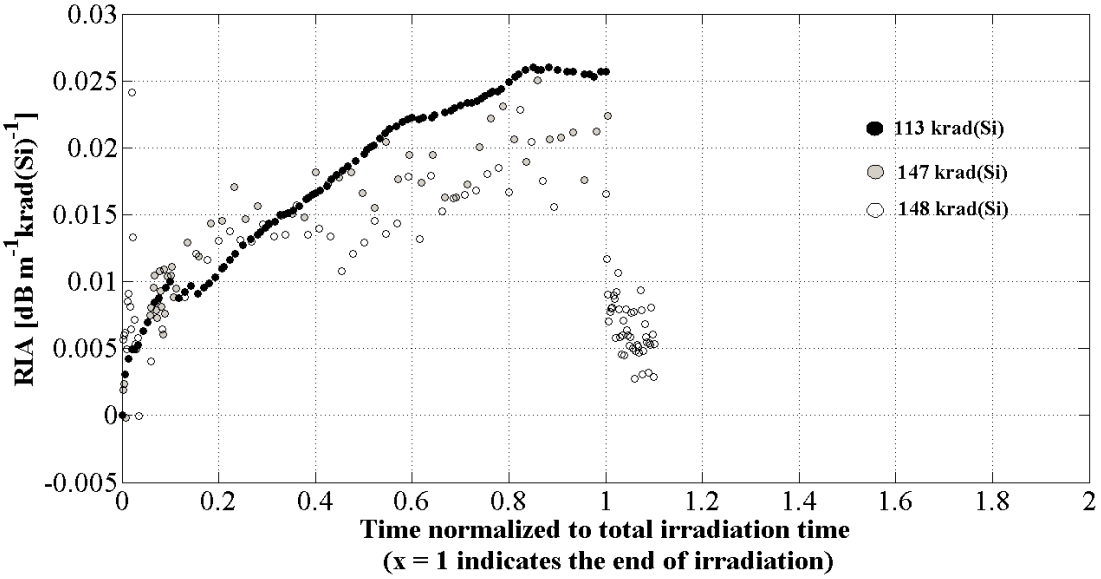

Figure 33. The RIA for ionizing only irradiations at different dose rates. The solid black dot curve is from SM YDFA irradiated by Co-60. The other two curves are from the 1064 nm transmission data through MM YDFs irradiated by Co-60. RIA values are normalized to total dose.

4.4 Summary

The degradation of the YDFs was measured *in-situ* during exposure to gamma irradiation from a Co-60 source. The SM YDFs operated as amplifiers examine the effect of gamma irradiation on the amplified signal output. Transmission of a white light source was measured through the MM YDFs in order to illuminate the damage effects in the SM YDFs. Passive fiber of a type typically used with the SM YDFs was irradiated in order to gauge the magnitude of its contribution to the observed degradation of the system.

The SM YDFs experience a degradation of the ASE intensity that does not directly correlate with the decreased amplified signal output. This result supports the theory that the absorption of the pump light is not a dominant factor in degradation of the performance of the SM YDFA under irradiation. The ASE intensity can be correlated to the excited Yb^{3+} ion concentration. Since the ASE intensity changes are small relative to the change in the amplified signal output, then the population of Yb^{3+} ions in the excited state is assumed to change very little as well.

The experiments conducted with the MM YDFs demonstrated the absorption at the pump wavelength (975 nm) is insignificant compared to the RIA at 550 and 1064 nm (Figure 34). The MM YDF transmission spectra compared to the RIA of the SM YDFA output indicate that the degradation to the output of the SM YDFA cannot be explained completely by the loss of transmission at the 1064 nm wavelength. The magnitude of the dose normalized RIA for the SM YDFA is higher than the same metric for the MM YDFs. The recovery rates of light transmission through the MM YDFs show that the degradation to the output signal following irradiation is based on defects that absorb in the UV as well as the IR wavelength ranges. This is due to the differences in activation energies of the two defects. The O_2 atom when situated at the center of a

ring of SiO_4 tetrahedra is in its lowest energy state (Bakos, 2003). The magnitude of the passive fiber transmission degradation and of the ceramic optical fiber connectors compared to that of the YDF is small enough to be excluded when considering the damage to YDFAs operating in harsh radiation environments.

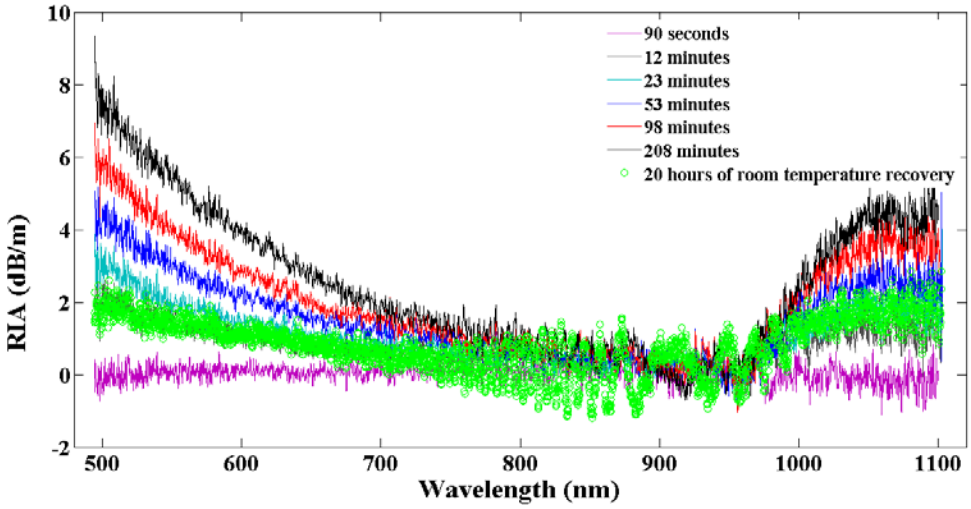

Figure 34. Spectral increase of radiation-induced absorption in a Co-60 irradiated multi-mode YDF overlaid with the RIA at 20 hours of room temperature recovery. There is a larger magnitude of recovery at the 550 nm range than at the 1064 nm range.

The set of gamma irradiations at low dose rates (compared to the reactor irradiations) demonstrated that the SM and MM YDFs would not be completely darkened within a short time of radiation exposure. This ensured that measurements of the change in the fiber transmission could be measured in the ACRR and OSU-NRL radiation environments without loss of signal.

5 Results of Gamma/Neutron Irradiation on YDFs

5.1 Chapter overview

The objectives of the OSU-NRL and ACRR tests were to produce the first results reported on the response of Yb-doped fibers in a mixed neutron/gamma environment. In addition, the results were used to further the knowledge of the relationship between the irradiation dose rate and damage and recovery of the fiber transmission at the pump and signal wavelengths (950-1100 nm).

The OSU-NRL tests were designed to expose the YDFs to a total neutron flux equivalent to the neutron flux that the single mode fibers were exposed to in the first series of ACRR tests. For the OSU-NRL tests, multi-mode fibers along with single-mode fibers were fielded. The multi-mode fibers were connected to a white light source during irradiation. The single mode fibers were operated as signal amplifiers during irradiation. Recovery data following irradiation for both ACRR and OSU-NRL tests was recorded for approximately 24 minutes to several hours following irradiation.

5.2 ACRR testing

5.2.1 Single mode fiber irradiations

A total of 20 tests were conducted at the ACRR. The first 10 tests were performed on pristine YDFs operated as YDFAs before, during, and after the pulse. This set of tests will be referred to as “series I” with alphabetical indicators for multiple shots. The second set of experiments involved three irradiations of the same YDF sample with the pulsed reactor output power increased with each shot. This set of tests, which also includes irradiation of a passive (undoped) MM DC fiber, is “series II”. The radiation exposure properties of each test are provided in Table 6. The fiber used in series II-2 tests was not operated as an YDFA during

irradiation. The transmission of the 1064 nm laser light through the fiber was monitored before, during and following the reactor pulse. Time-to-pulse + 3*FWHM is a value that represents the time at which over 90% of the pulse energy has been produced by the reactor.

Table 6 Details of ACRR Tests. The series II-2 tests, marked with a '*', involved a fiber transmitting the 1064 nm light only, and the last in the series, denoted with a '**', was a passive MM DC fiber.

Test	Total Reactor Output Power [MJ]	Ionizing Dose [krad]	1 MeV Equivalent Neutron Fluence [n/cm^2]	Neutron Fluence > 3 MeV [n/cm^2]	Time-to-Pulse + 3*FWHM [s]
I-1	6.38	9.31	4.55×10^{13}	3.47×10^{12}	0.70
I-2	23.75	42.81	1.69×10^{14}	1.54×10^{12}	0.60
I-3	49.5	76.16	3.18×10^{14}	2.90×10^{13}	0.44
I-4	52.1	78.43	3.13×10^{14}	2.86×10^{13}	0.44
I-5	12	21.88	9.20×10^{13}	8.40×10^{12}	0.62
I-6	25.5	41.13	1.61×10^{14}	1.48×10^{13}	0.61
I-7	75.4	117.93	4.97×10^{14}	4.54×10^{13}	0.40
I-8	14.4	22.55	9.14×10^{13}	8.35×10^{12}	0.71
I-9	29.6	45.56	1.84×10^{14}	1.68×10^{13}	0.57
I-10	76.9	121.86	5.07×10^{14}	4.63×10^{13}	0.40
II-1a	12	19.94	7.50×10^{13}	9.20×10^{12}	0.66
II-1b	27.3	43.51	1.67×10^{14}	1.84×10^{13}	0.60
II-1c	52.2	81.87	3.16×10^{14}	3.33×10^{13}	0.50
II-2a*	15.5	25.33	9.60×10^{13}	1.13×10^{13}	0.65
II-2b*	28.5	45.36	1.74×10^{14}	1.91×10^{13}	0.60
II-2c*	54.8	85.87	3.32×10^{14}	3.49×10^{13}	0.49
II-3a	12.7	21.01	7.92×10^{13}	9.62×10^{12}	0.66
II-3b	26	41.50	1.59×10^{14}	1.76×10^{13}	0.61
II-3c	50.6	79.40	3.07×10^{14}	3.24×10^{13}	0.51
II-4**	50.6	79.40	3.07×10^{14}	3.24×10^{13}	0.51

The RIA of the SM YDFA output signal along with the average reactor pulse power for three different power levels is plotted in Figure 35. The charts reveal that for the higher power pulses, the pulse width and subsequent total radiation exposure time decreases. The shape of the RIA for each power level is the same although the degree of degradation increases as pulse power increases. For the set of fibers in series I, the maximum RIA is reached at an average of 0.18 seconds following the peak of the pulsed reactor power output.

The degradation behavior does not vary much among the set of fibers from each series. The general trend is that output power decreases rapidly following the arrival of the pulse. The output pulses that are shorter and produce higher output energy lead to much more initial loss of output. The RIA does not saturate before the recovery phase begins. The overall model closely follows one that is found in a review of displacement damage effects in silicon devices following an incident neutron pulse (Srour, Marshall, & Marshall, 2003). The damage that anneals rapidly is referred to as transient damage. Once the annealing rate falls off to a much slower rate, the defects that are left are considered to be ‘permanent’ damage. This recovery behavior over several decades of time after the irradiation pulse as can be seen in Figure 36-39 for results from the series I and II tests.

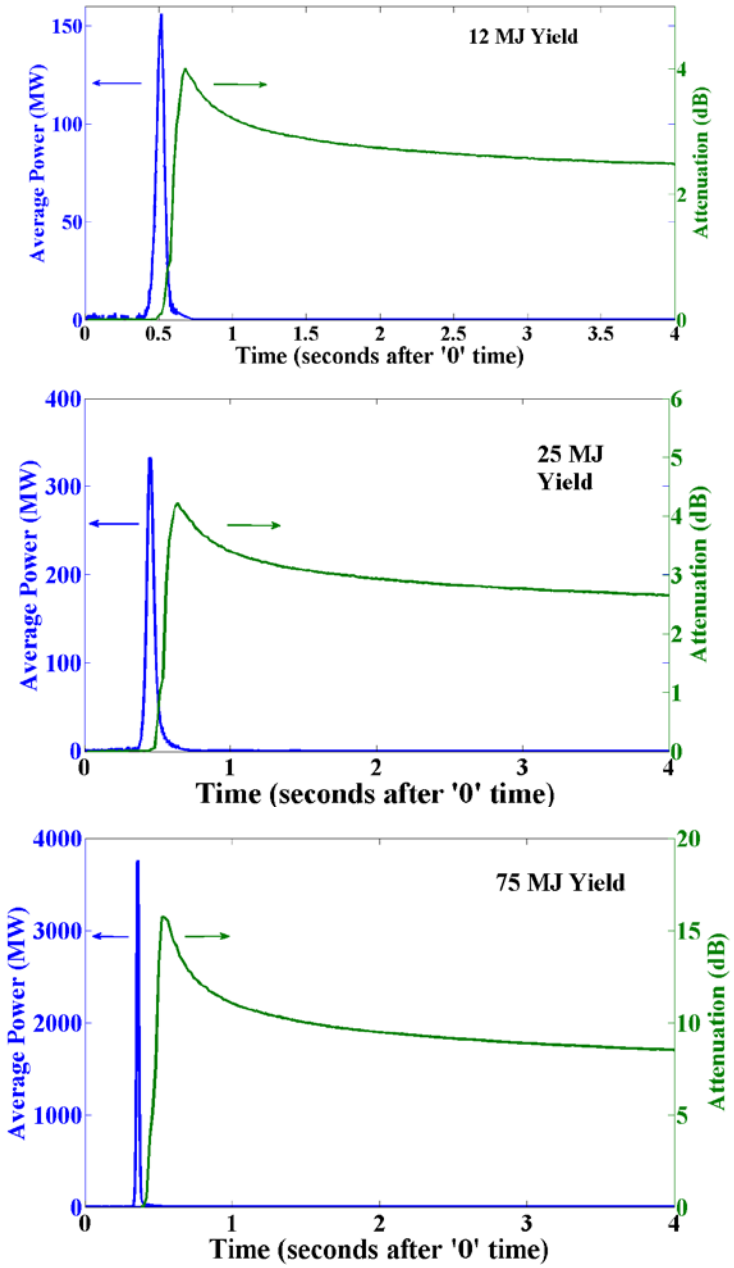

Figure 35. Output power along with RIA (dB) for the first 4 seconds following the zero time trigger for three different power levels.

The behavior of ACRR irradiated fibers showed that the magnitude of the transmission loss as well as the rate of recovery is dependent on the irradiation pulse power. Higher powers lead to higher damage and subsequently faster initial recovery. At the lowest reactor pulse power levels (12-16 MJ), the results are somewhat anomalous in that there is no correlation between reactor pulse power and the normalized magnitude of transmission loss. At these lower pulse

powers, the timing of the pulses can differ significantly. This timing variation changes dose delivery profile and can make the total calculated power difficult to estimate accurately.

The fiber for series II-2a-c tests was operated as an amplifier for a few minutes following initial setup, and approximately 30 minutes prior to the reactor pulse with the pump light removed from the fiber. The fiber was only transmitting the 1064 nm signal with no amplification. The output power was monitored before, during, and after the pulse. Following the first pulse, there was a slight loss in signal transmission, as shown in Figure 36. However, the amplifier fiber continued to amplify the signal. Thirty minutes after the first pulse, the output power of the amplifier fiber recovered to near the pre-irradiation level.

In all three tests, the recovery of the SM YDF that was not being pumped during irradiation initially proceeds at a higher rate than the recovery of the SM YDFA output. No excitation of the Yb^{3+} ions was anticipated in this irradiation. Thus, the rate of initial damage recovery in the SM YDFAs is partially dependent on (slowed down by) the rate of recovery of defects that are associated with the excitation process in the YDFAs. The de-excitation of the Yb^{3+} ions by energy transfer to defects created in close proximity fits this model. In the fiber that was transmitting only the signal light, with no excitation the transmission recovery was dependent only on the defect species that directly absorbs light at 1064 nm.

The higher degradation of the amplified signal is similar to results from the Co-60 irradiations of the single-mode and multi-mode YDFs. It was found during the Co-60 tests that the amplified spontaneous emission (ASE) of the irradiated single-mode fiber did not decrease at the same rate as the transmission of the signal wavelength decreased. The induced absorption of the maximum ASE wavelength was 40% lower at 150 krad(Si) than that of the signal wavelength. This indicates that radiation tests performed on YDFs that are operated in a passive

mode may provide results that could underestimate the actual degradation to the amplified system.

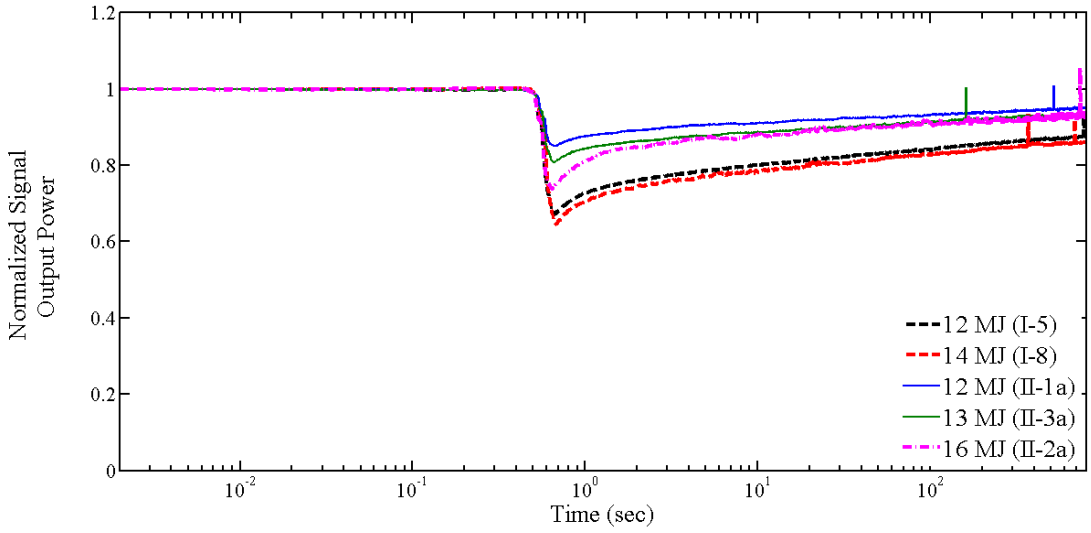

Figure 36. Normalized signal output power for series I and II fibers irradiated at the lower ACRR pulse power range (12-16 MJ).

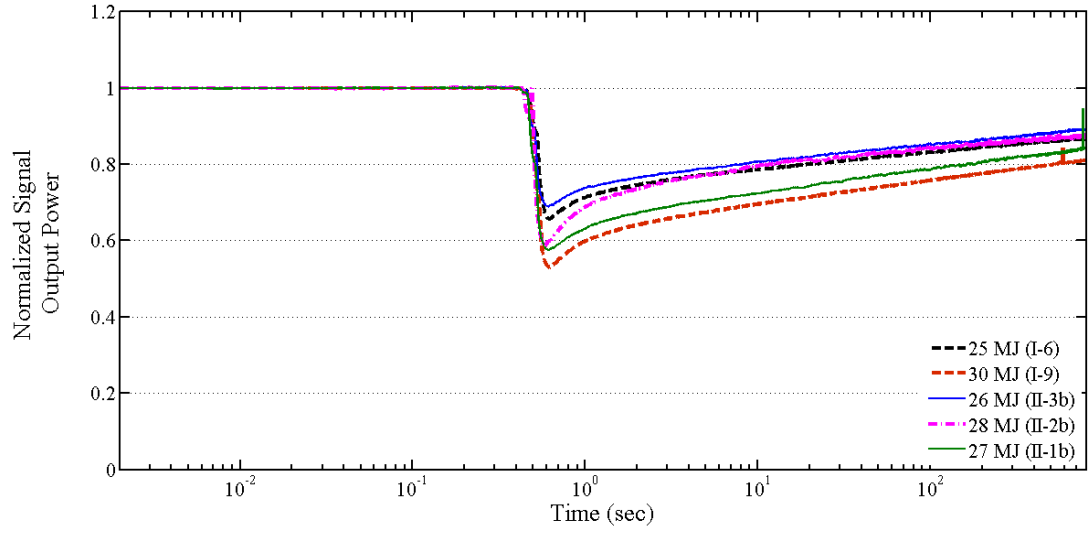

Figure 37. Normalized signal output power for series I and II fibers irradiated at the middle ACRR pulse power range (25-30 MJ).

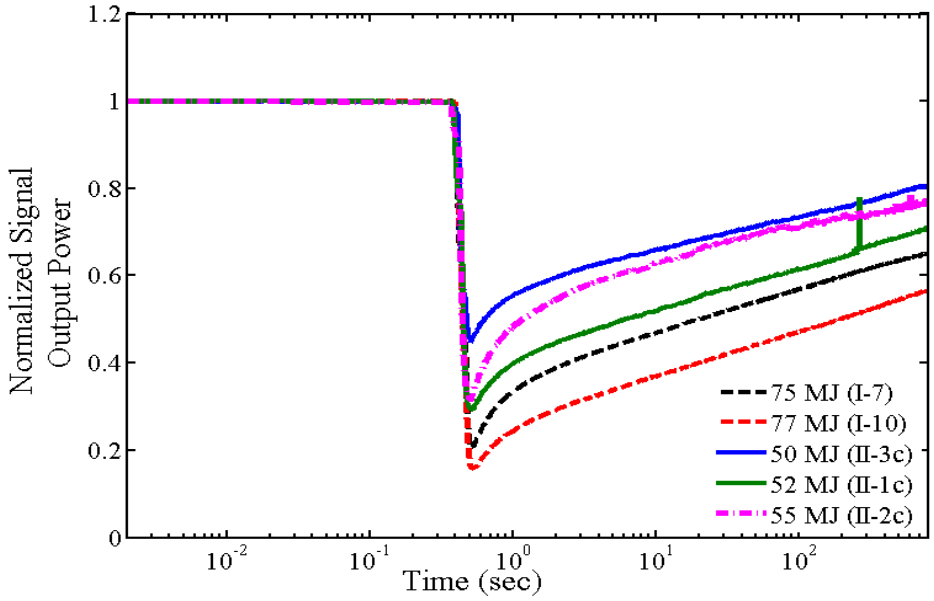

Figure 38. Normalized signal output power for series I and II fibers irradiated at the higher ACRR pulse power range (50-77 MJ).

When the RIA is normalized to the total ionizing dose, the result is that the higher the dose, the lower the normalized RIA value. From Figure 39, there is an obvious trend. As dose increases, there is less degradation per krad(Si) of dose. This is an indication of radiation insensitivity at higher total doses, likely due to the saturation effect of the damage. The relationship to total ionizing dose and RIA is, however, non-linear, and there are large differences between the results of tests with similar total doses.

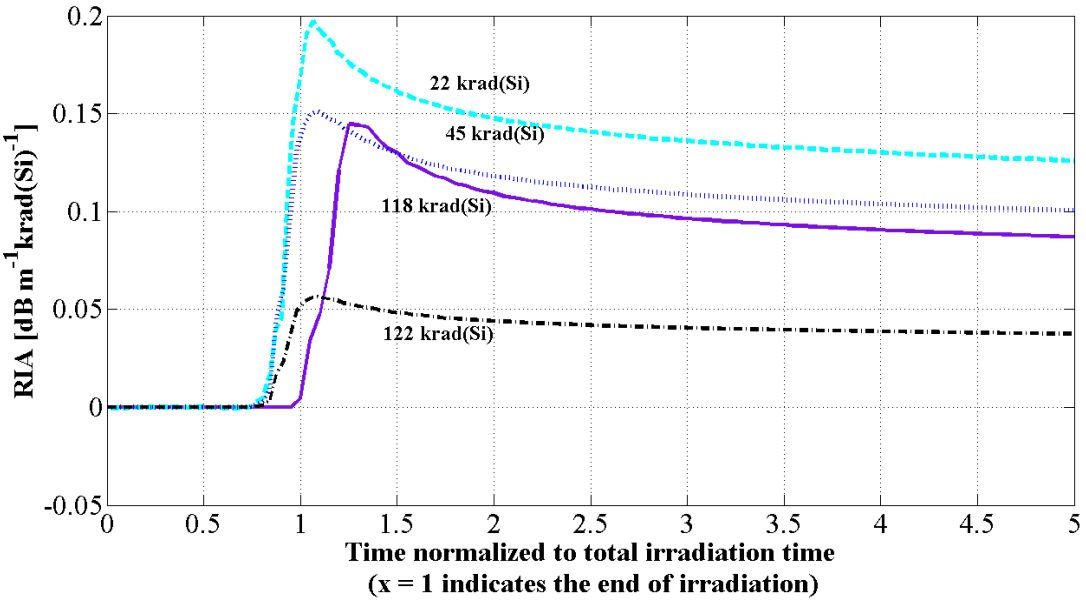

Figure 39. RIA normalized to the total ionizing dose value plotted on a timescale that is normalized to the total irradiation time.

Figure 40 provides the long term (beginning at half an hour after reactor pulse) recovery of series II-1c which was irradiated while being operated as an amplifier (black line) and the recovery of series II-2c, tested transmitting only the signal laser with no pump excitation (blues line). The amplified signal experiences a larger normalized reduction in output power. The transmission of both signals recovers at the same rate.

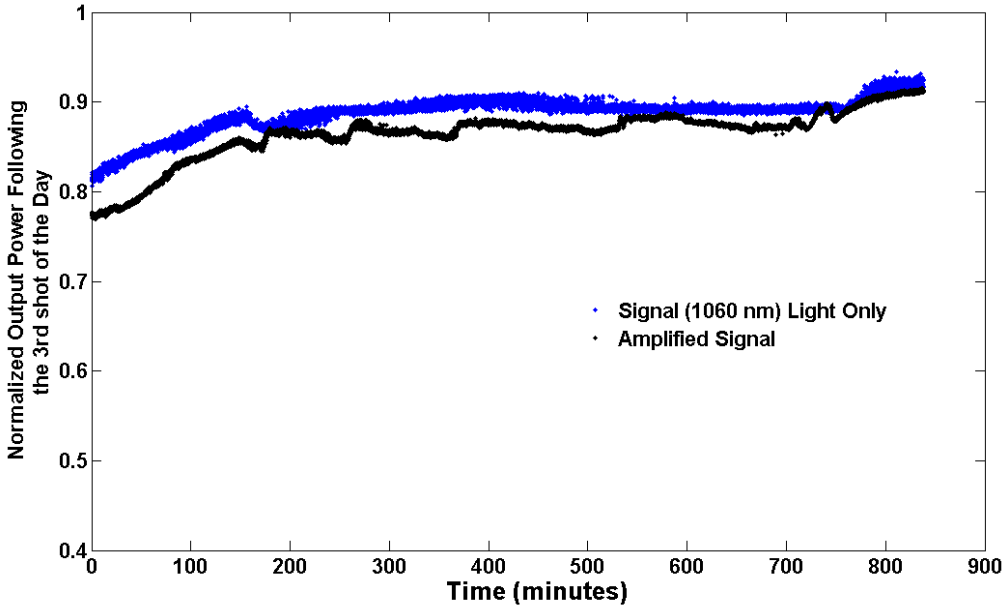

Figure 40. Output power following the 3rd shot of the day for 2 different fibers. The values are normalized to the pre-shot (following shot #2) irradiation values. The output of the amplified signal experiences higher degradation than the fiber transmitting signal light only. The recovery rate is approximately the same.

5.2.2 Multi-mode fiber irradiations

Two, 20 meter long passive MM DC cables were coupled together, and the white light source turned was used to measure transmission through the fibers. Spectra were recorded using the CCD spectrometer every 1 minute prior to the pulse. Right before the pulse, the system was set to record 100 rapid spectra (a few milliseconds apart).

Figure 41 shows the normalized output power at three wavelengths through the passive MM DCF in the short time following the ACRR pulse. The light transmission through the passive multi-mode fiber changed slightly during the pulse yet returned to pre-irradiation levels at all measured wavelengths (500-1100 nm) within 5 minutes following the pulse. Among wavelengths of interest (900-1100 nm), the largest loss was experienced at the 1064 nm wavelength. The transmission loss at the 975 nm was less than 10%. This is a good indication

that the passive fiber will not contribute significantly to the transmission loss of an YDFA system.

The loss at 564 nm is actually not as significant as the loss at 1064 nm through the passive MM fiber. The recovery of transmission at both wavelengths is rapid and proceeds at the same rate. This is an indication that the increased damage at 564 nm experienced by the MM YDFs under irradiation (from Co-60 and OSU-NRL as will be shown in the next section) is an effect directly related to the incorporation of Yb^{3+} ions in the fiber.

The primary result of these measurements was that passive, double clad MM fiber anneals rapidly following the reactor pulse. Passive fibers in the test chamber did not contribute significantly to the measured degradation and have no effect on the recovery rates measured.

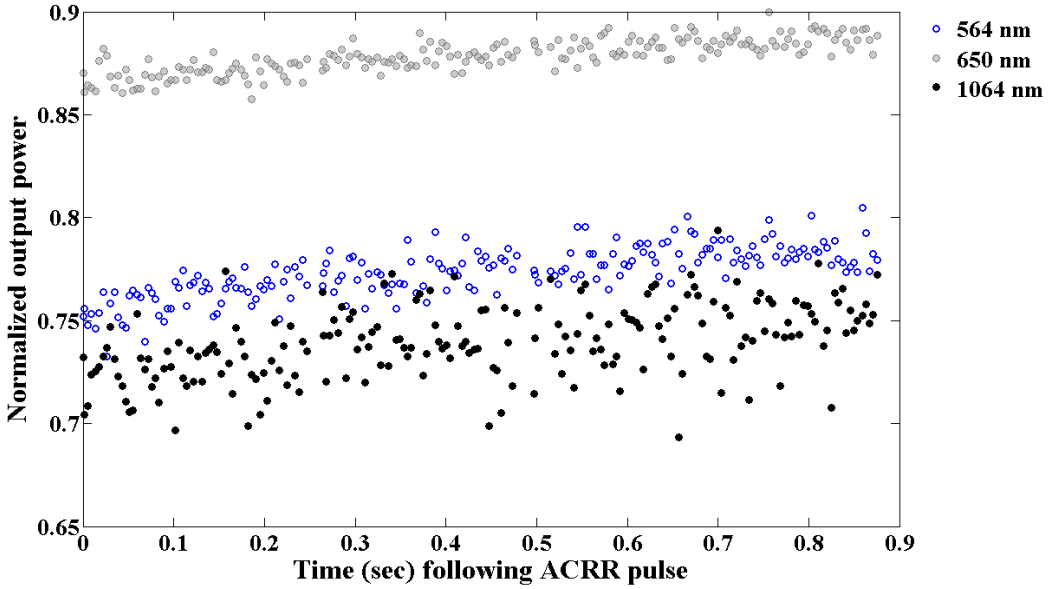

Figure 41. Normalized loss at three wavelengths through the passive MM DC fiber following an ACRR pulse.

5.3 OSU-NRL radiation tests

All of the fibers irradiated during the reactor tests were placed at the same location adjacent to the reactor core, and the reactor was operated at the same power level output for each irradiation (450 kW). The Yb-doped portion of the fibers tested, were placed inside a Cd box and lowered into position inside a dry tube prior to the reactor start up.

5.3.1 Single-mode fiber irradiations

SM YDFAs were operated *in-situ* during exposure to radiation from the OSU-NRL. The YDFAs were placed inside a Cd box and lowered into a moveable dry tube that was placed adjacent to the reactor core. The data collected from the SM YDFAs consisted of output power of actively operated SM YDFAs along with some spectral measurements from 970 to 1100 nm. Post-irradiation recovery was monitored through signal output power only (no spectral data).

For the single-mode fibers, the output power of the amplified signal was measured during irradiation. The power behavior of a fiber irradiated for 5 hours and allowed to recover (under continuous operation as an YDFA) is shown in Figure 42. The YDFA undergoes a rapid decrease in output power and then *semi-saturates* at a low (virtually dark) value. In the context of this work, semi-saturates it is meant to mean that the rate of decrease of the output power slows significantly, although the output power continues to decline throughout the entire irradiation period.

The recovery at the end of irradiation follows the same behavior as observed in fibers irradiated in the ACRR, with a rapid initial recovery that slows down and eventually follows a saturating exponential increase. In this case, Figure 43, the timeline for recovery is viewed over several hours. The recovery for the ACRR irradiated fibers reaches a saturated value after approximately 30 minutes.

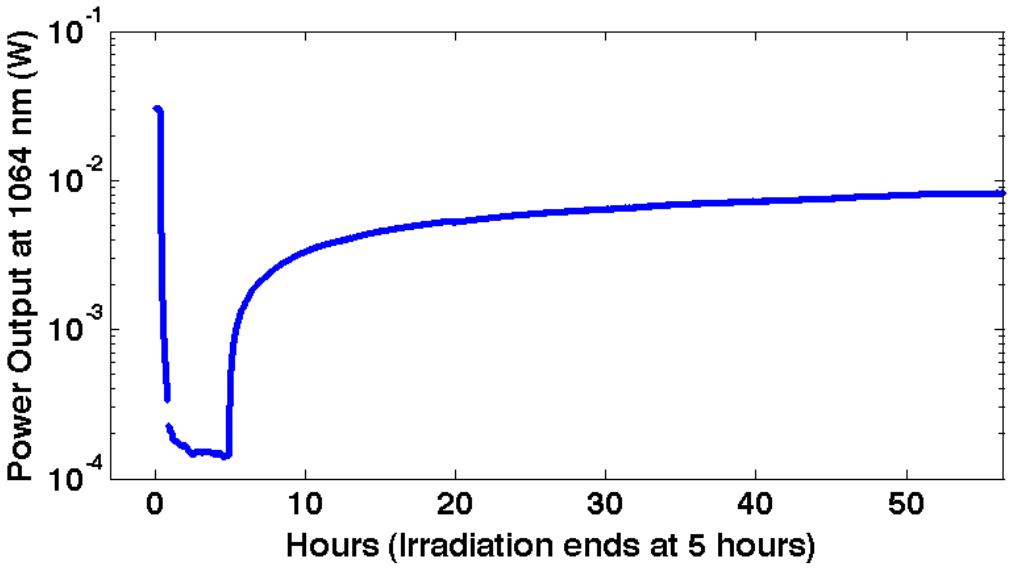

Figure 42. Power output of the amplified 1064 signal through a pumped single-mode YDF during and after irradiation at the OSU-NRL.

The initial drop occurs over a short period following the onset of reactor operation. The magnitude of the RIA is consistent for all three irradiated SM YDFAs. The RIA rises quickly to approximately 40 dB/m at an average rate of 1 dB/m per minute. The rate of increase of the RIA slows down and reaches a saturation level above 40 dB/m. At this level of degradation, the transmission of signal light through the fiber is insignificant.

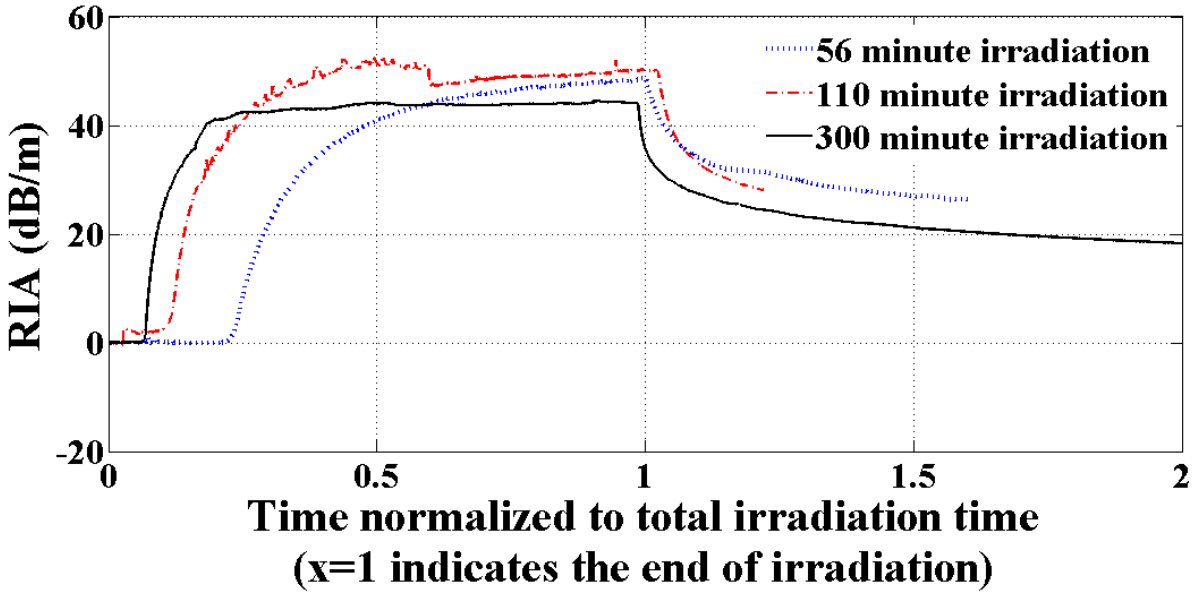

Figure 43. Time normalized RIA of the three SM YDFAs tested *in-situ* in the OSU-NRL.

The spectral data from a SM YDFA, Figure 44, shows that there is a clear decrease in the signal power output and an increase in the amount of pump light (inset) that is being transmitted through the fiber. The increased transmission of the pump light indicates that there is likely interference with the pump to Yb^{3+} energy transfer. There are multiple ways that this can occur. Primarily, a lower population of unexcited Yb^{3+} ions may be present that can accept the pump light. Thus, either more Yb^{3+} ions are already excited, or Yb^{3+} ions are changed to Yb^{2+} ions via interactions with incident radiation. There has yet to be a conclusive experiment in the literature that could answer whether or not Yb^{3+} ions change ionization state to Yb^{2+} following neutron irradiation of YDFs. Some publications have offered this as an explanation of their data, while others dispute the claim (Deschamps, Vezin, Gonnet, & Ollier, 2013) (Arai, Ichii, Tanigawa, & Fujimaki, 2009). The absorption of the Yb^{2+} ions has to be measured at very low wavelengths, in a region in which there is an increased absorption of silica itself. Therefore quantifying the Yb^{2+} concentration via absorption measurements is difficult. Additionally, as a result of non-radiative energy transfer from the excited Yb^{3+} ions to defect species, the Yb^{3+} ions may not fully relax to the ground state, but to an intermediate state that is not able to accept the 975 nm light.

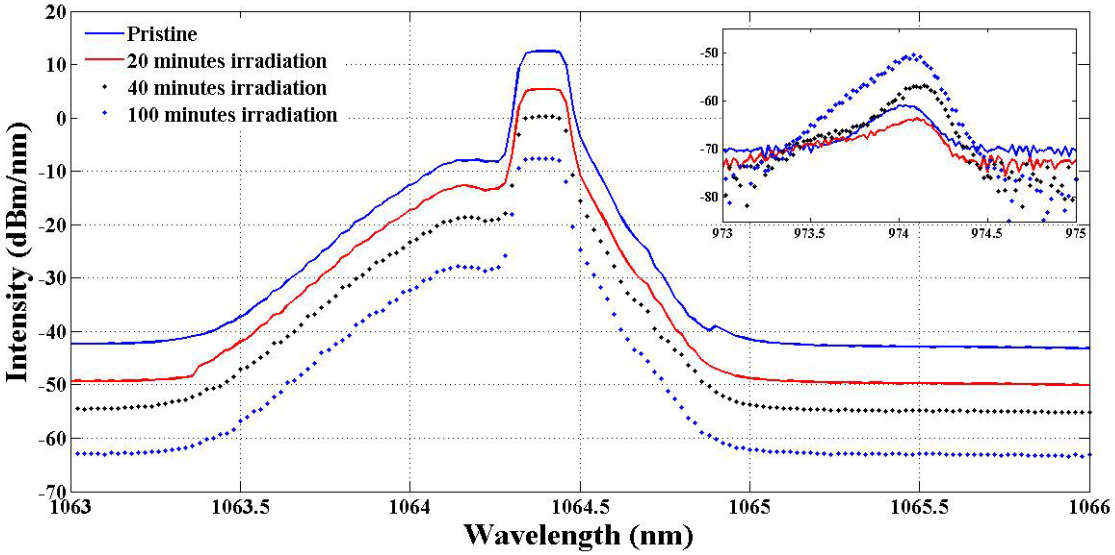

Figure 44. Spectral data from a SM YDFA at the OSU-NRL.

5.3.2 Multi-mode fiber irradiations

These tests documented saturating behavior in the RIA at all wavelengths. At 564 nm, the observed saturation of the RIA occurred at a significantly higher RIA than that at 1064 nm. The RIA at 1064 nm saturated after a relatively short time period. The MM YDFs also experienced a faster recovery of the RIA at 564 nm following irradiation. Figure 45 plots the RIA at 1064 nm with respect to irradiation time for each of the four MM YDFs tested. For each MM YDF, the RIA increases rapidly following approximately 15 to 20 minutes following the start up of the reactor. The RIA saturates at a level near 16 dB/m for this particular wavelength. A comparison of the RIA at different wavelengths for a single MM YDF is shown in Figure 46. The RIA at 564 nm increases well past that experienced at 1064 nm. Following irradiation, the RIA at 564 nm decreases much more rapidly than that at 1064 nm.

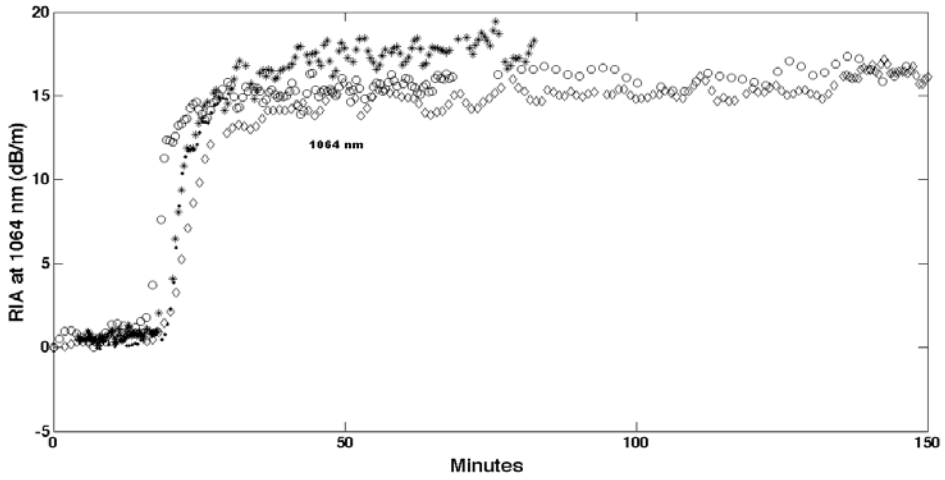

Figure 45. RIA for the 1064 nm wavelength through four of the multi-mode fibers during irradiation at the OSU-NRL. All fibers experience a similar rise in RIA following the start of irradiation and saturate at approximately 16 dB/m. Each symbol represents a separate MM YDF irradiation.

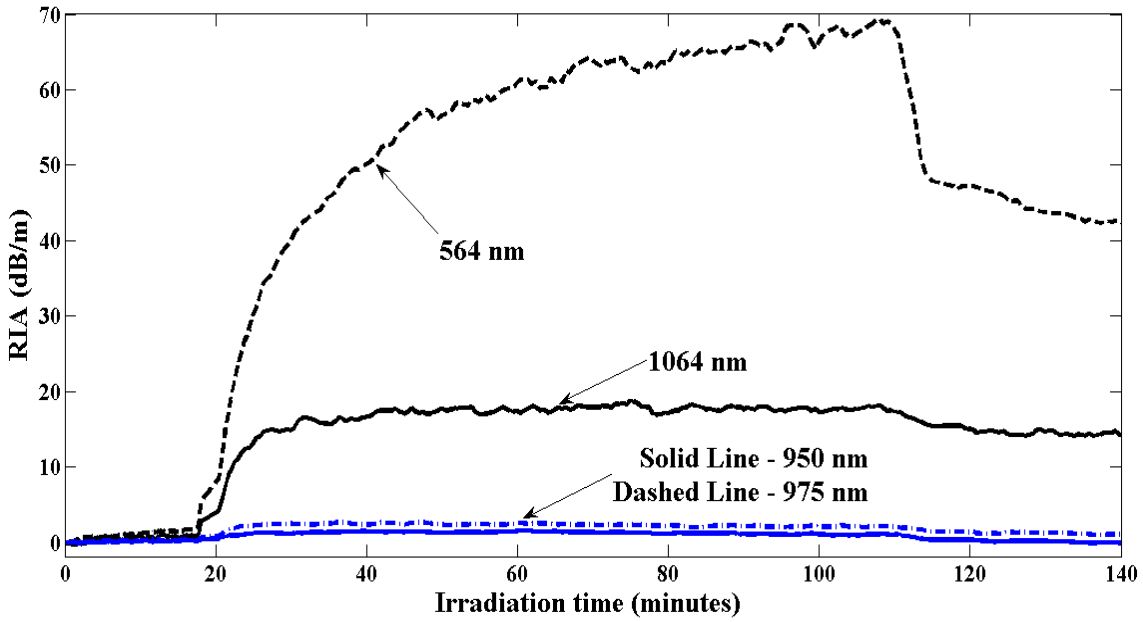

Figure 46. RIA for of a multi-mode YDF at select wavelengths during OSU-NRL irradiation. The irradiation ends at 108 minutes. The transmission of light at 950 nm and 975 nm changes little during irradiation. The recovery rate at the 564 nm wavelength is initially high. Recovery of the 1064 nm wavelength is minimal and slow.

The initial recovery rate corresponds well to the annealing of the damage at the 564 nm wavelength in the MM YDF. The recovery rate of the 1064 nm transmission in the MM YDF is lower than that of the amplified 1064 nm output of the SM YDFA exposed at the OSU-NRL. This indicates that the mechanism responsible for a large portion of the signal degradation through the YDFA during irradiation is related to the damage centers that have their maximum near 564 nm. These damage centers are created in close proximity to the Yb^{3+} ions. They are able to accept energy from the excited Yb^{3+} ions and thus degrade the amplified signal output. As the concentration of such transient defects is reduced, the long term damage representing more stable defects created in the fiber that can absorb the signal light directly and come to dominate the recovery.

The RIA with respect to wavelength for a MM YDF, shown in Figure 47 demonstrates a spectral behavior similar to that of the MM YDFs irradiated with a gamma only source shown in Figure 28. The RIA at the visible wavelengths increases more rapidly than that near 1064 nm during both irradiations. For the MM YDF exposed to the reactor radiation, the magnitude of the RIA is significantly higher and experiences a rapid increase a few minutes following the start up of the reactor that saturates at wavelength dependent times. The double arrow in Figure 47 indicates the change between two spectra taken 30 seconds apart. The entire span from the lowest curve to the highest RIA curve is taken over an irradiation time of 300 minutes.

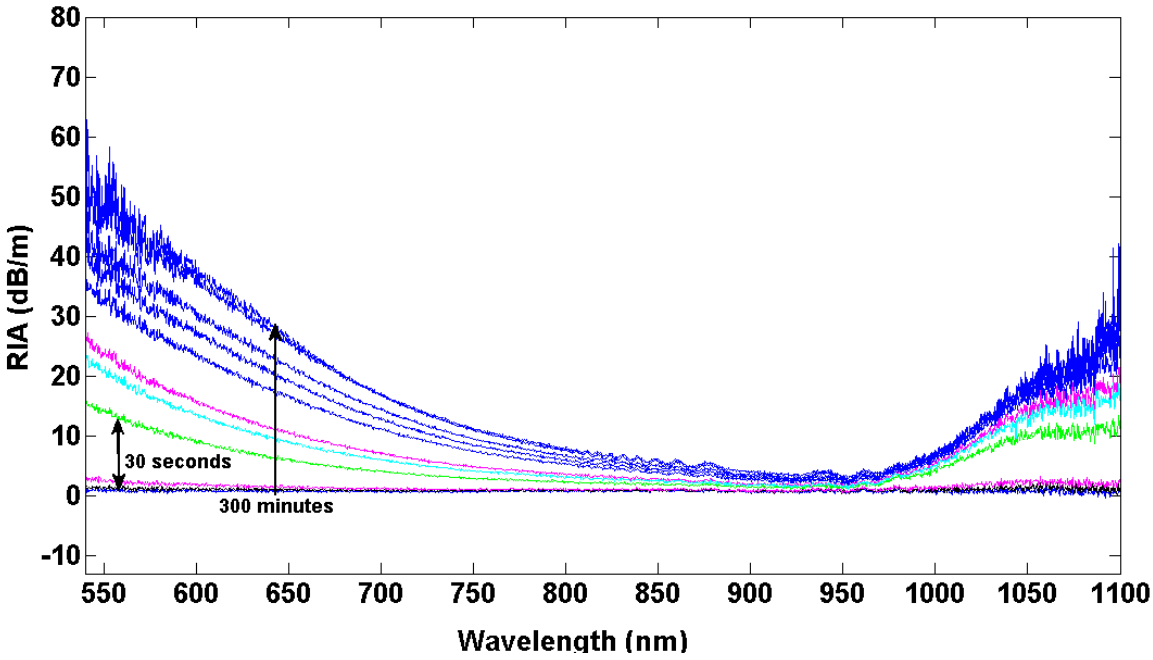

Figure 47. RIA of a multi-mode YDF across all measured wavelengths during OSU reactor irradiation. The RIA increases rapidly around 15 minutes after reactor start up and the the rate decreases to an eventual saturation.

What does it mean that the recovery of the SM YDFA output proceeds on pace with the 564 nm RIA but the degradation follows the pattern of the 1064 nm RIA of the MM YDF? Radiation-induced degradation of the SM YDFA amplified signal output is a result of two different mechanisms. The excited ions transfer their energy to defects instead of de-exciting through stimulated emission, and there are defects that are absorbing the 1064 nm light directly. The defects that affect the excited ion energy transfer anneal more rapidly than those that absorb 1064 nm light directly. In these fibers, there is indeed a saturation of the absorption leading to the signal loss at 1064 nm. There is no such saturation at the 564 nm wavelength at this dose (Figure 48). This implies that the degradation at the 1064 nm is related to a species in the fiber that is severely limited. This is indicative of an effect related to the Yb^{3+} ion concentration. There may be an increasing number of Al-based defects created in the close vicinity of the Yb^{3+} ions;

however, there are a limited number of Yb^{3+} ions that can transfer their energy to those defects. The production of interstitial O_2 molecules is likewise limited by the pre-irradiation precursors.

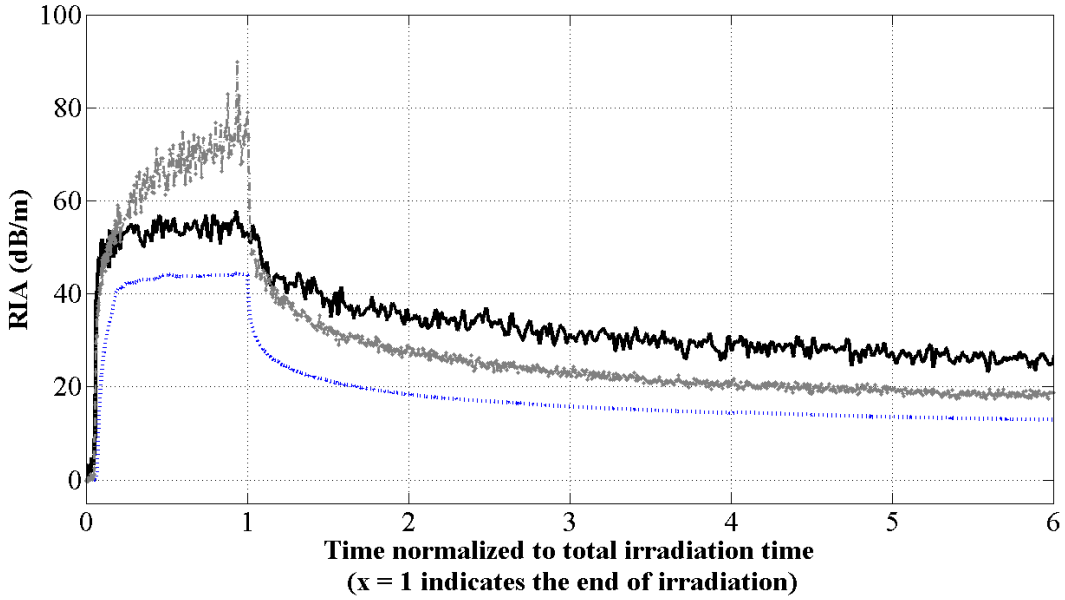

Figure 48. Time normalized RIA for the 5 hour irradiation of a MM YDF and SM YDFA. The dashed line is the output power of the YDFA. The gray line is the RIA of 564 nm through the MM YDF. The solid black line is the 1064 nm transmission through the MM YDF. The YDFA transmission saturates during irradiation similar to the 1064 nm transmission through the MM YDF. However, following irradiation, the RIA decreases at a rate that follows the rate of recovery of the 564 nm signal through the MM YDF.

5.3.3 Temperature effects on absorption

Increasing the fiber temperature results in a shift in the population density of the various Stark levels of the upper and lower energy regions. This will affect the absorption and emission at the corresponding wavelengths of transition. (Moore 2011). The increase in absorption in the 1010 to 1100 nm range is significant for temperatures of 600°C or more. For lower temperatures the absorption coefficient in the signal band increases from 2 to 5 dB/m when the temperature is raised from 25 to 167°C.

The temperature of the ACRR test chamber is maintained at 25°C throughout the test and recovery portions of the experiments. The OSU-NRL test chamber, however, is not actively

temperature controlled. Temperatures near the core range from 21 to 52°C during reactor operation and are dependent on ambient temperatures. The tests detailed in this work were conducted during late November and early December where average temperatures at the site were below freezing. Therefore, it can be assumed that the ambient temperature did not contribute changes in absorption due to excessive heating.

5.4 Conclusions

The power law was applied to the recovery curves of the amplified signal output power for the SM YDFs. For the Co-60 irradiated fibers, the power law effectively fits the entire range of RIA increase during irradiation. For the OSU-NRL irradiated SM fibers, the RIA increase is better fit using a saturating exponentials model (SEM), as in (18).

$$RIA(D) = \sum_i a_i (1 - \exp(-D / \tau_i)) \tag{18}$$

The white light source used to examine the absorption through the multi-mode (MM) fiber was not of a sufficient spectral power density to induce significant excitation in the fiber. For brevity, the results of the attenuation in the multi-mode fiber at 1064 nm were studied for each of the fibers irradiated by the reactor. The evolution of the RIA at 1064 nm involves a rapid rise beginning at approximately 15 minutes after the start of the reactor to a saturating value (~16 dB/m) within approximately 10 minutes. This behavior is plotted in Figure 45.

A power law fit of the RIA data from the MM YDFs was conducted for the 1064 nm curves. Examining the recovery of the transmission at 1064 nm during the first 40 minutes of recovery reveals a correlation with the exponent of the recovery time (-6.99 to -5.7). For the recovery over the entire time, the recovery is fit with exponentials that are significantly different (-6.99 to -1.04). For longer irradiation times, the exponent is less negative, which would indicate

a slower recovery. For shorter irradiation times, the exponent is more negative, indicative of a faster recovery.

A quadratic relationship of RIA increase with dose during the first ten minutes has been suggested for some RE doped fibers irradiated under high dose rate radiation (Lezius, et al., 2012). In the report, dose rates greater than 21 rad/sec were considered high dose rates. The ACRR and reactor tests both surpass this value. Based upon the initial increase in RIA for a MM fiber, the RIA growth fits very well to a quadratic function with respect to dose, Figure 49.

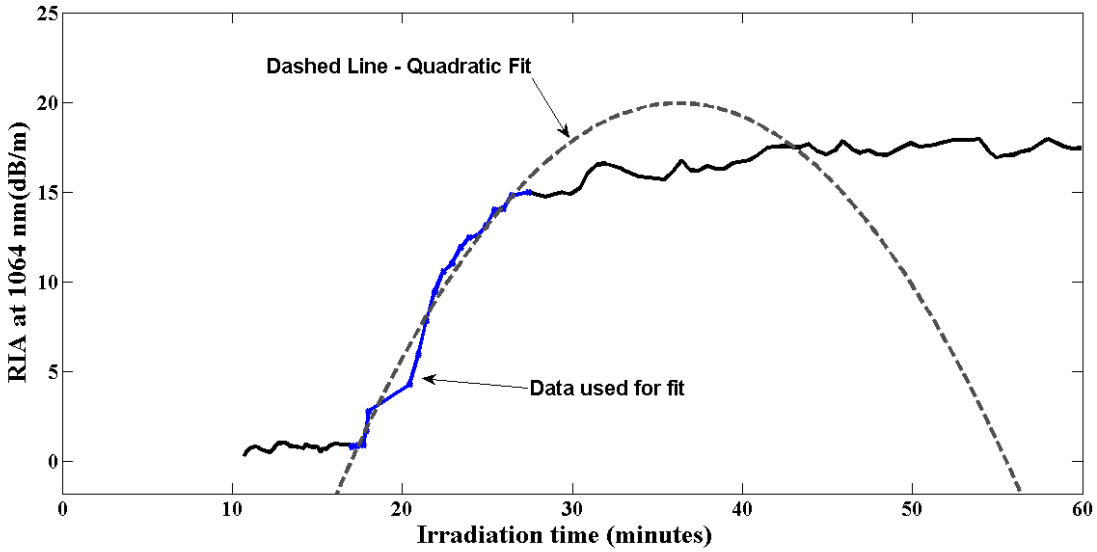

Figure 49. Initial RIA growth at 1064 nm fitted with a quadratic function.

The YDF that is not pumped shows an initial recovery of the 1064 nm transmission that proceeds more rapidly than the recovery of the amplified signal through the YDFAs. The transmission of the amplified signal is dependent on the processes associated with Yb^{3+} excitation and emission. These are the pump light to Yb^{3+} energy transfer, de-excitation of Yb^{3+} by stimulated emission and the absorption of the signal light in the fiber. In an unpumped fiber, the absorption of the signal light is a result of defect species that are created that can directly absorb the signal light as opposed to the energy transfer of the de-activation scenario in the

YDFA. The long term recovery rate of both the pumped and unpumped YDF occurs at the same rate. Therefore the permanent damage associated with the long term recovery is attributed to the same defect(s) for both fibers.

The loss in output of the amplified signal is attributed primarily to the Yb^{3+} deactivation and 1064 nm absorption. If the deactivation is a result of energy transfer to defects formed close to the Yb^{3+} ions, then it is most likely driven by the formation/annealing rate of the Al-based defects (with absorption centers around 564 nm). Absorption of 1064 nm light is a result of defects formed that absorb light at 1064 nm. The initial rate of recovery is more closely approximated by the recovery of the light at the 564 nm wavelength, an indication that deactivation of the excited Yb^{3+} ions is a primary damage mechanism in the YDFA. The long term degradation can be attributed to the absorption at the 1064 nm wavelength, possibly from interstitial O_2, which takes longer to anneal.

Jetschke et al. observed Yb^{3+} deactivation (not necessarily reduction to Yb^{2+}) in photodarkened fibers that was reversed with photobleaching. The report suggests that color centers in close vicinity to the Yb^{3+} ions function as a source of non-radiative transfer (Jetschke, et al., 2013).

It is interesting to see in the OSU-NRL and ACRR irradiation of MM fibers that the 564 nm wavelength exhibits an initial rapid recovery followed by a much slower revcovery. The 1064 nm transmission does not experience this. This can be an indication that the defects that absorb near the 564 nm wavelength are quickly annealed at room temperature. However, those at the 1064 nm wavelength are more stable at room temperature. This speculation is supported by Jetschke (2013) and the data of this research. Jetschke (2013) writes:

The absorption of color centers spectrally overlaps with Yb^{3+} emission; they can thus be hypothesized as acceptors of transferred energy if they remain in close vicinity to the Yb^{3+} ions after the PD process. Moreover, the complete recovery of ***fluorescence intensity and lifetime*** *after thermal bleaching of PD loss (temperature 600 degrees C) points to the color centers as the real acceptors of energy in the photodarkened fibers.*

The atomic defects generated during photodarkening in Yb fibers function not only as absorbing color centers for photons in the wavelength range from the visible up to near-IR (Jetschke, et al., 2013). They also are speculated to absorb energy from excited Yb^{3+} ions directly, because a strong, nearly linear correlation of photodarkening loss (proportional to density of color centers) and reduction of fluorescence is found. From the distinct efficiency of this non-radiative energy transfer this research support the conclusion that colors centers remain in close vicinity of the Yb^{3+} ions where they were generated during the pump-induced photodarkening process.

This energy transfer can cause additional loss of laser efficiency by the deactivation of Yb^{3+} ions that absorb pump power without contributing to the laser process. Further investigations, including modeling of Yb-doped fibers lasers, must be pursued to understand the impact of both color center absorption and Yb^{3+} deactivation on the performance of high power fiber lasers and amplifiers.

6 Analysis and Conclusions

6.1 Damage caused by gamma and gamma/neutron irradiation

The gain through the SM YDFA is primarily impaired by defects created at 564 nm and 1064 nm. The Al-based defects at 564 nm are responsible for the rate of recovery of the amplified signal in the short time following the end of irradiation. These defects cause the short time recovery of the SM YDFA to slow down in relation to a YDF that is not functioning as an amplifier. The long term recovery is governed by the recovery of the defects at 1064 nm. Both sets of defects are concentration limited. Therefore the SM YDFA experiences saturation of absorption after a specific total dose although the absorption of the defects at 564 nm continues to increase.

No significant contribution to the system degradation under irradiation by the passive fibers was observed. Under pulsed reactor irradiation, the passive fiber demonstrated a higher degradation of transmission at 1064 nm than at 564 nm, which is opposite of that in the MM YDFs irradiated in the OSU-NRL. The increased and slowly saturating damage at 564 nm in the MM YDF directly results from the incorporation of Yb^{3+} ions into the fiber. This result also further supports the supposition that the damage centers created by irradiation that influence Yb^{3+} de-activation are created in close proximity to the Yb^{3+} ions.

There are three mechanisms for light absorption from radiation-induced defects that can lead to degradation to YDFA performance. The first mechanism involves absorption of pump light by defects other than the Yb^{3+} ions. In other words, active ion excitation decreases, which constrains the number of photons that can be amplified. The second is the non-radiative transfer of energy from excited Yb^{3+} ions to defects instead of light emission. These defects are presumed to be created and remain in close vicinity to the Yb^{3+} atoms. This mechanism is

referred to as Yb^{3+} deactivation (Jetschke, 2013). The third mechanism is the increased absorption of the signal light (in 1000+ nm range) by defects in the fiber. This absorption affects the signal light input into the fiber along with any signal light that happens to get amplified by the Yb^{3+} ions. All three mechanisms can be present at the same time.

There is evidence that the second and third mechanisms dominate the degradation of signal light amplification. For instance, during reactor irradiation, the light transmission through the multi-mode fiber at the pump wavelength decreased by an insignificant amount. Indeed spectral measurements from the SM YDFA indicated that as radiation exposure increased, the amount of pump light absorbed in the fiber decreased. This implies that the creation of defects that absorb the pump light was minimal. However, defects are created that interfere with the excitation and de-excitation of Yb^{3+} ions. The light absorption at the signal wavelength increased significantly, leading to the conclusion that excited Yb^{3+} deactivation along with signal light absorption dominate the loss of gain.

Comparing the recovery of the signal amplification of the SM YDF amplifiers to the wavelength dependent transmission recovery of the MM YDFs provided insight as to whether or not deactivation is primary for absorption of the signal wavelength. The signal light absorption dominates the long term recovery. In addition, the signal light that is amplified also suffers absorption as it travels through the fiber. In the short time following irradiation, deactivation dominates and the rate of recovery resembles the recovery of the transmission of light wavelengths below 800 nm. As the color centers anneal, the non-radiative decays from the Yb^{3+} ions to the color centers will decrease and the light emission will increase.

A majority of transient damage in YDFA output is from species that absorb at 564 nm. This is indicative of the de-activation mechanism being the prime source of signal degradation in

the short time following irradiation. The longer lived effects are a result of defects that absorb light directly at 1064 nm. (It has been suggested that there is interstitial O_2.)

Co-60 irradiations of passive and active operated SM YDFAs along with passive irradiations of MM YDFs formed the first half of this current research. For the SM YDFAs, the data collected was comprised of amplified output signal power and spectral measurements from 970 to 1100 nm. In the SM YDFAs, it was found that the intensity of the output of the ASE decreased at a slower rate than that of the output amplified signal. This indicated that the excitation of Yb^{3+} ions is not significantly affected by irradiation; however direct absorption of the signal light and non-radiative transfer of energy to defects increased.

The measurements of a white light source transmission through the MM YDFs revealed that RIA is greater at wavelengths below 900 nm than it is at wavelengths above 980 nm. The standard approach to this absorption pattern has been to attribute it to color centers produced in the visible portion of the spectrum that have wide band-tails which absorb well into the near IR (thus leading to the absorption above 980 nm). However, fitting of the known Al-defects to the absorption curve does not correspond well with regards to the absorption at 1064 nm. This absorption is attributed to the formation of interstitial O_2 molecules in the YDF. Formation of these molecules is based on the concentration of precursors in the fiber and is concentration limited. The absorption at 1064 nm saturates after a given total dose exposure, whereas the absorption at 564 nm does not.

The set of gamma irradiations at low dose rates (compared to the reactor irradiations) demonstrated that the SM and MM YDFs would not be completely darkened within a short time of radiation exposure. This ensured that measurements of the change in the fiber transmission could be measured in the ACRR and OSU-NRL radiation environments without loss of signal.

ACRR pulse irradiation of the SM YDFAs demonstrated that the damage to the output of the amplified signal increases with increased reactor pulse power. Pulse power is synonymous with gamma dose and neutron flux and inversely to radiation exposure time. At the highest pulse powers tested, there was no indication of saturation of the damage before the system began to recover. Following irradiation, there is an initial rapid recovery period followed by a much slower recovery that does not reach complete recovery in the times monitored (over 8 hours in some cases). The initial recovery of the SM YDFA is dominated by the recovery of the Al-based defects. The long term recovery is influenced by the recovery of defects that absorb the signal light directly. A passive MM DC fiber was tested in the ACRR as well. The result was that minimal loss occurred during the pulse (less than 30% for all wavelengths) and recovered to pre-irradiation levels in minutes following the pulse. The observation was made that in the passive fiber, the 1064 nm loss is greater than that of the 564 nm. In the Yb-doped fiber, the 564 nm loss is significantly higher than that at 1064 nm. This indicates that the increased loss at 564 nm is a direct result of the Yb-do\ping.

Steady state reactor irradiations of SM YDFAs and MM YDFs provided data on the rate of loss and recovery which verified that in the operation of the SM YDFA, the Al-based defects and the absorption of light at 1064 nm are responsible for the degradation experienced under irradiation. The spectral data analyzed indicated a decrease in the intensity of the 1064 nm signal during irradiation, but also included an apparent increase in the transmission of the residual pump light at 975 nm, as expected. The conclusion is that there is some damage induced that interferes with the excitation of the Yb^{3+} ions, thus leading to a lower absorption of pump light.

Based upon the initial increase in RIA for a MM fiber, the RIA growth at 1064 nm fits very well to a quadratic function with respect to dose. The loss of the 1064 nm amplified signal saturates at a level that is far below the input signal level indicating a negative gain through the SM YDFA. However, the loss of light at 564 nm through the MM YDF slows but does not saturate during irradiation. The loss and recovery of the signal through the SM YDFA can be modeled as a result of the loss and recovery at 564 nm and 1064 nm. The initial recovery of the signal is dominated by the recovery of the Al-based defects and the long term recovery follows that of the 1064 nm absorption centers.

The losses measured in each radiation scenario were found to recover at room temperature although very slowly following an initial rapid recovery of a portion of the loss. No fiber experienced recovery to pre-irradiation transmission. The permanent damage induced in the fibers affects the absorption of light at the signal wavelength and in the visible light wavelength range. Both regions of absorption involve defect species that degrade the performance of SM YDFAs.

Examining the three sets of irradiation experiments reveals an overarching relationship between the concentration of Al-dopants incorporated in the fiber along with the Yb^{3+} ions and the amount of precursors to the formation of interstitial O_2. Both have an effect on the RIA through the formation of defects that contribute to the loss of intensity of the 1064 nm light either through direct absorption or through precluding amplification through de-activation of the excited Yb^{3+} ions.

6.2 Numerical model results

The profile of the absorption with respect to ionizing dose for the MM YDFs irradiated in the OSU-NRL was used to update the numerical model. Two additional Gaussian curves were

added to the Yb-doped fiber absorption spectrum calculation. The first Gaussian, representing the absorption from the Al-based defects was centered at 550 nm. The absorption of a MM YDF exposed to the reactor irradiation was used to determine the coefficients for the Gaussian curves. The second Gaussian was centered at 1064 nm. For the case in which only the 550 nm absorption is included, the coefficients used spanned a range equivalent to the 70 dB/m RIA measured. The modeled RIA for the signal output is minimal (less than 1 dB/m). Even for the highest coefficient values, there was little increase in the RIA produced by the model. For the case of only the 1064 nm added absorption, the output signal experienced much more intense power loss and also negative gain for absorption coefficient values relative to those measured. The result that is calculated when both Gaussians are included in the model produced an output signal degradation closer to what is measured. However, there was still less of a degradation on the gain that is expected, see Figure 50.

In order to model the de-activation of the Yb^{3+} ions as a mechanism of damage, the absorption at the signal wavelength was increased at a magnitude nearly equivalent to that of the absorption at the 550 nm wavelength (equivalent to 70 dB/m). This approach will not properly estimate the signal absorption through a fiber in passive mode, but it does simulate the increased signal loss in an active SM YDFA.

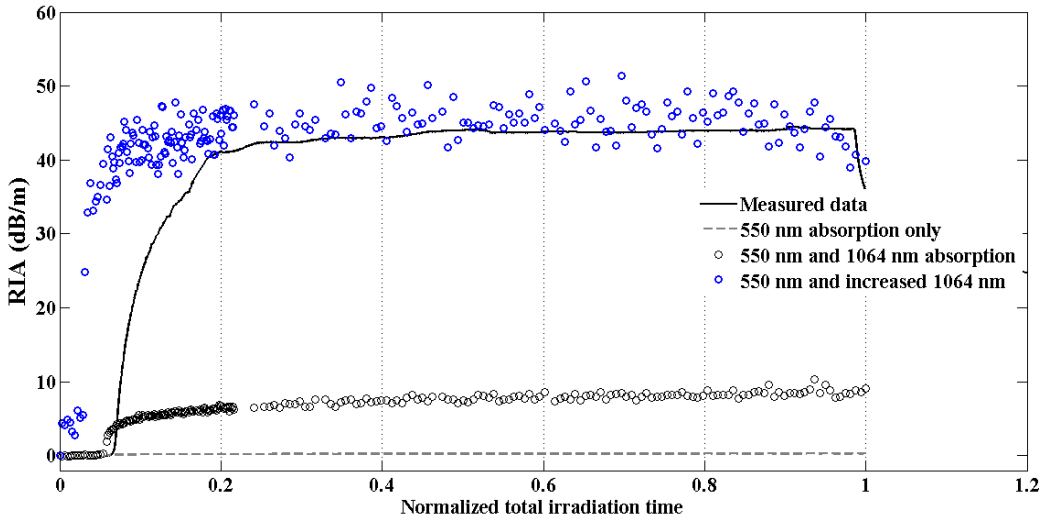

Figure 50. RIA of the 1064 nm output signal from an OSU-NRL irradiated SM YDFA plotted with the RIA that results from the effects of modeling the absorption curves in the simulation.

6.3 Future research

More research on the radiation effects on Yb-doped and other RE-doped optical fiber materials is needed to produce a robust body of knowledge that can lead to radiation-insensitive optical systems. To determine the neutron-specific sensitivity of the fibers, a neutron-only exposure should be performed on the YDFs. The results can then be compared to the gamma only and gamma/neutron irradiations. In addition, a broader range of dose rates for gamma irradiation should be performed to effectively determine the dose-rate effect on RIA. MM YDFA experiments for high power applications should also be performed in the ACRR and OSU-NRL. The common approach to an all-fiber laser incorporates the use of MM and SM YDFs. A representative system should be evaluated in a radiation environment as this will most likely be an optical of system of great interest to those planning for the use of optical based materials in harsh environments. The source of absorption at 1064 nm should be verified using luminescence measurements. If interstitial O_2 is involved, there should be characteristic luminescence at 1270 nm in the presence of 1064 nm laser light.

REFERENCES

Ahrens, R. G., Abate, J. A., Jaques, J. J., Presby, H. M., Fields, A. B., DiGiovanni, D. J., LuValle, M. J. (1999). Radiation reliability of rare earth doped optical fibers for laser communication systems (LT). *Military Communications Conference Proceedings* (pp. 694-697). IEEE.

Ahrens, R. G., Jaques, J. J., LuValle, M. J., DiGiovanni, D. J., & Windeler, R. S. (2001). Radiation effects on optical fibers and amplifiers. *Testing, Reliability, and Applications of Optoelectronic Devices.* SPIE.

Alam, M., Abramczyk, J., Madasamy, P., Torruellas, W., & Sanchez, A. (2007). Fiber Amplifier Performance in Gamma-Radiation Environment. *OSA Optical Fiber Conference - Paper OMF4.*

Arai, T., Ichii, K., Tanigawa, S., & Fujimaki, M. (2009). Photodarkening Phenomenon in Yb-doped Fibers. *Fujikara University Technical Review*, pp. 6-11.

Bakos, T. (2003, December). Defects in Amorphous SiO2: Reactions, Dynamics and Optical Properties. Nashville, Tennessee: Dissertation Graduate School of Vanderbilt Univeristy.

Barnes, C. E., & Wiczer, J. J. (1984). *Radiation Effects in Optoelectronic Devices.* Albuquerque, NM: Sandia National Laboratory, Technical Report.

Berghmans, F., Brichard, B., Fernandez Fernandez, A., Gusarov, A., Van Uffelen, M., & Girard, S. (2008). An Introduction to Radiation Effects on Optical Componenents and Fiber Optic Sensors. In W. J. Bock, I. Gannot, & S. Tanev, *Optical Waveguide Sensing and Imaging* (pp. 127-165). Dordrecht, The Netherlands: Springer.

Bjarklev, A. (1993). *Optical Fiber Amplifiers: Design and System Applications.* Norwood, MA: Artech House, Inc.

Brichard, B., & Fernandez, A. F. (2005). Radiation effects in silica glass optical fibres. *RADECS 2005 Conference Short Course on New Challenges for Radiation Tolerance Assessment from Deep Space Environments to Fusion Reactor Environments*, (pp. 95-138).

Brückner, R. (1970). Properties and Structure of Vitreous Silica I. *Journal of Non-Crystalline Solids, 5*, 123-175.

Budz, A. J., Waisman, J., Tiedje, H. F., & Haugen, H. K. (2009). Short-Pulse Dual-Wavelength System Base on Mode-Locked Diode Lasers With a Single Polarization-Maintaining Yb:Fiber Amplifier. *Journal of Lightwave Technology, 27*(16), 3416-3424.

Bussjager, R. J., Hayduk, M. J., Johns, S. T., & Taylor, E. W. (2002). Comparison of radiation-induced passive and dynamic response in two erbium-doped fiber lasers. *IEEE Aerospace Conference* (pp. 3-1369-3-1379). Rome, Italy: IEEE.

Cheeseman, M., Bowden, M., Akinci, A., Knowles, S., & Webb, L. (2012). Neutron testing of high-power optical fibers. In G. J. Exarhos, V. E. Gnuzdev, J. A. Menapace, R. M. Detlev, & M. J. Soileau (Ed.), *Laser-Induced Damage in Optical Materials. 8530*, pp. 18-1 to 18-17. SPIE.

Choate, L. M., & Schmidt, T. R. (1979). *Sandia Laboratories Radiation Facilities.* Kirtland AFB, NM: Sandia Laboratories.

Deschamps, T., Vezin, H., Gonnet, C., & Ollier, N. (2013, March 29). Evidence of AlOHC responsible for the radiation-induced darkening in Yb doped fiber. *Optics Express, 21*(7), 8382-8392.

Dicks, B.-M., Heine, F., Petermann, K., & Huber, G. (2001). Characterization of a Radiation-Hard Single-Mode Yb-Doped Fiber Amplifier at 1064 nm. *Laser Physics, 11*(1), 134-137.

DiGiovanni, D. J., Shubochkin, R., Morse, T. F., & Lenardic, B. (2007). Rare Earth-Doped Fibers. In A. Méndez, & T. F. Morse, *Specialty Optical Fibers Handbook* (pp. 195-242). Burlington, MA: Elsevier Academic Press.

Dragic, P. D., Carlson, C. G., & Croteau, A. (2008). Characterization of defect luminescence in Yb doped silica fibers: part I NBOHC. *Optics Express, 16*(7), 4688-4697.

Fox, B. P. (2013). *Investigation of Ionizing-Radiation-Induced Photodarkening in Rare-Earth-Doped Optical Fiber Amplifier Materials.* PhD Dissertation, University of Arizona.

Fox, B. P., Schneider, Z. V., Simmons-Potter, K., Thomes, J. W., Meister, D. C., Bambha, R. P., & Kliner, D. A. (2008). Spectrally Resolved Transmission Loss in Gamma Irradiated Yb-Doped Optical Fibers. *IEEE Journal of Quantum Electronics, 44*(6), 581-585.

Fox, B. P., Schneider, Z. V., Simmons-Potter, K., Thomes, W. J., Meister, D. C., Bambha, R. P., Soderlund, M. J. (2007). Gamma Radiation Effects in Yb-Doped Optical Fiber. *Fiber Laser IV: Technology, Systems, and Applications. 6453.* SPIE.

Fox, B. P., Simmons-Potter, K., Kliner, D. A., & Moore, S. W. (2013). Effect of low-earth orbit space on radiation-induced absorption in rare-earth-doped optical fibers. *Journal of Non-Crystalline Solids, 378*, 79-88.

Fox, B. P., Simmons-Potter, K., Moore, S. W., Fisher, J. H., & Meister, D. C. (2009). Gamma-Radiation-Induced Photodarkening in Actively Pumped Yb3+ - Doped Optical Fiber and

Investigation of Post-Irradiation Transmittance Recovery. *Optical Technologies for Arming, Safing, Fuzing, and Firing V.* San Diego, CA: SPIE.

Fox, B. P., Simmons-Potter, K., Thomes Jr., W. J., & Kliner, D. A. (2010). Gamma-Radiation-Induced Photodarkening in Unpumped Optical Fibers Doped With Rare-Earth Constituents. *IEEE Transactions on Nuclear Science, 57*(3), 1618-1625.

Friebele, E. J. (1992). *Correlation of single mode fiber fabrication factors and radiation response.* Washington, D.C.: Naval Research Laboratory, Technical Report.

Friebele, E. J., Schultz, P. C., & Gingerich, M. E. (1980). Compositional effects on the radiation response of Ge-doped silica-core optical fiber waveguides. *Applied Optics, 19*(17), 2910-2916.

Gill, K., Grabit, R., Persello, M., Stefanini, G., & Vasey, F. (1997). Gamma and neutron radiation damage studies of optical fibres. *Journal of Non-Crystalline Solids, 216*, 129-134.

Girard, S. (2003). *Analyse De La Reponse Des Fibres Optiques Soumises a Divers Environnments Radiatifs.* L'Universite Jean Monnet de Saint-Étienne, PhD Dissertation.

Girard, S., & Marcandella, C. (2010). Transient and Stead State Radiation Responses of Solarization-Resistant Optical Fibers. *IEEE Transactions on Nuclear Science, 54*(4), 2049-2055.

Girard, S., Kuhnhenn, J., Gusarov, A., Brichard, B., Van Uffelen, M., Ouerdane, Y., Marcandella, C. (2013). Radiation Effects on Silica-Based Optical Fibers: Recent Advances and Future Challenges. *IEEE Transactions on Nuclear Science, 60*, 2015-2036.

Girard, S., Ouerdane, Y., Boukenter, A., & Meunier, J.-P. (2006). Transient radiation responses of silica-based optical fibers: Influence of modified chemical vapor deposition process parameters. *Journal of Applied Physics, 99*, 023104.

Girard, S., Ouerdane, Y., Tortech, B., Marcandella, C., Robin, T., Cadier, B., Blackmore, E. W. (2009, December). Radiation effects on ytterbium- and ytterbium/erbium-doped double-clad optical fibers. *IEEE Transactions on Nuclear Science, 56*(6), 3293-3299.

Girard, S., Tortech, B., Régnier, E., Van Uffelen, M., Gusarov, A., Ouerdane, Y., Thienpont, H. (2007). Proton- and Gamma-Induced Effects on Erbium-Doped Optical Fibers. *IEEE Transactions on Nuclear Science, 54*(6), 2426-2434.

Girard, S., Vivona, M., Laurent, A., Cadier, B., Marcandella, C., Robin, T., Ouerdane, Y. (2012). Radiation hardening techniques for Er/Yb doped optical fibers and amplifiers for space application. *Optics Express, 20*(8), 8457-8465.

Griscom, D. L. (1985). Defect Structure of Glasses - Some outstanding questions in regard to vitreous silica. *Journal of Non-Crystalline Solids, 73*, 51-77.

Griscom, D. L., Gingerich, M. E., & Friebele, E. J. (1993). Radiation-Induced Defects in Glasses: Origin of Power-Law Dependence of Concentration on Dose. *Physcial Review Letters, 71*, 1019-1022.

Gusarov, A., Van Uffelen, M., Hotoleanu, M., Thienpont, H., & Berghmans, F. (2009). Radiation sensitivity of EDFAs based on highly Er-doped fibers. *Journal of Lightwave Technology, 27*(11), 1540-1545.

Hecht, J. (2006). *Understanding Fiber Optics* (5th ed.). Upper Saddle River, New Jersey: Pearson Prentice Hall.

Henschel, H., & Köhn, O. (1993). Radiation sensitivity of passive fibre optic components. *SPIE Proceedings Vol. 1973*, (pp. 250-261).

Henschel, H., Köhn, O., Schmidt, H. U., Kirchhof, J., & Unger, S. (1998, June). Radiation induced loss of rare earth doped silica fibers. *IEEE Transactions on Nuclear Science, 145*(3), 1552-1557.

Hosono, H., & Kawazoe, H. (1994). Radiation-induced coloring and paramagnetic centers in synthetic SiO2:Al glasses. *Nuclear Instruments and Methods in Physics Research Section B, 91*(1-4), 395-399.

Jetschke, A., Schwuchow, A., Unger, S., Leich, M., Jager, M., & Kirchhof, J. (2013). Deactivation of Yb3+ ions due to photodarkening. *Optical Materials Express, 3*(4), 452-458.

Jockusch, S., Turro, N. J., Thompson, E. K., Gouterman, M., Callis, J. B., & Khalil, G. E. (2007). Singlet molecular oxygen by direct excitation. *Photochemical & Photobiological Sciences, 7*, 235-239.

Johns, S. T., Hayduk, M. J., Bussjager, R. J., Gerhardstein, C. M., Vettese, E. K., Fanto, M. L., & Taylor, E. W. (2003). Temporal responses of actively modelocked erbium-doped fibre laser irradiated by gamma-rays. *Electronics Letters, 39*(18), 1310-1312.

Johnston, A. (2004). Optical Sources, Fibers, and Photonic Subsystems. *Nuclear and Space Radiation Effects Conference, Course Materials.* Atlanta, GA: IEEE.

Kajihara, K., Masahiro, H., Motoko, U., Morimoto, Y., Skuja, L., & Hosono, H. (2005). Interstitial oxygen molecules in amorphous SiO2 I.Quantitative concentration analysis by

thermal desorption, infrared photoluminescence, and vacuum-ultraviolet optical absorption. *Journal of Applied Physics, 98,* 013527-1 to 7.

Koester, C. J., & Snitzer, E. (1964). Amplification in a Fiber Laser. *Applied Optics, 3*, 1182-1186.

Kokki, T., Koponen, J., Laurila, M., & Ye, C. (2010). *Fiber amplifier utilizing an Yb-doped large-mode-area fiber with confined doping and tailored refractive index profile.* Lohja, Finland: nLight Corporation, Technical Report.

Koponen, J. (2008). *Measuring Photodarkening from Yb Doped Fibers.* Helsinki, Finland: Helsinki University of Technology, PhD Dissertation.

Lezius, M., Predehl, K., Stöwer, W., Türler, A., Greiter, M., Hoeschen, C., Holzwarth, R. (2012). Radiation Induced Absorption in Rare Earth Doped Optical Fibers. *IEEE Transactions on Nuclear Science, 59*, 425-433.

Liu, H. (2011). *Ytterbium-Doped Fiber Amplifiers: Computer Modeling of Amplifier Systems and a Preliminary Electron Microscopy Study of Single Ytterbium Atoms in Doped Optical Fibers.* McMaster University, Open Access Dissertations and Theses, Master's Thesis.

Mady, F., Benabdesselam, M., Mebrouk, Y., & Dussardier, B. (2010). Radiation effects on ytterbium-doped silica optical fibers: traps and color centers related to the radiation-induced optical losses. *RADECS Proceedings - Paper LN2.*

Mattern, P. L., Watkins, L. M., Skoog, C. D., & Barsis, E. H. (1975). Absorption Induced in Optical Waveguides by Pulsed Electrons as a Function of Temperature, Low Dose Rate Gamma and Beta Rays, and 14 MeV Neutrons. *IEEE Transactions on Nuclear Science, 22*(6), 2468-2474.

Ollier, N., Planchais, R., & Boizot, B. (2008). EPR study of Yb-doped irradiated glasses. *Nuclear Instruments and Methods in Physics Research B, 266,* 2854-2858.

Ott, M. (2004). *Radiation Effects Expected for Fiber Laser/Amplifier Rare Earth Doped Optical Fiber*. NASA. Retrieved 2012 from www.misspiggy.gsfc.nasa.gov/tva/

Ouerdane, Y., Girard, S., Tortech, B., Robin, T., Marcandella, C., Boukenter, A., Crochet, P. (2009). Vulnerability of rare-earth-doped fibers for space missions: origins of radiation-induced attenuation. *Fiber Optic Sensors and Applications VI. 7316.* San Francisco, CA: SPIE.

Paschotta, R., Nilsson, J., Tropper, A. C., & Hanna, D. C. (1997, July). Ytterbium-doped fiber amplifiers. *IEEE Journal of Quantum Electronics, 33*(7), 1049-1046.

Pask, H. M., Carman, R. J., Hanna, D. C., Tropper, A. C., Mackechnie, C. J., Barber, P. R., & Dawes, J. M. (1995). Ytterbium-Doped Silica Fiber Lasers: Versatile Sources for the 1-1.2 micrometer Region. *IEEE Journal of Selected Topics in Quantum Electronics, 1*(1), 2-13.

Rose, T. S., Gunn, D., & Valley, G. C. (2001). Gamma and Proton Radiation Effects in Erbium-Doped Fiber Amplifiers: Active and Passive Measurements. *Journal of Lightwave Technology, 19*(12), 1918-1923.

Rumbaugh, L. (2013, July 22). *Fiber Lasers and Amplifiers Design Toolbox - File Exchange.* Retrieved August 3, 2013, from MATLAB Central File Exchange: http://www.mathworks.com/matlabcentral/fileexchange/42122-fiber-lasers-and-amplifiers-design-toolbox

Salh, R. (2011). *Silicon Nanocluster in Silicon Dioxide: Cathodoluminescence, Energy Dispersive X-Ray Analysis, Infrared Spectroscopy Studies.* Retrieved Sep 23, 2012, from INTECH: http://www.intechopen.com/books/crystalline-silicon-properties-and-uses/silicon-nanocluster-in-silicon-dioxide-cathodoluminescence-energy-dispersive-x-ray-analysis-infrared

Singleton, B. J., Jones, B. S., Bickley, A. A., Petrosky, J. C., McClory, J. W., & Kowash, B. R. (2011). Radiation effects on YAG:Ce scintillating fiber. *IEEE Nuclear Science Symposium and Medical Imaging Conference* (pp. 1935-1940). Valencia, Spain: IEEE.

Singleton, B., Petrosky, J., Pochet, M., Usechak, N. G., & Francis, S. A. (2014). Gamma radiaton-induced degradation of actively pumped single-mode ytterbium-doped optical fibers. *Optical Components and Materials XI. 8982.* San Francisco, CA: SPIE.

Skuja, L. (2000). Optical Properties of Defects in Silica. In G. Pacchioni, L. Skuja, & D. L. Griscom, *Defects in SiO2 and Related Dielectrics: Science and Technology* (pp. 73-116). Dordrecht, The Netherlands: KluwerAcademic Publishers.

Skuja, L., Güttler, B., Schiel, D., & Silin, A. (1998). Infrared photoluminescence of preexisting or irradiation-induced interstitial oxygen molecules in glassy SiO2 and α-quartz. *Physical Review B, 58*, 14296-14304.

Snitzer, E., & Woodcock, R. (1965). Yb3+-Er3+ Glass Laser. *Applied Physics Letters, 6*, 45-46.

Soh, D. B., Bisson, S. E., Patterson, B. D., & Moore, S. W. (2011). High-power all-fiber passively Q-switched laser using a doped fiber as a saturable absorber: numerical simulations. *Optics Letters, 36*(13), 2536-2538.

Srour, J. R., Marshall, C. J., & Marshall, P. W. (2003, June). Review of Displacement Damage Effects in Silicon Devices. *IEEE Transactions on Nuclear Science, 50*(3), 653-670.

Sumimura, K., Yoshida, H., Hisanori, F., & Nakatsuka, M. (2006). Yb fiber mode locked laser with a wide tuning range for chirped pulse amplification systems. *IEICE Electronics Express, 3*(11), 233-237.

Tammela, S. K., Söderlund, M. J., Koponen, J. J., Philippov, V., & Stenius, P. (2006). The Potential of Direct Nanoparticle Deposition for the Next Generation of Optical Fibers. *Photonics West OPTO Symposium. 6116.* SPIE.

Taylor, E. W., & Liu, J. (2005). Ytterbium-doped fiber laser behavior in a gamma-ray environment. *Photonics for Space Environments X. 5897.* Bellingham, WA: SPIE.

Taylor, E. W., McKinney, S. J., Sanchez, A. D., Paxton, A. H., Craig, D. M., Winter, J. E., Kaliski, R. (1998). Gamma-ray induced effects in erbium-doped fiber optic amplifiers. *Photonics for Space Environments VI. 3440.* San Diego, CA: SPIE.

Van Uffelen, M., Girard, S., Goutaland, F., Gusarov, A., Brichard, B., & Berghmans, F. (2004). Gamma Radiation Effects in Er-Doped Silica Fibers. *IEEE Transactions on Nuclear Science, 51*(5), 2763-2769.

West, R. H., Dowling, S., Lewis, R. B., Sikora, E. S., & Wright, J. V. (1992). The effects of ionising radiation and hydrogen on erbium doped fibre amplifiers. *Optical Materials Reliability and Testing. 1791.* SPIE.

White, S. (2013, September 9). *Personal communication*.

Williams, G. M., Putnam, M. A., & Friebele, E. J. (1996). Space radiation effects on erbium doped fibers. *Photonics for Space Environments IV. 2811.* SPIE.

Wright, A. C. (2000). Defect-free Vitreous Networks. In G. Pacchioni, L. Skuja, & D. L. Griscom, *Defects in SiO2 and Related Dielectrics* (pp. 1-35). Dordrecht: Kluwer Academic.

REPORT DOCUMENTATION PAGE		*Form Approved* *OMB No. 0704–0188*

The public reporting burden for this collection of information is estimated to average 1 hour per response, including the time for reviewing instructions, searching existing data sources, gathering and maintaining the data needed, and completing and reviewing the collection of information. Send comments regarding this burden estimate or any other aspect of this collection of information, including suggestions for reducing this burden to Department of Defense, Washington Headquarters Services, Directorate for Information Operations and Reports (0704–0188), 1215 Jefferson Davis Highway, Suite 1204, Arlington, VA 22202–4302. Respondents should be aware that notwithstanding any other provision of law, no person shall be subject to any penalty for failing to comply with a collection of information if it does not display a currently valid OMB control number. PLEASE DO NOT RETURN YOUR FORM TO THE ABOVE ADDRESS.

1. REPORT DATE (DD–MM–YYYY) 02-06-2014	2. REPORT TYPE Doctoral Dissertation	3. DATES COVERED *(From — To)* Oct 2010 – May 2014

4. TITLE AND SUBTITLE Radiation Effects on Ytterbium-doped Optical Fibers	5a. CONTRACT NUMBER
	5b. GRANT NUMBER JON 13P290/JON14P270
	5c. PROGRAM ELEMENT NUMBER
6. AUTHOR(S) Singleton, Briana J., Major, USAF	5d. PROJECT NUMBER
	5e. TASK NUMBER
	5f. WORK UNIT NUMBER
7. PERFORMING ORGANIZATION NAME(S) AND ADDRESS(ES) Air Force Institute of Technology Graduate School of 2950 Hobson Way WPAFB OH 45433-7765	8. PERFORMING ORGANIZATION REPORT NUMBER AFIT-ENP-DS-14-J-15
9. SPONSORING / MONITORING AGENCY NAME(S) AND ADDRESS(ES) Dr. Brett Bedeaux USAF Nuclear Weapons Center 498 NSW/NWASA 1551 Wyoming Blvd SE Kirtland AFB, NM 87117 (505) 853-3838 brett.bedeaux@kirtland.af.mil	10. SPONSOR/MONITOR'S ACRONYM(S) USAFNWC
	11. SPONSOR/MONITOR'S REPORT NUMBER(S)

12. DISTRIBUTION / AVAILABILITY STATEMENT
DISTRIBUTION STATEMENT A: APPROVED FOR PUBLIC RELEASE; DISTRIBUTION UNLIMITED.

13. SUPPLEMENTARY NOTES
This material is declared a work of the U.S. Government and is not subject to copyright protection in the United States.

14. ABSTRACT
This work focused on the impact of gamma and mixed gamma/neutron radiation on transmission through single-mode and multi-mode ytterbium-doped single-mode fibers operated as amplifiers for a 1060-nm light source. Ytterbium-doped optical fibers demonstrate sensitivity to gamma and mixed neutron/gamma radiation exposures that is independent of the operational configuration of the fiber during irradiation. No identifiable dose rate damage production mechanism was encountered. However, fiber damage recovery following irradiation was found to be dependent on the radiation dose rate.

15. SUBJECT TERMS
Radiation effects, rare-earth doped optical fibers, Yb-doped optical fibers, reactor exposure

16. SECURITY CLASSIFICATION OF:			17. LIMITATION OF ABSTRACT	18. NUMBER OF PAGES	19a. NAME OF RESPONSIBLE PERSON James C. Petrosky, PhD (ENP)
a. REPORT U	b. ABSTRACT U	c. THIS PAGE U	UU	130	19b. TELEPHONE NUMBER (Include Area Code) (937) 255-3636 x7300 james.petrosky@afit.edu